Bio-physical controls on tidal network geomorphology

Belliard, Jean-Philippe

UNIVERSITÀ DEGLI STUDI DI TRENTO

QUEEN MARY
UNIVERSITY OF LONDON

Erasmus Mundus Joint Doctorate School in Science for MAnagement of Rivers and their Tidal System

---

Jean-Philippe Belliard

Bio-physical controls on tidal network geomorphology

Erasmus Mundus

October 2014

Doctoral thesis in Science for MAnagement of Rivers and their Tidal System,
Cycle: 1
Primary Institution:
Department of Civil, Environmental and Mechanical Engineering, University of Trento, Trento, Italy
Secondary Institution:
School of Geography, Queen Mary, University of London, London, UK
Associate partner:
UNESCO-IHE, Delft, Netherlands
Supervisors:
Dr. Marco Toffolon, University of Trento
Dr. Kate Spencer & Dr. Gemma Harvey, Queen Mary, University of London
External advisors:
Dr. Alessandra Crosato, UNESCO-IHE
Dr. Luca Carniello, University of Padua, Padua, Italy
Dr. Stijn Temmerman, University of Antwerp, Antwerp, Belgium

Front cover: Lagoon of Venice, Veneto, Italy.

Academic year 2014/2015

This page is intentionally left blank

The SMART Joint Doctorate Programme

Research for this thesis was conducted with the support of the Erasmus Mundus Programme[1] , within the framework of the Erasmus Mundus Joint Doctorate (EMJD) SMART (Science for MAnagement of Rivers and their Tidal systems). EMJDs aim to foster cooperation between higher education institutions and academic staff in Europe and third countries with a view to creating centres of excellence and providing a highly skilled 21st century workforce enabled to lead social, cultural and economic developments. All EMJDs involve mandatory mobility between the universities in the consortia and lead to the award of recognised joint, double or multiple degrees. The SMART programme represents a collaboration among the University of Trento, Queen Mary University of London, and Freie Universität Berlin. Each doctoral candidate within the SMART programme has conformed to the following during their 3 years of study:

(i) Supervision by a minimum of two supervisors in two institutions (their primary and secondary institutions).

(ii) Study for a minimum period of 6 months at their secondary institution.

(iii) Successful completion of a minimum of 30 ECTS of taught courses.

(iv) Collaboration with an associate partner to develop a particular component / application of their research that is of mutual interest.

(v) Submission of a thesis within 3 years of commencing the programme.

[1]This project has been funded with support from the European Commission. This publication reflects the views only of the author, and the Commission cannot be held responsible for any use which may be made of the information contained therein.

A mes parents,
Philippe et Marie

Acknowledgements

My first thoughts go to my supervisors Dr. Marco Toffolon, Dr. Kate Spencer and Dr. Gemma Harvey for their guidance, support, patience and kindness throughout this PhD. In particular, I wish to thank Marco who has invested a lot of his time guiding me from the very beginning and has paid very detailed attention to every aspect of my work. Benefiting his experience, knowledge and enthusiasm has been a source of inspiration and which has opened my mind to new research interests and perspectives. I would like to thank Kate and Gemma who have introduced me to different research approaches. Their expertise and intuitions have been central to the outcome of this thesis.

I would like to thank Pf. Andrea Defina and Dr. Luca Carniello for enabling me to use and further develop their modelling framework. A special thanks to Luca for his patience in explaining me the model with its underlying theories and numerical aspects so that I could proceed efficiently. I also would like to thank Dr. Andrea D'Alpaos for his definite insights into the modelling work.

Warm thanks go to Dr. Alessandra Crosato for providing me with a placement at UNESCO-IHE. Her constructive advice have helped me to hold better critical thinking on the modelling work.

I would like to express my sincere gratitude to Dr. Stijn Temmerman for giving me the opportunity to spend several weeks at the University of Antwerp and letting me use the different facilities there. His expertise and enthusiasm have helped me to achieve the field-based framework of my research.

I would like to expressly acknowledge all the academic and administrative staff involved in the SMART programme who have successfully designed a joint Doctorate program offering an international and inter-disciplinary approach which has resulted in one of the most memorable experiences of my life.

A big thanks to each and every one of the PhD colleagues encountered in the different institutions. I have met fantastic scientists and great people, and although they are too many to be listed here, I am sure they will recognise themselves! I am grateful

to all the SMART doctoral candidates for contributing to my personal and professional time. Special thanks go to the first "family" cohort, particularly those based in Trento; Marco and Simone for helping me settled down there and for having succeeded in turning me as a Trentino lover!; Hossein and Cagri for being tightened the three of us in the good and bad moments as being expatriates!

I am personally indebted to Prima who has now been part of my life since my Master studies and who has constantly pushed me to unveil my potential while helping me in many ways on a daily life basis.

Last but not least, I would like to show my gratitude to my family: my parents Philippe and Marie, my little brother Pierre-Olivier and my two sisters Caroline and Julie for their endless patience and encouragements.

Abstract

Looking over a tidal wetland, the tidal network characterised by its intricate system of bifurcating, blind-ended tidal courses clearly stands out from the overall landscape. This tidal landform exerts a fundamental control on the morphology and ecology within the tidal environment. With today's recognition of the ecological, economical and societal values provided by tidal wetlands, which has been notably reflected in the development of restoration management strategies across Europe and USA, there is a need to fully understand the nature and development of tidal networks as well as their relationships with associated landforms and biotic components (e.g. vegetation), to eventually guarantee the success of current and future restoration practices. Accordingly, this research aims to bring further insights into the bio-physical controls on the geomorphology of tidal networks. To this end, a combination of remote sensing, modelling and field activities was employed.

A geo-spatial analysis was performed at Queen Mary, University of London (UK), to address the variability of tidal network patterns. A series of network scale morphometric variables was extracted using airborne LiDAR data among selected tidal networks across the UK depicting different planview morphologies, and supplemented with the collection of corresponding marsh scale environmental variables from published sources. Multivariate statistics were then performed to characterise the variability of tidal network patterns and identify the inherent environmental controls. The analysis has revealed that every network type can be characterised based upon measures of network size and complexity, with each network pattern depicting proper morphometric aspects. Particularly, the stream Strahler order and the median depth of the network main channel have the highest discriminating weight on the patterns investigated. High correlation between the latter variable and network main channel width has revealed that linear, linear-dendritic and dendritic networks followed a transitional gradient in their aspect ratio approximated by a power law and thus are seen to depict similar erosional processes. To the contrary, meandering networks clearly depart from this

relationship, and show particular segregation in their aspect ratios with respect to dendritic networks. Globally, differentiation on network morphometric properties has been linked to environmental conditions specific to the marsh physiographic setting within which a tidal network develops. Conceptually, tidal networks seem to adapt to marsh environmental conditions by adopting suitable morphologies to drain their tidal basin effectively.

An eco-geomorphic modelling framework was developed at University of Trento (Italy), to address tidal network morphological development. In line with current theories as well as modelling advances and challenges in the field of tidal network ontogeny, emphasis was thus placed on the investigation of tidal channel formation and evolution in progressive marsh accretional context. Under these environmental conditions, tidal network development can be ascribed to the combination of two channel-forming processes: channel initiation results from bottom incisions in regions where topographic depressions occur; channel elaboration results from differential deposition, contributing to the deepening of the tidal channels relative to the adjacent marsh platform. Further evolutionary stages including channel reduction proceed from the horizontal progradation of the marsh platform which may lead eventually to channel infilling. Moreover, both qualitative and quantitative results allude to an acceleration of the morphological development of the synthetic tidal networks with increasing sediment supply. These different observations thus emphasise the prevalence of depositional processes in shaping tidal channels. In a second stage, the investigation was extended to the role of the initial tidal flat morphology as an inherent control on tidal network development, by considering different scenarios of topographic perturbations, which has revealed its legacy on tidal network morphological features. Modelling experiments have also acknowledged salt marsh macrophytes as a potential control on network evolution depending on their biomass distribution within the tidal frame. However, tidal channel morphodynamcis appears to be sensitive to the way biomass growth is mathematically parameterised in the model.

In view of the current challenges in transcribing mathematically such a dynamic process and the relevance of bio-physical interactions in driving salt marsh and tidal network evolution, a field survey was conducted in a temperate salt marsh in the Netherlands, as part of the mobility to UNESCO-IHE (Netherlands) in partnership with University of Antwerp (Belgium), to assess vegetation distribution and productivity in the tidal frame. Particularly, emphasis was placed on extending investigations on the possible presence of relationships involving vegetation properties in different climatic

and ecological conditions from those characterising these previously documented relationships. Regression analysis has revealed that biomass growth can be expressed as a linear function of marsh relative elevation, providing therefore direct empirical validation for corresponding assumptions reported in the literature and used in the present modelling framework; surprisingly, that increase did not correlate with an increase in species richness and diversity. Analysis of likely associations between vegetation morphometrics and total standing biomass yielded only a single linear relationship linking the latter variable to stem height. In truth, these observations may bear reconsiderations on the global validity of the assumptions used in the formulation of some eco-geomorphic processes which are applied in the study and prediction of wetland resiliency facing climate change.

Contents

List of Figures

List of Tables

Chapter 1

Introduction

1.1 Rationale and research scope

In recent decades, large areas of coastal wetlands have been lost or seriously degraded as a result of both natural and anthropogenic pressures. Natural challenges include subsidence, erosion, climate change manifestations such as increasing storminess and sea-level rise (Kirwan and Murray, 2007). Human threats include land reclamation, sea-defence construction and water quality deterioration resulting from over-population in littoral zones. In truth, coastal land reclamation has been a common practice in Europe which originally dated back to Roman times (Rotman et al., 2008; Watts et al., 2003), emphasising thus how much the ecological, economical and societal values of these ecosystems have been long disregarded.

Although coastal wetlands only cover 4% of Earth's total land area (Spencer and Harvey, 2012), they provide a wide range of ecosystem services benefiting national economies (Barbier et al., 2011; Costanza et al., 1997). For temperate coastal wetlands, main benefits include the sustainable protection of coastal settlements against storm surges and marine flooding; the sequestration of carbon, nutrients and pollutants; and the provision of rare and unique habitats supporting nursery grounds for fish, and breeding/feeding grounds for birds (Jones et al., 2011). The increasing popularity of the ecosystem services concept has been reflected in a range of legislative and policy frameworks at the European level for the management and preservation of aquatic ecosystems (e.g. European Parliament and the Council of the European Union, 2000). Coupling this with the increasing awareness in the general public regarding the economical and societal values offered by these environments, concerns about restoration have progressively arisen over the last decades (Garbutt et al., 2006), in an

attempt to stop the human pressure which is itself suspected to have contributed to the degradation of up to 50% of salt marshes worldwide (Barbier et al., 2011).

A coastal management strategy, now well implemented across Europe and USA, and having the potential to restore salt marshes and deliver ecosystem services, is Managed Realignment (MR) (Spencer and Harvey, 2012). This restoration technique is described as a "soft engineering" approach whereby the building of a sea-wall at the back of a site is performed followed by the deliberate breaching, lowering, or even removal of the old sea-wall seaward to eventually allow tidal waters to inundate the previously protected low-lying intertidal area (French, 2006). Such schemes offer sustainable coastal flood defence, habitat restoration and ecosystem services which may help EU member states to achieve good ecological status imposed by the Water Framework Directive. Accordingly, more than 50 MR sites have been created in UK since the first one in 1991 (Pendle, 2013). In practice however, designing and assessing a MR scheme is highly complex. The success of such an engineering intervention is theoretically assessed by means of criteria indicative of the restored site's ecological performance, which are however not clearly defined and difficult to measure presently(Scott et al., 2011). Many restoration schemes may seem to deliver high ecological and biodiversity values in a short time scale, but often depict poorer or slower habitats than expected over longer term, particularly for salt marshes, to the complete reversion to tidal flats sometimes (Burgin, 2010). Despite pre-breaching engineering operations can be conducted such as sediment excavation/re-charge (e.g. Allfleet's marsh, Essex, UK) to control elevation and hydroperiod within the site, or the creation of an artificial tidal network (e.g. Freiston marsh, Lancashire, UK) to promote landward sediment transport and drainage within the system (Symonds and Collins, 2007), usually restored sites show less variation in topography than natural wetlands (Elsey-Quirk et al., 2009) and remain poorly drained (Crooks et al., 2002). In fact, the entire difficulty resides in designing relevant schemes to guarantee the success of the intervention due to the current incomplete understanding of the processes and their interplays governing the morphological evolution of the wetland and its components, particularly the tidal network, being key to the well-functioning of such an ecosystem (Perillo, 2009).

A distinctive feature of tidal networks are their intricate system of branching usually blind-ended channels that clearly stands out from the overall landscape as illustrated in Figure 1.1. Therefore, upon viewing Figure 1.1, one may typically wonders how such a striking landform forms; how it morphologically evolves; why it adopts various patterns; and whether it constitutes a product of eco-geomorphic interplays. Practically,

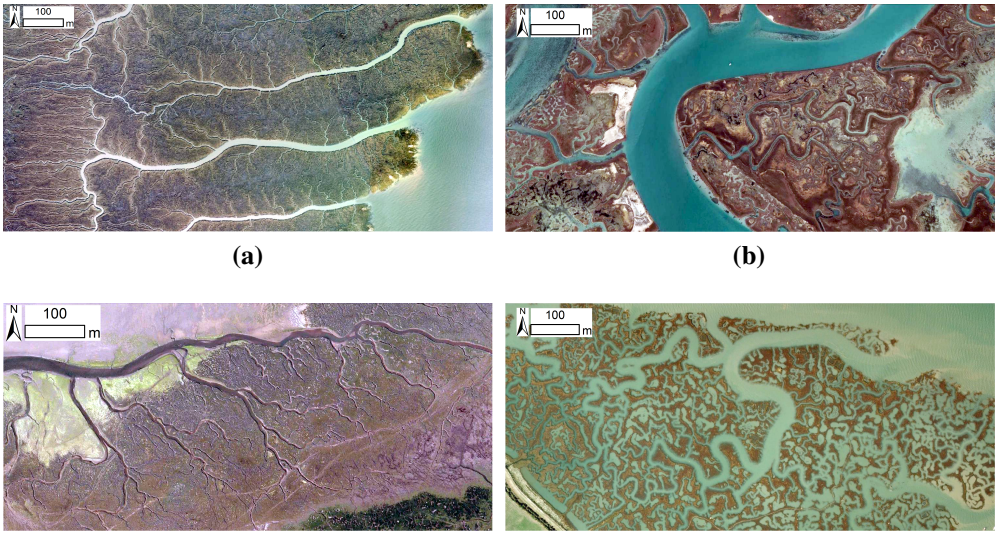

Figure 1.1: Examples of salt marshes: (a) Dengie peninsula, Essex, UK; (b) San Felice salt marsh, Venice Lagoon, Italy; (c) Dyfi estuary, Wales, UK; (d) Tollesbury marsh, Essex, UK.

these questions encompass the study of the description, nature, and development of such a landform and its relationship with associated environments and biotic components (e.g. vegetation), thence, of the geomorphology of tidal networks. Accordingly, having set these research directions, the present contribution aims to bring further insights into the bio-physical controls on the geomorphology of tidal networks.

1.2 Research questions and outline of the dissertation

Studying the eco-geomorphology of tidal wetlands mainly involves two research methodologies, which have been widely adopted by environmental engineers and geomorphologists. The first methodology derive results based upon empirical or experimental data from real study cases. Additional information can be collected from published sources. Geomorphological tools are mostly based on this methodology whereby statistical evidences support and verify results. The second methodology regards modelling and analytical theory. This approach usually calls for simplifications of the dynamic processes at work and solve the problem mathematically. Unlike the statistical approach, the method does not directly require observational data to be carried out, but needs empirical data for validation. Each methodology presents its own

advantages and drawbacks. For instance, one particular constraint for the first approach is the assembly of a data set preferably large and internally-consistent for subsequent analysis.

The present research is underpinned by three elements, involving these two methodologies. Firstly, Chapter 2 presents an overview of the physical features over which the subsequent research elements will be performed, and provides the necessary knowledge to grasp their main morphological characteristics. Chapter 3 which was conducted at Queen Mary, University of London (UK) addresses the diversity of network patterns to answer, following a review on the different tidal network planform and drainage characteristics, the successive research questions:

(i) What factors characterise a particular network pattern?
(ii) Do these factors respond to environmental controls?

Chapter 4 which was conducted at the University of Trento (Italy) addresses tidal channel ontogeny. A review on the various theories regarding tidal channel formation and evolution processes as well as the advances and challenges in transcribing the knowledge in a numerical modelling perspective is first presented. Chapter 4 will focus on the following research questions:

(i) How do tidal channels form and evolve in different marsh sedimentary contexts?
(ii) How do tidal channels form and evolve starting from different initial tidal flat bathymetric configurations?
(iii) How do tidal channels respond to eco-geomorphic feedbacks involving different ecological scenarios and mathematical parameterisations?

Lastly, in view of the growing interest in the research field of bio-morphodynamics, and which recent contributions have shown the relevance of a range of bio-physical interactions and feedbacks in driving the morphological evolution of salt marshes and their intertwining tidal networks, the last part of the thesis falls within this scope accordingly. Thus, Chapter 5 which was conducted at UNESCO-IHE (Netherlands) in partnership with the University of Antwerp (Belgium) looks at vegetation spatial distribution and productivity in salt marshes, following a review on salt marsh vegetation dynamics, with the subsequent research questions:

(i) How halophytes are spatially distributed in a temperate salt marsh?
(ii) Does total standing biomass respond to marsh elevation and if so what relationship does it depict?

(iii) Do relationships exist between vegetation morphometric characteristics and total standing biomass?

Finally, Chapter 6 concludes the research by exposing a summary of the main outcomes per research element, supplemented with future research considerations.

Chapter 2

Tidal network: the reference framework

This chapter presents an overview of the physical features discussed within this research including general aspects of the associated global geomorphic setting, characteristics of tidal networks and related micro-features in temperate climate. A more detailed literature review accompanies the subsequent chapters.

2.1 Tidal wetlands: overview

Prior to discussing on the tidal network and its embedded micro-features, important is first to refer to the wetland setting and its spatially-associated landforms in order to appreciate better the environmental conditions within which they occur.

2.1.1 General character and system composition

Tidal (and coastal) wetland ecosystems occur within an elevation gradient that ranges from sub-tidal depths at which light penetrates to support photosynthesis of benthic plants to where the sea passes its hydrologic influence to groundwater and atmospheric processes (Wolanski, 2009). Examples of such ecosystems comprise salt marshes, mangroves, tidal flats and seagrasses. Typically, tidal wetlands occur in environmental settings characterised by low-hydraulic energy and gentle slopes, thus favouring sediment depositional and accretional activities. Wetland development relies on complex interplays between physical and biological processes contributing to the unique character of such ecosystems. In fact, tidal wetlands represent perhaps the most striking

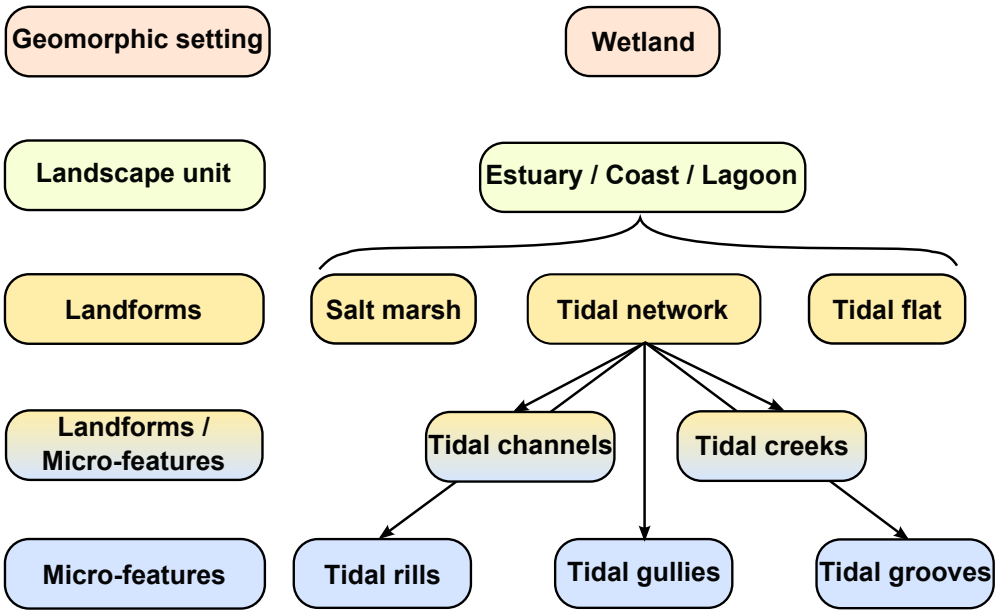

Figure 2.1: Geomorphic description system of a tidal wetland in temperate climate with its geomorphological components based on the convention of Schoeneberger and Wysocki (2012).

example of a system whose adaptation to changing environmental conditions (e.g. climate change) may be controlled by eco-geomorphic interactions (Langley et al., 2009).

From a geomorphological perspective, wetlands are termed as geomorphic settings that develop among different landscape units which themselves constitute unique or broad regional groups of spatially-associated landforms (Schoeneberger and Wysocki, 2012). In turn, these landforms encompass so-called micro-features which represent physical features too small to delineate at common survey scale. In the case of tidal wetlands occurring in temperate climate being the object of the present research, the corresponding geomorphic description system is illustrated in Figure 2.1. The following sections will thus follow this description system to progressively downscale the discussion to the physical features of interest.

2.1.2 Landforms

Tidal wetlands in temperate latitudes are mostly manifested by the presence of salt marshes and their associated tidal flats. Salt marshes are complex tidal landforms regularly flooded by tides and chiefly covered by halophytic vegetation (Fagherazzi

et al., 2012). Together with the contiguous tidal flats, these tidal wetlands make a major contribution to the environments of the lowland coastal zone in Northwest Europe (Allen, 2000), although they are also widespread in similar landscape units located in other temperate regions across the world. In Great Britain, Burd (1989) recorded a total of 443.7 km^2 covered by salt marshes; in North America, this area amounts to 300,000 km^2, primarily in Canada and Alaska (Mitsch and Gosselink, 2000). Morphological evolution of salt marshes results from complex eco-geomorphic interactions mostly in the form of feedbacks involving several processes and forcing factors (Figure 2.2). For instance, a fundamental feedback mechanism links the processes of marsh sedimentation with marsh elevation and tidal inundation, being driven by the sediment availability and the hydrodynamics (green loop in Figure 2.2). Marsh ecology notably manifested by vegetation productivity supplements this feedback mechanism (blue loop in Figure 2.2) as it contributes to surface sedimentation via a range of eco-geomorphic processes which will be reviewed in chapter 5. Another feedback mechanism connects marsh sedimentation to marsh relative elevation and autocompaction (blue loop in Figure 2.2). The different involved processes act on a wide range of characteristics scales. For instance, although some halophytic species depict biennial or even perennial life cycle, the evolution of their biomass is known to act on interannual scales (Morris and Haskin, 1990). Apparent marsh morphological change is expected to take place over annual or decadal scales whereas extrinsic forcing factors depict a rather wide spectrum of time scales, ranging from seconds (e.g. waves) to decades and beyond (e.g. sea level rise) (Coco et al., 2013).

Similar to their tidal wetland analogues, salt marshes form in low-energy estuarine or coastal environments under all tidal regimes (Allen and Pye, 1992). Pye and French (1993) have recognised seven types of marshes based on physiographic settings and planar morphology (Figure 2.3). Although this classification was built upon marshes in the UK, comparable marsh morphological types can be encountered across the European coastline (Allen, 2000). Open coast marshes (Figure 2.3a) are usually sandy or sandy-muddy if sheltered by back-barriers or spits (Figure 2.3b). Estuarine fringing marshes (Figure 2.3d) mostly occur parallel to the flow direction and are thus relatively elongated (EstSim Consortium, 2007). This type is predominantly muddy similarly with the Estuarine back barrier setting (Figure 2.3c) where the enclosed spit(s) provides a certain degree of obstruction of the estuary mouth, hence limiting tidal wave penetration. Marshes of types open embayment (Figure 2.3e) and restricted entrance embayment (Figure 2.3f) are usually sandy to sandy-muddy and are rather large in size due to the

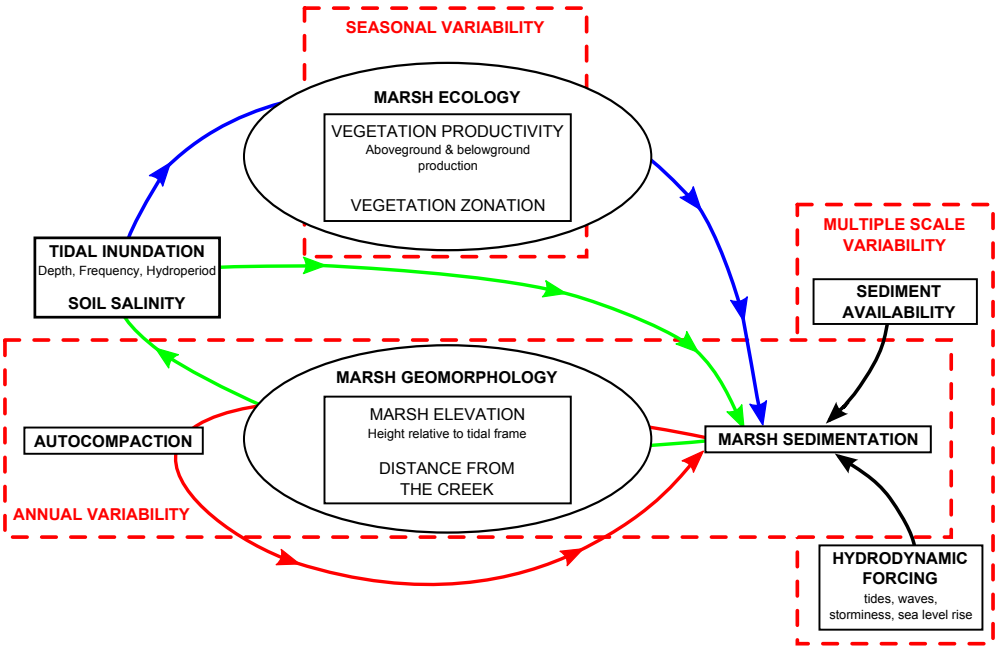

Figure 2.2: Main drivers, processes and feedbacks in salt marsh evolution.

extensive intertidal zones characteristic of these physiographic settings. As rias (Figure 2.3g) are typically drowned v-shaped valleys with valley sides being relatively steep and composed of hard rocks (Steers, 1964), the corresponding marshes are usually located in the inner side of this estuarine environment. This above trend in marsh sediment composition in relation to the physiographic setting can however show strong within-site variability depending on the marsh location inside the tidal landscape and on the presence of river inflows (Pye, 2000).

In these different tidal systems, marshes are generally associated with two other tidal landforms: the tidal flats and the tidal network as outlined in Figure 2.1 and illustrated in Figure 2.4 (D'Alpaos et al., 2005; Fagherazzi et al., 2006).

Tidal flats extend over the lower elevations within the tidal frame and are usually deprived of vegetation. They require an environment characterised by an abundant supply of fine-grained sediments and the predominance of tides and tidal currents over other hydrodynamic forces (Klein, 1985). Indeed, tidal flats cannot form when wave action prevails as wave breaking typically induces an offshore transport of the fine-grained sediments (King, 1972). Thus, sediment transport should be dominated by tidal currents rather than wave breaking to allow for the accumulation of fine-grained sediments (Gao, 2009) and consequently the formation of tidal flats.

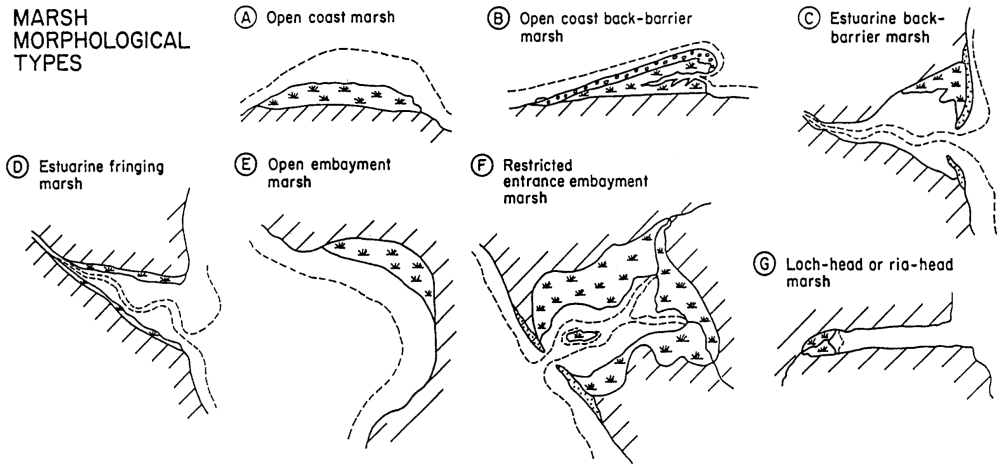

Figure 2.3: Geomorphological classification of UK salt marshes (adapted from Pye, 2000, after Pye and French, 1993).

Lastly, the tidal network with its noticeable appearance completes the wetland picture. Its function is to transport tidal waters, sediments and nutrients in and out of the marsh platform (D'Alpaos et al., 2005). As being the primary target of this research, from now on the focus will be placed on the description of this landform and its geomorphic components; salt marshes and tidal flats to which tidal networks are tightly coupled will be discussed only when necessary.

2.2 Tidal network characteristics

The tidal (drainage) network and its intrinsic tidal courses represent one of the most important landforms within the tidal landscape, and constitutes a chief control on the morphology and ecology of the tidal wetland (Fagherazzi and Furbish, 2001). Prior to exposing the present knowledge on the characteristics of the tidal network and its embedded physical features, a brief recall on the inherent definitions is provided in order to set the topic appropriately.

2.2.1 Tidal courses: definitions and classification

Fundamentally, tidal networks constitute a circulatory system through which tidal waters, suspended sediments and nutrients are distributed over the marsh platform during the flood tide and drained to the sea during the ebb tide (Allen, 2000). Due to this key function, they provide various ecosystem services and are therefore essential

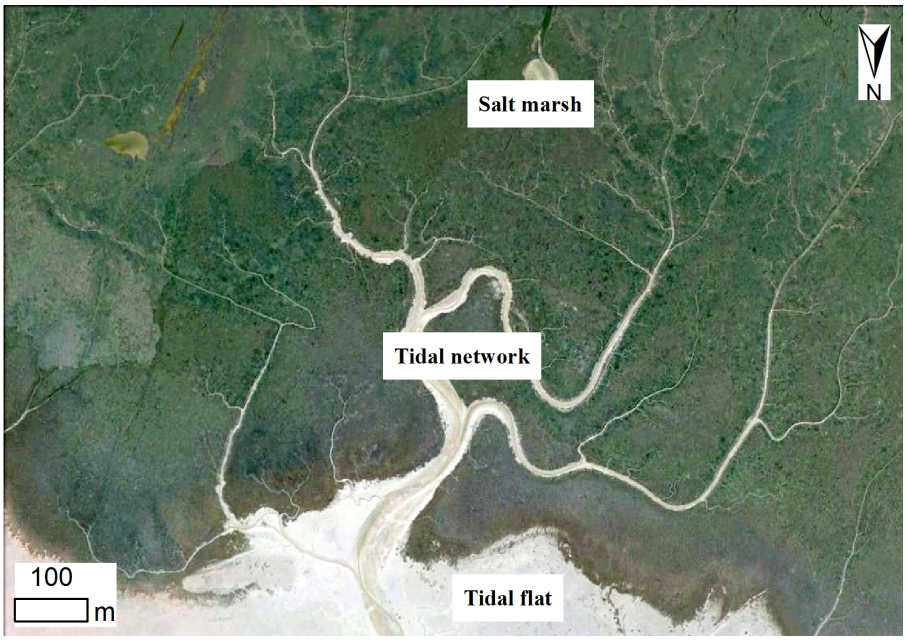

Figure 2.4: Aerial image ($\sim$ 1.7 x 1.1 km, north towards bottom) of an estuarine landscape in the Bay of Mont Saint-Michel, France, and its associated tidal landforms: salt marsh, tidal flat and the tidal network.

for the life within tidal wetlands (Barbier et al., 2011). From a morphological point of view, tidal networks consist of a complex system of bifurcating, usually blind-ended tidal courses that dissect the wetland (Coco et al., 2013), although through-flowing tidal courses that essentially connect channels to channels or to lagoons can sometimes occur (Hughes, 2012). Here, tidal course is a generic name for designating all valley features cutting through the wetland such as channels and creeks. Despite the fact that the latter names are often used interchangeably in the literature, distinctions between the different tidal courses still exist and are worth to recall so as to avoid any confusion and also to better grasp every tidal course geomorphological characteristics.

Perillo (2009) proposed an inclusive classification of tidal courses based on course size, namely the width and depth of a course cross-section measured at bankfull level, as well as the persistence of water on the course during low tide conditions as displayed in Table 2.1.

Following these criteria, 5 tidal courses were classified whose planview morphology is illustrated in Figure 2.5. Correspondingly, tidal rills which are materialised by very small indentations formed along the unvegetated margins of larger courses during the ebb tide represent the smallest tidal courses in size (Figure 2.5a - tr). They usually

Table 2.1: General classification of tidal courses (adapted from Perillo, 2009).

Tidal course	Water persistence at low water slack	Course depth (cm)	Course width (cm)	Cross-sectional area (cm^2)
Tidal rills	No	< 1	< 2	< 1
Tidal grooves	No	1-5	2-10	< 50
Tidal gullies	No	< 1	< 2	50 - 1,000
Tidal creeks	Yes	10 - 200	10 - 200	100 - 4,000
Tidal channels	Yes	> 100	> 200	> 2,000

constitute the primary stage towards the development of a large tidal course. Their formation is ascribed to the presence of a small layer of fine sediments being intersected by low flowing waters or from the action of groundwater outflows usually occurring on sandy beaches. Topographic slope and soil sediment characteristics contribute to the diversity in rill morphology.

If the morphological structure of the rill is persistent enough or the magnitude of the forming hydrodynamic processes is balanced enough to ensure its maintenance, the rill can thus evolve towards a tidal groove (Figure 2.5a - tr). Tidal grooves are thus relatively deeper and wider than tidal rills, which make them more liable to resist tidal inundation. Similar to the former micro-feature, grooves develop along channel banks but also marsh fronts. A steeper slope is however necessary so that the resulting erosive action of the ebb tidal flow and groundwater discharges can shape them.

Tidal gullies (Figure 2.5b) can form upon the concentration of flows and waves in some of the grooves along the channel margins or the marsh edge (Priestas and Fagherazzi, 2011), leading to deeper and much wider indentations than the previous tidal courses. Unlike rills and grooves, their courses are preserved and even enhanced by the hydrodynamic forcing. Gullies may reach similar geometrical characteristics as tidal creeks, the difference residing however in the absence of tidal waters on the course at low tides.

Therefore, while rills, grooves and gullies are characterised by the lack of a permanent tidally-driven baseflow during low tides, tidal creeks and tidal channels on the contrary are marked by water persistence along their course even at low water slack (Perillo, 2009). Strictly speaking, tidal creeks (Figure 2.5c) are partially inundated at low tides, typically at the creek mouth whereas creek head may be completely dried up. Thus, only tidal channels (Figure 2.5d) always have tidal waters along their entire

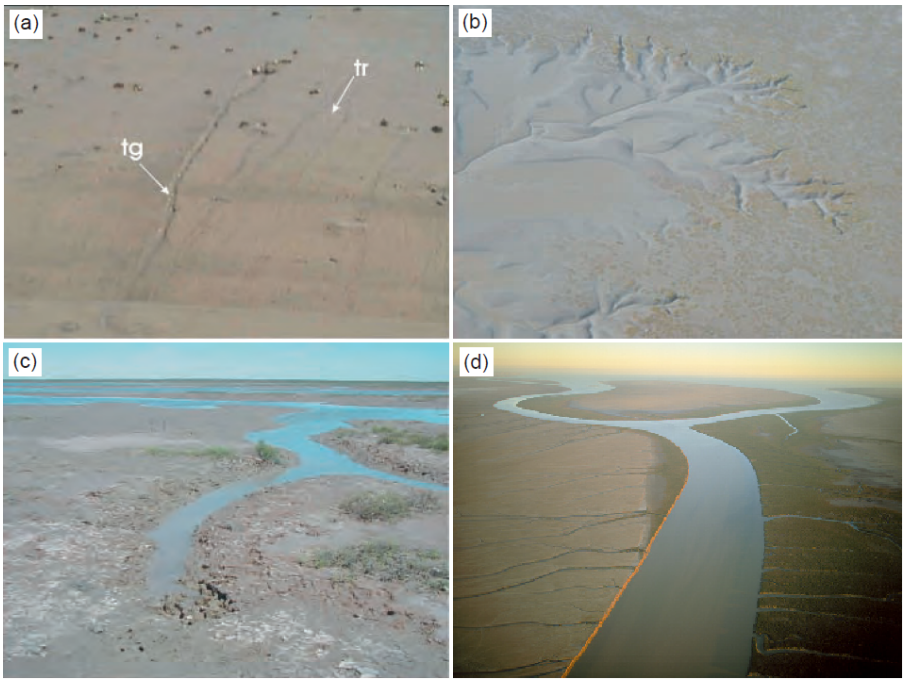

Figure 2.5: Examples of different tidal courses (adapted from Perillo, 2009). (a) Tidal rills (tr) and tidal grooves (tg); (b) tidal gullies; (c) tidal creeks; (d) tidal channels.

course at any stage in the tidal frame. Distinctions between creeks and channels also regard their geometrical aspects; where tidal creeks show strong variations in depth and a rather constant width over their whole course, tidal channels depict a constant depth to the detriment of a varying width (Perillo, 2009). Such morphometric properties reveal the high and complex dynamics governing their geomorphology. Rills, grooves, gullies and creeks are tributaries of tidal channels, yet only creeks and channels intertwine both tidal flats and salt marshes.

As creeks and particularly channels are the largest tidal courses in size, they constitute the most distinctive features of the tidal network, exerting a strong control on the hydrodynamics and sediment transport in the tidal landscape, hence on its short and long term morphological evolution (Dronkers, 2005). In view of their influential character, various comprehensive studies have attempted to describe their characteristics. Accordingly, in the following will be summarised the main peculiarities of tidal courses with special considerations on tidal channels and creeks.

2.2.2 Tidal course characteristics

Spatial and temporal flow patterns

Tidal environments commonly experience variations in tidal, fluvial and wave energy (Dalrymple and Choi, 2007), yet tidal currents are the preeminent hydrodynamic forcing in the generation and preservation of tidal channels (Hughes, 2012). Wind driven waves may indeed occur along large tidal channels, producing large erosion of the marsh front and channel margins, and may lead to the formation of tidal gullies (Pethick, 1992; Priestas and Fagherazzi, 2011), but wave effect rapidly decreases with distance from the sea. The intensity of fluvial hydrodynamics on the other hand reduces seaward from the landward extent of the tidal wave.

Tidal hydrodynamics in tidal channels is a highly complex phenomenon. In general, the flow in tidal channels is highly non-uniform where the water slope differs from the bottom slope (Allen, 2000; Rinaldo et al., 1999a), except occasionally in small first-order tidal creeks where the flow can be topographically driven due to the high bed slope locally. However, the main peculiarity of tidal hydrodynamics in tidal courses regards the presence of an asymmetry between the magnitude of flood and ebb velocities and the respective periods over which they occur. The morphology of the platform flanking the tidal courses constitutes a primary control of these flow inequalities (Hughes, 2012). Indeed, large intertidal areas with extensive vegetation colonization typically induce a slower propagation of the flood and ebb currents over the platform, and thus a retard in the passage from flood to ebb tide. A shortened ebb is therefore observed. As a consequence, the timing of the ebb tide and, consequently the magnitude of its peak velocity become modified (Fagherazzi et al., 2008). Tidal asymmetry can also vary depending on the location of the tidal course within the tidal system. Typically, course flow is flood-dominated near the head of the tidal basin, ebb-dominated in the middle reach and balanced at the seaward end (Allen, 2000).

Spatial variations in the absolute magnitude of tidal velocities also occur along the tidal network. Low-order tidal creeks and gullies experience a complex velocity-stage relationship where the bankfull level acts as a geomorphic threshold materialising the transition from undermarsh to overmarsh tides (Pethick, 1980). Indeed, they commonly observe a high flood velocity pulse (or surge) close to bankfull conditions, essentially when the water overtops the channel banks due to the sudden variation in tidal prism as the huge storage capacity of the marsh platform comes into play (i.e., overmarsh tidal prism) (Bayliss-Smith et al., 1979; French and Stoddart, 1992). Comparatively,

due to the delayed ebb flow, the highest ebb velocity pulse occurs at a slightly lower water stage than the flood velocity peak and is sensibly stronger (Figure 2.6). Indeed, principles of conservation requires faster flows to convey the same tidal prism for a shorter period of time. Likewise, as the flow in the course is more inertia driven compared to the overmarsh flow being more frictionally-dominated due to the presence of vegetation, the water surface slope between the platform and the course during the ebb tide is relatively steep, creating faster flows.

However, high-order tidal creeks and channels are more likely to experience their highest flood and ebb velocities near mid-tide and have a lower tidal asymmetry (Ashley and Zeff, 1988; Hughes et al., 2009). Thereby, maximum current velocities in tidal courses do not necessarily correspond with the highest water depth unlike river systems.

Implications on sediment transport

This non-uniform and greatly unsteady tidal flow has significant effect on the geomorphological work within tidal courses and for the net transport of water and sediments onto the marsh platform. Low flow velocities occurring at undermarsh stages and at high water slack (see Figure 2.6) favour the deposition of suspended sediments in the channel and in the nearby regions of the marsh platform. Such a process dominates so long as the water level is not too close to bankfull level.

However, erosion and transport of sediments prevail during the drowning and emptying of the marsh platform which are characterised by their respective high flood and ebb velocities (Miller et al., 1977). Moreover, this re-entrainment and transport capacity are partly dependent on the character and lithological composition of the local soil stratigraphic sequence which determines the rate of sediment autocompaction (Allen, 2000). If sediment have just settled down and have not yet attained a certain degree of compaction, tidal flows can easily resuspend and transport them, which may jeopardise thus the preservation of small tidal courses.

On overall, sediment transport within intertidal system is highly complex owing to the very intricate tidal hydrodynamics depicting large spatial variability and tidal asymmetry. Bi-directional flows lead to landscape-forming flow rates being either flood or ebb dominated depending on the hydraulic geometry of the tidal course itself, the elevation of the marsh platform, the spatial distribution of the vegetation and the tidal amplitude. Thus, the flood or either ebb dominance measured at a particular course does not necessarily imply that the whole tidal network experience a similar net flux of sediments (Hughes, 2012). The dependence of the erosion and deposition processes on

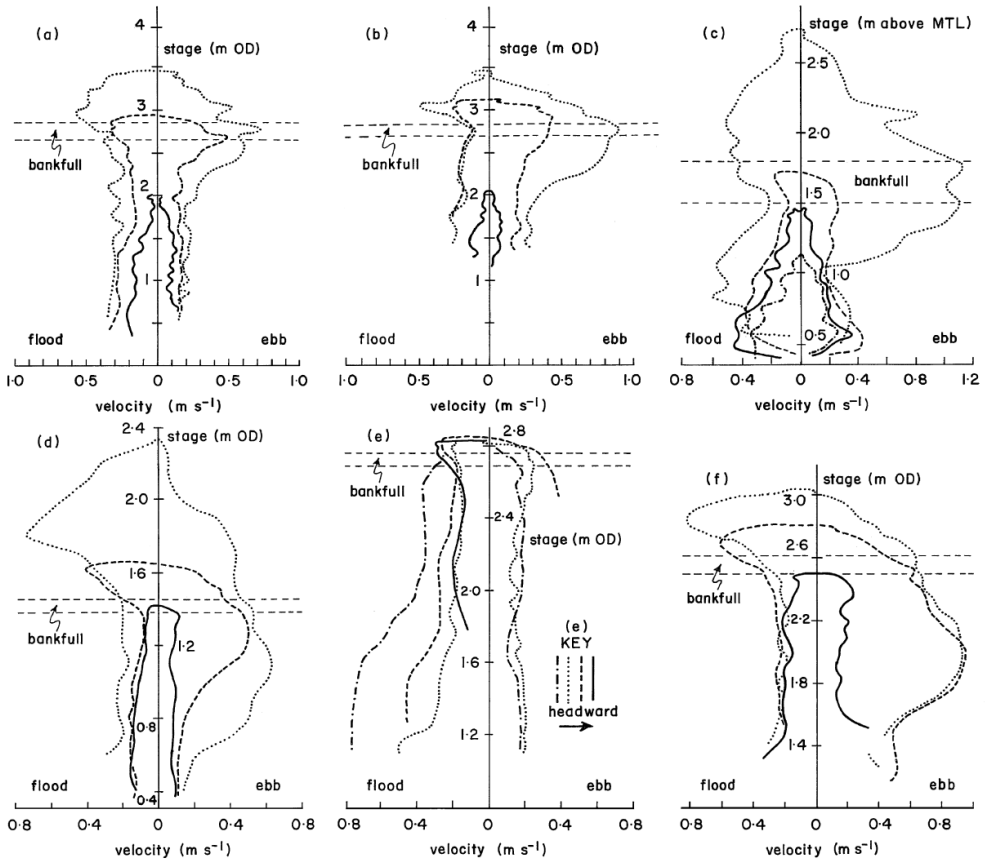

Figure 2.6: Velocity stage curves measured within different tidal creeks at undermarsh, bankfull and overmarsh tides (from Allen, 2000). (a,b) Hut Creek, Scolt Head Island, North Norfolk; (c) Tidal creek, Ems-Dollard marshes, Dutch-German border; (d) Tidal creek, Warham marshes, North Norfolk; (e) Tidal creek, Warham marshes, North Norfolk. The corresponding key only regards this subplot; (f) Tidal creek, Dengie Peninsula, Essex.

local conditions lead to a diversity in course morphometric features consequently.

Course topology

Several studies have provided insights into the cross-sectional shapes of salt marsh channels and their environmental controls (Allen, 2000; Collins et al., 1987; D'Alpaos et al., 2006; Fagherazzi and Furbish, 2001; French and Stoddart, 1992; Pestrong, 1965; Toffolon and Crosato, 2007).

Accordingly, tidal channels portray a variety of cross-sections. V-shaped and U-shaped cross-sections are frequent in small and linear tidal courses. Although asymmetric cross-sections commonly materialise meandering channels, they may occasionally occur in linear channels subject to lateral migration (Ginsberg and Perillo, 2004). Complex cross-sections take place especially in wide tidal channels containing geomorphic features such as mid-channel bars. They can be interpreted as bimodal cross-sections representing two channels separated by the bar, and depicting a residual circulation associated with flood and ebb dominance (Kjerfve, 1978). However, the formation process of this particular type of cross-section remains still under debate. Overhanging cross-section types in contrary testify to the differential sedimentary characteristics of the channel banks (Perillo, 2009). Physically, this distinct form is explained by the erosion of the lower portion of the channel bank by the tidal currents whereas the more cohesive materials composing the upper portion of the channel margin, whose resistance is reinforced by plant roots, allow instead for its preservation.

The diversity in cross-sectional shape therefore reflects the influence of a range of factors comprising tidal range, marsh stratigraphy, its associated plant cover, and channel sinuosity. Conceptually, Bendoni et al. (2014) distinguished two main processes responsible for the erosion of channel banks and marsh front based on the size of the removed material: surface erosion and mass failure. On one hand, surface erosion refers to the quasi-continuous breaking-up of sediments into small particles and aggregates whose size is much smaller with regard to bank dimensions. Mass failure, on the other hand, alludes to the discontinuous process of block failure whose dimensions are comparable to those of the banks. As previously studied by several authors (e.g. Allen, 1989; Pringle, 1995), mass failure is manifested in various ways including rotational slips characterising banks located at the outer bend of meanders of large or deep channels, as well as cantilever and toppling failures which occur along the banks of shallow to moderately deep creeks.

Bed profile and morphologies

The longitudinal bed profile of tidal rills, grooves and gullies is commonly shallow convex-up for most of their course, except at their blind-ended heads where a certain degree of upward concavity is observed (Toffolon and Lanzoni, 2010). As a matter of fact, bed slope at the head of these small tidal courses can be relatively high, being highlighted by the development of a characteristic micro-cliff which in turn favours fast ebb flows and a deeper thalweg consequently (Minkoff, 2007). Typically, a very irregular disordered morphology consisting of ruptured sediment clasts, crumbs, plant patches and crustaceous burrows occur at course heads if the bed materials is compacted. Moving seaward along the course, these irregulatrites in channel bed and banks tend to be progressively smoothed out under the action of tidal currents.

To the contrary, the bed profile of tidal channels and creeks portrays a somewhat higher relief towards the mouth (Perillo, 2009), being materialised notably by the presence of irregularities in the form of depositional features at the mouth of blind tributaries. These sediment deposits located at the confluence between blind tributaries and higher-order creeks are attributed to the sudden settling of the suspended and bed load materials at or near low water slack following their transport during ebb tide. These deposits can be flushed away or instead further accumulate and form eventually islands depending on the magnitude of the tidal flows or the possible supply of fluvial sediments to compensate the export of sediments to the sea. As observed by Hood (2010), with additional sediment supply, these islands can potentially fill the gap with the marsh mainland, triggering the formation of a meander bend. This reveals that the hydrodynamics of blind tributary / high-order creek junctions generate depositional zones near tributary outlets and favour confluence morphodynamics (Hood, 2010).

Other geomorphic features comprise scour holes which form at the mouth of tributaries in pure tide-dominated systems instead of mid-channel bars. Scour holes in tidal settings differ significantly from those encountered in fluvial settings. Discrepancies notably arise in their topology with the stoss side oriented landward and the lee side oriented seaward, being exactly opposite to the orientations of scour holes observed in river systems. Several authors have previously related the variations in fluvial confluence bed morphologies to asymmetries in confluence angle, the proportion between tributary and main river discharge, sediment erodibility and bed elevation (Ashworth, 1996; Best, 1988; Boyer et al., 2006). In fluvial systems, the depth of the confluence scour hole decreases together with the ratio of tributary to main stream discharge (Best, 1988). In tidal systems, significant differences in hydraulic geometry between blind tributaries

and their higher-order channels may exist, notably in terms of comparative width, depth and ebb velocities. Correspondingly, the proportion of tributary to high-order channel discharge can be particularly low, thus sometimes resulting in ill-defined or absent scour holes.

Geomorphic measures and relationships

Empirical synthesis of complex dynamic processes is a common practice in geomorphology (D'Alpaos et al., 2009). Accordingly, a number of field and remote sensing studies have attempted to derive geomorphic measures and relationships allowing to grasp and quantify the morphodynamics of tidal channels (e.g. Fagherazzi et al., 1999; Marani et al., 2002, 2003; Rinaldo et al., 1999a,b; Steel and Pye, 1997; Vandenbruwaene et al., 2012). The width to depth ratio $\beta = w/D$, with $w = 2B$ being the channel width, B the channel half-width and D the channel depth, represents a simple measure indicative of the morphology of tidal courses and their inherent controls. Despite a great variability across various tidal systems translating a diversity in the processes controlling section shape, globally, β suggests a distinction between marsh creeks and tidal flat channels as displayed in Figure 2.7.

Such a differentiation suggests tidal creeks from these two landform populations, (i.e., salt marsh and tidal flats) seem to respond to different erosional and depositional processes, leading thus to different types of incisions (D'Alpaos et al., 2005). Physically, the presence of halophytic vegetation and of fine and cohesive sediments on the marsh platform result in salt marsh creeks being deeply incised ($5 < \beta < 8$), as opposed to tidal flat channels ($8 < \beta < 50$). This bi-modal distribution can be ascribed to the bank erosion processes in relation to the presence of vegetation as well as sediment characteristics. As previously mentioned, heavily rooted banks near the marsh surface promote creek bank stability. Moreover, as vegetation impedes flow through its canopy promoting the deposition of sediments particularly close to creek margins where biomass density is significant (Leonard and Luther, 1995), this leads eventually to an increased creek depth. On the opposite, the coarser and less cohesive soils being deprived of vegetation alongside tidal flat channels promote instead wider and shallower channel geometry (D'Alpaos et al., 2005).

Various geomorphic relationships combining channel morphometric characteristics with landscape forming flow rates have arisen in the literature. O'Brien (1969) proposed a relationship linking the channel mouth minimum cross-sectional area Ω and the tidal prism P, i.e., the total volume of water being exchanged through the outlet of a channel

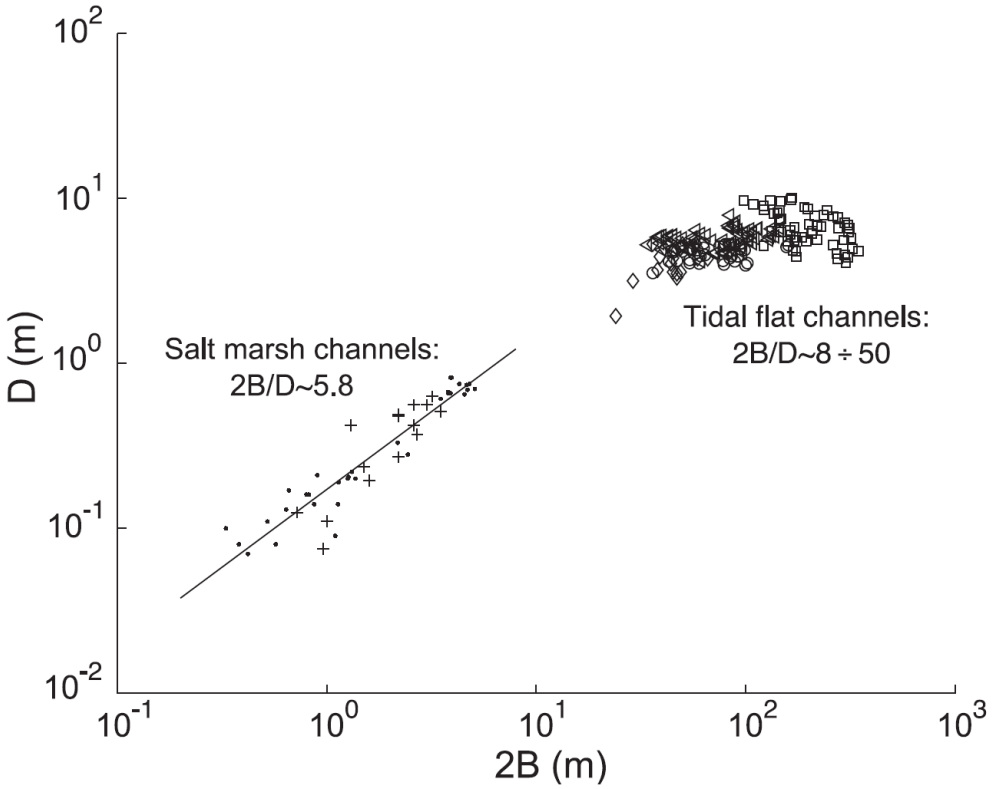

Figure 2.7: Channel width w vs depth D for salt marsh and tidal flat channels in the Venice lagoon (from Marani et al., 2002). Square and triangle symbols represent two distinct tidal flat channels with measurements taken along their respective winding path. Similarly, dot and cross symbols indicates two different salt marsh creeks.

during flood or ebb, such that:

$$\Omega \propto kP^{\alpha} \tag{2.2.1}$$

where k and α are empirically derived constants. Jarrett (1976) confirmed the validity of the above relationship by extending the analysis to a large number of tidal inlets depicting different locations and structures. Other authors have also found this relationship to be satisfied in sheltered sections of tidal systems (e.g. Byrne et al., 1980; Hume, 1991; Rinaldo et al., 1999b). Figure 2.8 displays values of channel cross-sectional area versus tidal prism for field and laboratory data (Hughes, 2002). Further studies have attempted to provide theoretical grounds for this empirical relationship, among which Marchi (1990) introduced a general framework to rationally include all of the various theoretical treatments of this concept. Consequently, D'Alpaos et al. (2009) has proposed to term this tidal prism - channel cross-sectional area relation as the "O'Brien-Jarrett-Marchi" law.

Moreover, as reported by several authors following investigations in various tidal systems (e.g. Friedrichs, 1995; Lanzoni and Seminara, 2002; Rinaldo et al., 1999b), replacing the tidal prism P by the closely related spring peak discharge Q, (i.e., driven by spring tidal fluctuations), bears also a relationship with channel mouth cross-sectional area Ω, in the form:

$$\Omega \propto Q^{\alpha_q} \tag{2.2.2}$$

where the scaling coefficient $\alpha_q \sim 1$ (Friedrichs, 1995). In fact, Friedrichs (1995) explains this relationship by relating the equilibrium cross-sectional geometry to the so-called stability shear stress, namely the total bottom shear stress being just above the critical shear stress and that is just necessary to maintain a null along-channel gradient in net transport.

Further studies have shown that a power law also exists between channel cross-sectional area Ω and its drainage area A (e.g. Fagherazzi et al., 1999; Rinaldo et al., 1999a,b), yielding:

$$\Omega \propto A^{\alpha_a} \tag{2.2.3}$$

where $\alpha_a \sim 1$. The drainage area A is therefore a representative of the volume of water which flows through it, and is an extension of the "O'Brien-Jarrett-Marchi" law (D'Alpaos et al., 2005). Figure 2.9 illustrates this relationship although an apparent

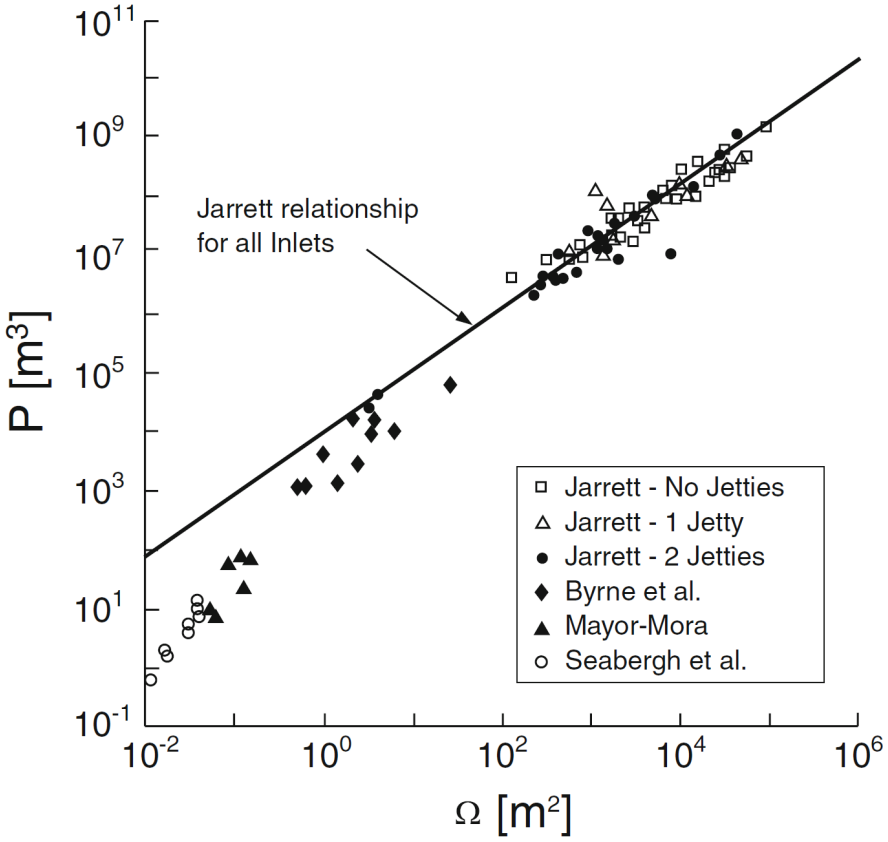

Figure 2.8: Equilibrium cross-sectional area Ω versus tidal prism P for field and laboratory data derived from various authors (from D'Alpaos et al., 2009 after Hughes, 2002).

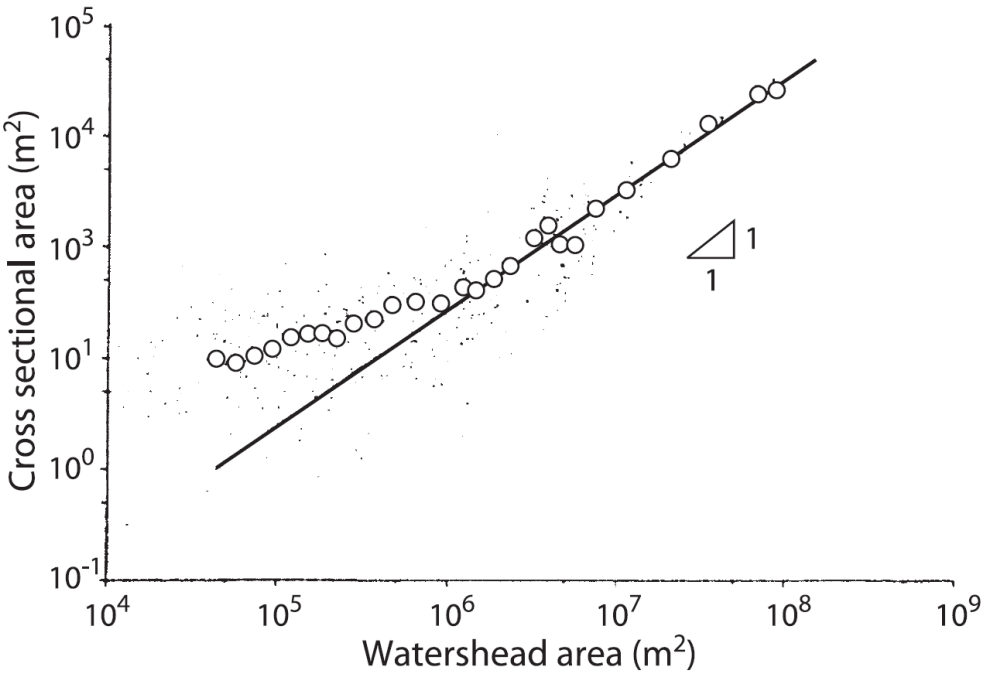

Figure 2.9: Cross-sectional area Ω versus drainage area A for individual cross-sections symbolised by the dots and ensemble mean of at least 50 cross-sections (from Marani et al., 2004, adapted from Rinaldo et al., 1999b).

break in the power law can be observed. Other power law relationships between channel hydraulic geometrical variables such as total network length l and drainage area A or flow properties, i.e., P and Q, were also documented (e.g. Fagherazzi et al., 1999; Marani et al., 2003; Rinaldo et al., 1999a,b; Steel and Pye, 1997).

2.3 Summary

Tidal courses and the networks they form constitute, through their functions, an essential element within the wetland landscape. The review presented in this chapter has outlined their main characteristics, providing a comprehensive basis for the subsequent research chapters. The numerous field and theoretical studies, some of which have been pointed out through this review, have led to great advances in the physical knowledge of these tidal landforms.

However, a balanced understanding of their geomorphology still calls for additional research. In truth, this lack of sufficient comprehension is related to the complexity and variability so much characterising tidal courses, which stem from the many conflicting

dynamic processes acting at overlapping spatial scales. For instance, spatial variations in flow magnitude as well as tidal asymmetry and their interplays with sediment heterogeneity and marsh vegetation have shown to affect the relevant morphodynamics, resulting eventually in different course and network morphologies. Moreover, the intricacy of these dynamic landscape-forming processes complicates the understanding of tidal course ontogeny. The present research intends to bring further insights into these issues.

Chapter 3

Assessing the bio-physical controls on tidal network patterns

The focus of this chapter is the variability of tidal network morphology. At first, a brief review on the different network patterns and drainage characteristics is addressed, providing grounds for the motivation for this research element. Then, the methodology of the proposed work will be described prior to detailing the results.

3.1 Network patterns and drainage characteristics

Tidal networks bear apparent similarities in form to fluvial networks (Steel and Pye, 1997), such that they have been primarily granted as drainage systems serving a distinct area on the tidal basin (Ragotzkie, 1959; French and Stoddart, 1992). This has lead a number of authors to explore the properties of tidal networks to see how they are similar to, and how they differ, from fluvial networks.

Based upon examinations of a series of large scale estuarine channels, Hibma et al. (2004) distinguished two tidal channel patterns namely fractal and braided. The fractal pattern refers to dendritic networks whereas the braided pattern describes multi-thread tidal channels intersected by shoals. Eisma (1998) proposed a more detailed classification built upon investigations of salt marsh creeks and tidal flat channels within different physiographic settings, which recognises 10 network patterns grouped into three categories: single channels, channel systems and few or no channels. Moreover, following investigations of British salt marshes, Pye and French (1993) classified seven network types, which complement those of Eisma (1998), and being illustrated in

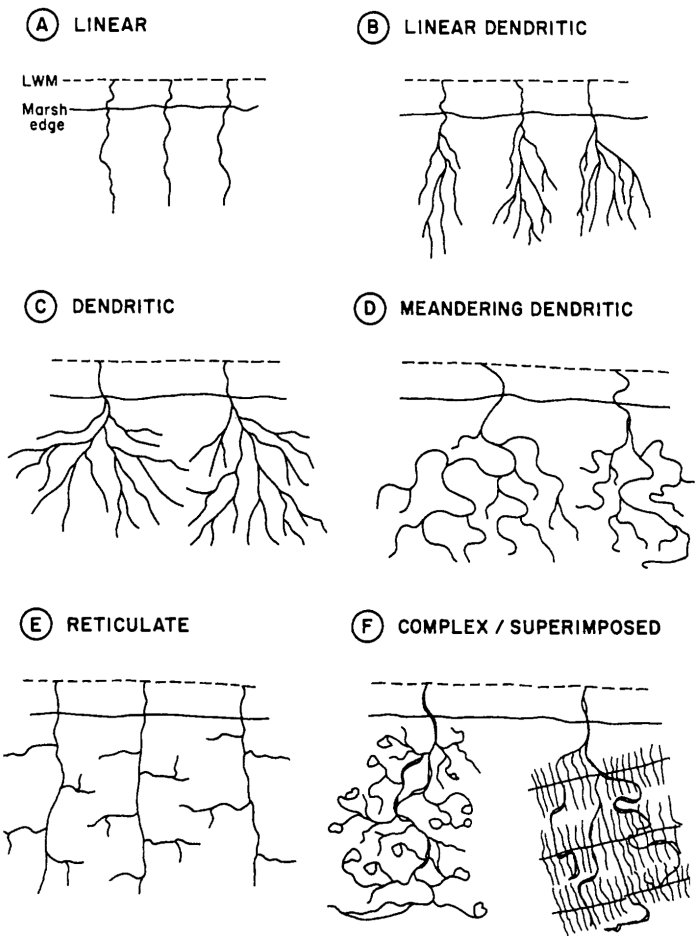

Figure 3.1: Network type classification in British saltmarshes (from Pye, 2000, adapted from Pye and French, 1993).

Figure 3.1. As the aforementioned network style classifications cover different spatial scales, overlaps and distinctions exist between the different categories. However, unlike Hibma et al. (2004), the classifications of Eisma (1998) and Pye and French (1993) discern network patterns based on the degree of channel complexity as well as on the presence of either single channel or developed networks.

First morphometric analyses of tidal channels were conducted using hydraulic geometry concepts developed in river channels (e.g. Myrick and Leopold, 1963), whilst other studies focused on the drainage properties of tidal networks employing the classical Hortonian topological measures typically applied to fluvial networks (e.g. Knighton et al., 1992; Pestrong, 1965; Pethick, 1980; Ragotzkie, 1959). Kirchner (1993) and Rodríguez-Iturbe and Rinaldo (1997) have pointed out that these fluvial-based metrics

(including Horton's branching and length ratios, and Tokunaga's cyclicity) are only applicable for tidal networks composed of blind-ended tidal courses. Therefore, other quantitative measures presenting higher flexibility in their range of application in relation to different network structures are needed. Moreover, the drainage density defined by Horton (1945) as being the inverse of the ratio of the total network length over its watershed area is generally unable to distinguish network structures when applied to tidal basins. Indeed, in spite of apparent site-specific features and morphological variability in tidal networks, Hortonian drainage density depicts some degrees of constancy in time and space, indicative of a similarity of form and a lack of distinctiveness. Marani et al. (2003) have shown this similarity of form to be an artefact of the Hortonian measure which does not capture relevant geomorphic controls such as marsh elevation and vegetation type. In reality, site specific features and differences in tidal network morphologies may only be captured by determining the unchanneled flow lengths on the marsh platform, which statistical properties constitute physical indices of the tidal network capability to drain its basin, and therefore provide an alternative definition of the drainage density (Marani et al., 2003).

In fact, differences related to hydraulic and ecogeomorphic considerations clearly separate tidal from fluvial networks. One of the most noticeable distinctions lies in the large size of the tidal channels with respect to the size of the system, with channelised areas constituting a substantial part of the total area of the tidal wetland (D'Alpaos et al., 2005). Also, although its importance in river morphology has been also demonstrated, the role of the vegetation should be particularly considered in tidal networks because vegetation has a great control on creek shape and lateral migration (Garofalo, 1980; Pestrong, 1965) and, in tidal flats where halophytes are typically absent, channel meanders and loops are rare and the drainage density appears to be smaller (Fagherazzi et al., 1999).

Fluvial catchment are defined topographically, whilst tidal basins, except when the basin extent meets the inland side of the marsh or the rear of any natural or artificial barriers are divided hydraulically (Allen, 2000; Perillo, 2009), hence the relevance of determining flow directions and associated gradients as a measure of drainage density. The probability density function of the unchanneled flow lengths generally depicts an exponential decay, and therefore a pointed absence of scale-free distributions. Other scaling relationships typically observed in fluvial networks do not yield any scaling property when applied to tidal networks (Marani et al., 2003). For instance, Hack's law, (Hack, 1973), which relates the total contributing basin area to the mainstream

length portrays a well-defined power law relationship in fluvial systems whose scaling parameters show a certain degree of consistency through many scales. However, testing such a relationship in tidal networks bears not any single power law, which tends to reveal that Hack's law does not seem to apply to tidal basins (Rinaldo et al., 1999b). Other power law relationships notably linking watershed area with drainage density or channel width prevailing in fluvial catchments do not seem to hold through various investigated spatial scales in tidal networks or differ significantly from site to site. These different results prove that tidal networks do not depict scale invariant features, a characteristic of fractals yet so prevalent in fluvial networks. This scale dependent character transcribes the spatial variability of the landscape-forming flow rates in tidal systems and the competing dynamic processes acting at overlapping spatial scales (D'Alpaos et al., 2005). Flow bi-directionality and tidal asymmetry highlights the dependence of geomorphic processes on local conditions as pointed out in Chapter 2, triggering variations in channel morphometric features such as channel widths and curvature which is unusual in fluvial morphology (Marani et al., 2002), thence the lack of scaling features accordingly.

Other fundamental differences in flow regime with fluvial networks such as the manifestation of null discharge near the highest water level or the occurrence of maximum flood velocities generally when the water overtops the channel flanks have suggested that the primary function of tidal networks may not be to feed and drain the marsh during the respective flood and ebb tides, but instead to dissipate the tidal and wave energy entering into the system (Pethick, 1992).

3.2 Objectives

Although a notable amount of work on the morphometric properties of tidal networks and their intrinsic channels has been documented in the literature, a number of issues still remain, including controls on the variability of tidal network patterns. Different network patterns exist in nature and have been classified accordingly (e.g. Eisma, 1998; Pye and French, 1993). However, there is little understanding of why a specific network pattern develops at a particular location (Perillo, 2009). The slope of the associated wetland, its sediment characteristics and age of the system may all be controlling factors (Pethick, 1969; Steel and Pye, 1997), and variability, unless artificially impacted, reflects the combined influence of several natural controls whose full identity is not known. Moreover, to what extent each of them is responsible for the occurrence of a

distinct network pattern also remains unknown.

Accordingly, in this study a geospatial analysis was performed on a number of salt marshes across the UK aiming to i) characterise the variability in salt marsh network patterns and ii) identify the related environmental controls. This study makes use of the growing development of remote-sensed technologies, offering the possibility to access to large data sets for a low research cost.

3.3 Methods

3.3.1 Data sources

Two types of remote-sensed data were used to perform the geospatial analysis: airborne LiDAR data and sequential aerial images. Recent individual date and time stamped LiDAR data already processed as Raster bare-earth DTMs (Digital Terrain Models) were obtained from Environment Agency (2014b). LiDAR data were measured using an Optech Gemini LiDAR sensor mounted on an aircraft. Resulting elevation data meet high accurate standards with a RMSE close to $\pm$5cm for the late surveys and with spatial resolutions of 25cm, 50cm and locally 1m for a few sites. Elevations units are in meters AODN (Above Ordnance Datum Newlyn).

Google Earth imagery, which has been used successfully to obtain morphological information in previous contributions (e.g. Goudie, 2013), was also used in this study. Google Earth offers the advantage of providing a vast quantity of freely available images often at high resolutions and spanning several years, which therefore allow for extracting accurate information about the morphology of a broad range of geomorphic settings. Other data were obtained from published sources.

3.3.2 Site selection

Salt marsh systems are widely distributed along the UK coastline (Allen, 2000), and the study site selection has attempted to transcribe this geographical variability (Figure 3.2).

Site selection was based on the following criteria. Firstly, based on the Pye and French (1993) classification of network patterns, only the first 4 network types consisting of linear, linear-dendritic, dendritic and meandering were investigated in this analysis (see Figure 3.1). Complex network types, (e.g., Tollesbury marshes, Essex) are rarely encountered across the British coast, whilst reticulate and superimposed network

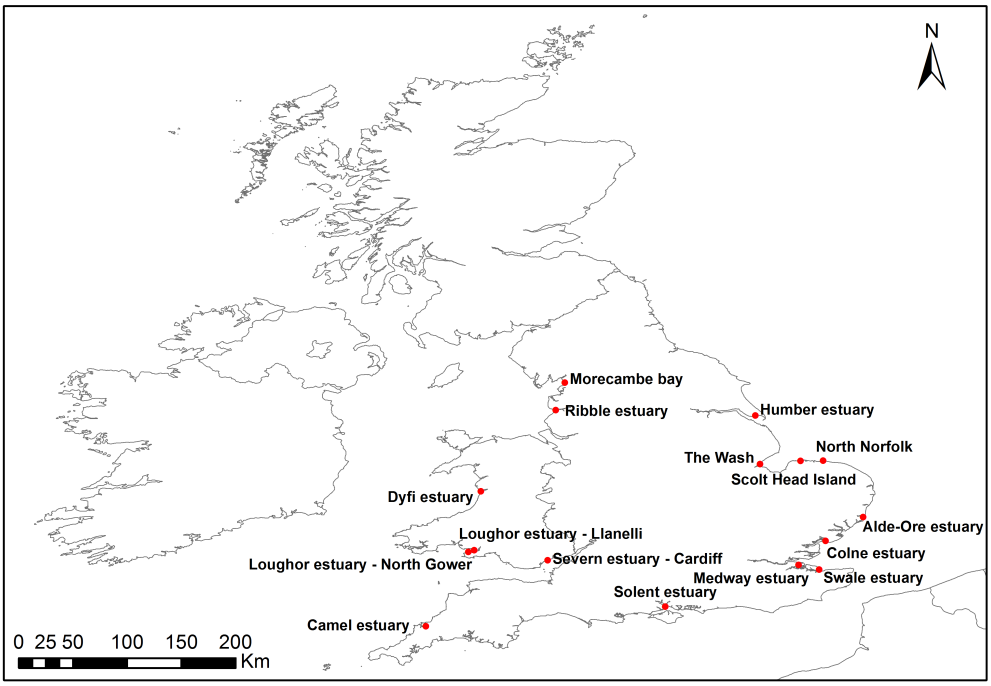

Figure 3.2: Location of the study sites

types are influenced by human interference, and are not strictly natural systems. They were thus excluded from the present analysis. 4 marsh systems per network type were selected, with a total of 16 sites. At each site, 3 tidal network replicates were extracted to account for the possible within-site variability in tidal channel morphometric aspects. As this randomly stratified selection of the salt marshes and their embedded tidal networks were based on the qualitative classification of Pye and French (1993), in practice distinguishing the different tidal network types may not be straightforward, therefore special care was brought on this issue. Figure 3.3 displays an example of selected tidal networks being representative of a particular network type from 4 different salt marsh systems. This above consideration combined with the necessity that, for a given site, both a high LiDAR spatial resolution and a relevant amount of information should be available from the literature eventually reduces the number of possibilities.

3.3.3 Variable definition and data extraction

To characterise the variability in network pattern and identify the related environmental controls, a series of variables extending over different spatial scales and covering various features proper to the tidal wetland have been extracted accordingly.

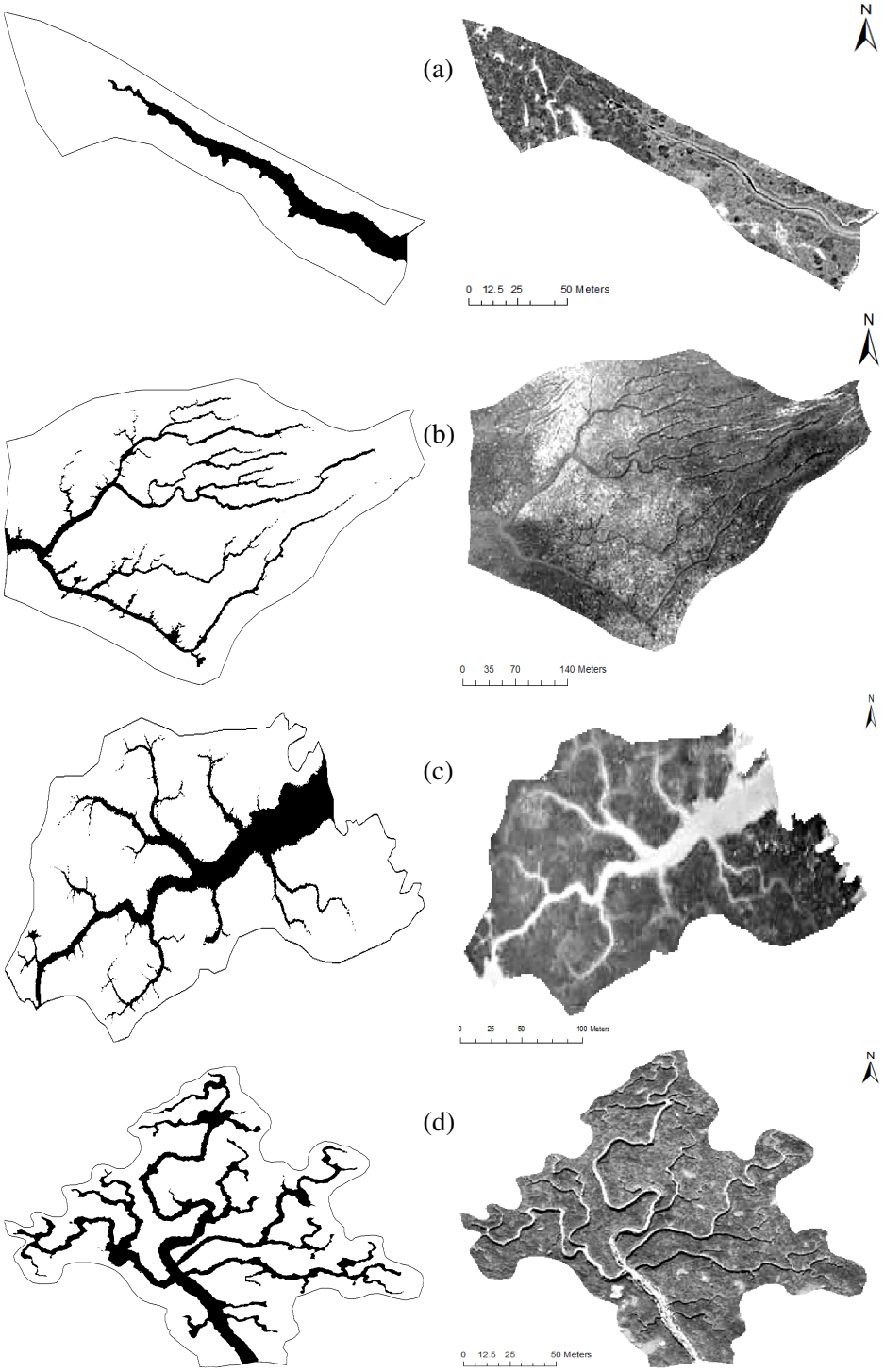

Figure 3.3: Replicate network skeletons per network type and corresponding aerial photos from 4 study sites. (a): linear type, Morecambe bay, Lancashire; (b): linear-dendritic type, Ribble estuary, Lancashire; (c): dendritic type, Solent estuary, Hampshire; (d): meandering type, Scolt Head Island, North Norfolk.

Marsh environmental characteristics

Marsh scale data on hydrodynamics, sedimentology and eco-geomorphology were collected from secondary sources. These data comprise tidal range at spring tides, relative sea level rise (RSLR), marsh sediment composition based on Shepard (1954) classification and marsh physiographic settings following the types defined by Pye and French (1993). Comprehensive studies were reviewed to compile the desired data. Table 3.1 presents these marsh characteristics for every site investigated.

Further data on marsh eco-geomorphology were gathered at the sub-basin scale (i.e., network basin) and processed in ArcGIS v10.2. Google Earth images were used to estimate the vegetation area proportion, defined as the proportion of the network basin that is vegetated.

Concretely, for each study site, an aerial image was saved in Google Earth which was dated as close as possible to the date of the corresponding LiDAR data (i.e., the date of the respective survey flight). This aerial image was then loaded as a multi-band raster in ArcGIS and geo-referenced against the respective projected DTM using control points. Then, a contrast stretch was applied on the raster display to increase the visual contrast of the vegetated features of interest. In this respect, image pixel DN (Digital Number) values were stretched on the basis of the corresponding band histogram in such a way that the bulk of the frequency distribution was expanded over a wider range of display (grey) levels, and leaving a shorter range for the less frequently occurring DN values. This contrast manipulation was performed both on the red and green bands, to accentuate the respective spectral reflectances and thus capture the spectral signature of the vegetation.

The resulting RGB true colour composite served as a support to perform a classification of land cover types subsequently. Training samples were first outlined to define "signature classes" representative of the features of interest. Then, by means of a maximum likelihood numerical classifier, every pixel was compared to the "key" pixels composing the training samples and assigns it to the most similar signature class. Figure 3.4 provides an example of a colour composite and associated land cover classification for one of the sub-basin investigated. In Figure 3.4a, the application of the manual contrast stretch highlighted two distinct vegetated features, which might indicate either a difference in biomass density or simply the presence of two vegetation species. Yet, these features are grouped into a single vegetation class and knowing *a priori* the pixel resolution and now the number of pixels belonging to the vegetation class, the total vegetation area can be computed and be then divided by the total sub-basin area to

Table 3.1: Whole marsh scale characteristics.

Site location	Network pattern	Spring tidal range (cm)	RSLR (mm/yr)	Sediment composition	Marsh physiographic setting	References
Morecambe Bay	Linear	8.3	0.69	Sand	Restricted-entrance embayment	Gray (1972); Allen (2000); Gehrels (2010)
Ribble estuary	Linear-dendritic	8	1.7	Sandy silt	Estuarine fringing	Steel and Pye (1997); Gehrels (2010)
Dyfi estuary	Dendritic	4.5	-4.65	Sandy silt	Estuarine back-barrier	Steel and Pye (1997); Allen (2000)
Loughor estuary (Ti Morfar)	Dendritic	6.6	-0.76	Sandy silt	Estuarine back-barrier	Steel and Pye (1997); Gehrels (2010)
Loughor estuary (North Gower)	Meandering	6.6	1.5	Sandy silt	Estuarine back-barrier	Allen (2000); Goudie (2013)
Severn estuary (Cardiff Bay)	Linear	12.3	3.3	Clayey silt	Estuarine fringing	Allen (1989); Allen and Duffy (1998); Allen (2000)
Camel estuary	Dendritic	6.3	1.19	Silt	Ria	Gehrels (2010); Goudie (2013)
Solent estuary	Dendritic	3.2	-0.49	Clayey silt	Estuarine back-barrier	Goudie (2013)
Medway estuary	Linear	5.6	-0.8	Silty clay	Estuarine back-barrier	van der Wal and Pye (2004); Spencer et al. (2003); Kirby (2013)
Swale estuary	Linear-dendritic	5.2	-0.67	Clayey silt	Estuarine back-barrier	Steel and Pye (1997); van der Wal and Pye (2004)
Colne estuary	Meandering	4.6	-0.85	Silty clay	Estuarine back-barrier	van der Wal and Pye (2004); Gehrels (2010); Goudie (2013)
Alde-Ore estuary	Linear	3.2	2.4	Silty clay	Estuarine back-barrier	Allen (2000); Pye (2005)
North Norfolk (Blakeney point)	Meandering	6.4	2	Silty clay	Open coast back-barrier	French and Stoddart (1992); French (1993); Allen (2000); Goudie (2013)
North Norfolk (Scolt Head Island)	Meandering	6.4	2	Silty clay	Open coast back-barrier	Stoddart et al. (1989); Allen (2000)
The Wash	Linear-dendritic	6	1.5	Silty clay	Open embayment	Pye (1995); Steel and Pye (1997); Allen (2000)
Humber estuary	Linear-dendritic	6	1.04	Silty clay	Estuarine back-barrier	Allen (2000); Lee and Cundy (2001)

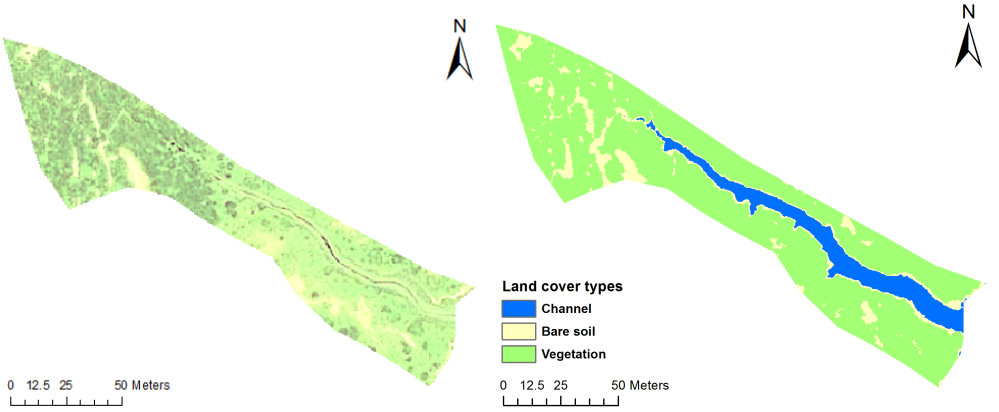

(a) **(b)**

Figure 3.4: **(a)**: RGB true colour composite; **(b)**: derived land cover classification of a network basin located at the Morecambe Bay.

eventually determine the vegetation area proportion.

Median marsh platform elevation was determined upon the extraction of the tidal network skeleton and its corresponding channelized area (see Section 3.3.3 for detail). Moreover, the median marsh elevation of the delineated network basin was used to compute the marsh relative height, defined as the elevation of the marsh platform relative to the local Highest Astronomical Tide (HAT). HAT levels were first collected at primary or secondary ports near the location of the study site using online databases including National Oceanographic Centre (2014) and Environment Agency (2014a). Then, Admiralty Tide Tables were used to convert HAT expressed in local Chart Datum (C.D.) to O.D.

The marsh relative height strictly represents the depth between HAT level and the median marsh platform elevation (i.e., marsh depth below HAT). It is an important measure as it implicitly refers to the age of the tidal basin considered (i.e., marsh relative age). Indeed, the age of a marsh is typically defined as the time elapsed since its initial colonisation by halophytes (Pethick, 1981). Following vegetation colonisation, the marsh accretes and gains elevation until it reaches a constant position relative to the tidal frame, while there is a concurrent asymptotic decrease in the surface deposition rate as a result of the reduced inundation frequency. The marsh has therefore attained dynamic equilibrium at a level below HAT and only receives enough sediment to counteract the combined effect of sea level rise and autocompaction (Allen, 2000). This local sedimentary surface adjustment is indicative of a mature or established marsh. Pethick

(1981) was the first to derive this asymptotic elevation-age relationship based on field data collected at North Norfolk which was later supported by several authors either empirically (Dijkema et al., 1990; Pye, 1995) or numerically (Allen, 1990; French, 1993).

Lastly, the slope of the marsh platform was also estimated based upon the transect materialising the distance from the furthest landward to the furthest seaward point within the corresponding network basin.

Channel/network hydraulic geometry

LiDAR data in tidal channels were analysed to assess their reliability as ground elevation data. To this purpose, 3D scenes, hillshade DEMs and creek cross-sections were successively generated and analysed for every network replicate in ArcGIS, which bear clear visualisation of the creek morphology and its thalweg. This distinct observation has to be put in line with the fact that the majority of the investigated tidal networks are composed of tidal creeks located relatively high in the intertidal zone, whose highest order creek further divides downstream as being usually of secondary level with respect to the large scale estuarine channels. This means that the salt marsh creeks were either dry or superficially inundated along their course during the corresponding LiDAR survey.

Geometrical measures of the tidal network mouth extracted in ArcGIS included mouth width w and mouth depth d while the associated aspect ratio β (i.e., width-to-depth ratio) and cross-sectional area Ω were computed subsequently. These measurements describe the size of the network and provide information on the magnitude of the landscape forming flow rates, and network hydrology (Jarrett, 1976; O'Brien, 1969; Rinaldo et al., 1999a,b).

Cross-sectional morphology was classified according to the mouth cross-sectional shape whose main types were defined in chapter 2: V-shape, U-shape, asymmetric, compound, complex, overhanging simple and complex (Figure 3.5). Cross-sections were examined using the profile graph tool included in the 3D analyst toolbox provided by ArcGIS.

All width and depth data were determined at bankfull stage. To do that, a width measurement was first carried out in Google Earth to make use of the vegetation line as an indicator of bankfull level, and was then adjusted in ArcGIS using the high resolution of the LiDAR data and the corresponding cross-sectional profile to better identify the overmarsh point (i.e., lateral knickpoint). Depth below the derived bankfull level were

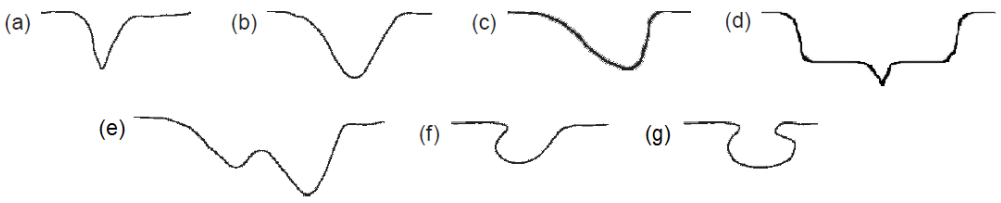

Figure 3.5: Cross-sectional shapes surveyed. (a) V-shape; (b) U-shape; (c) asymmetric; (d) compound; (e) complex; (f) overhanging simple; (g) overhanging complex (Adapted from Perillo, 2009).

measured consequently. Moreover, channel median width and depth were defined as the average between the minimum and the maximum width and depth measured in the main channel (i.e., channel with the highest Strahler stream order).

Several morphometric measurements of the network longitudinal profile, including channel and total network lengths were estimated in ArcGIS. For network length, a threshold was imposed on the extent over which the measurement was performed due to the fact that the LiDAR spatial resolution varies across the study sites. Here, measurements were conducted up to three Strahler orders with the main channel being the highest order (order 3), followed by its direct creek tributaries (order 2) and the successive ones (order 1). In fact, if considering more than three Strahler orders, the creek thalweg cannot be accurately identified for the lowest order creeks.

The main channel slope was calculated over the corresponding channel length, and the network slope was based on the course length between the furthest landward point of lowest order digitized creeks and the network mouth. Lastly, the bed longitudinal profile was characterised as being either convex-up, planar or concave-up, which may bring insights into the morphodynamic equilibrium of the tidal network.

Main channel sinuosity was calculated as the ratio of the channel length over the length of null-curvature. The latter measurement represents the line connecting the section of every meander bends having zero curvature, being also called the inflexion point (Marani et al., 2002). Measuring the sinuosity against a straight line would lead indeed to an overestimation of its value in the case of a curvilinear channel course.

Network topology

As mentioned earlier, the traditional Hortonian measure of drainage density does not provide a distinctive picture of tidal network geometry and its relationship with the salt marsh it dissects (Marani et al., 2003). Such a peculiarity combined with the usual

non-negligible size of the tidal network with respect to its catchment area suggests the introduction of alternative measures of drainage density. In the present study, the channel area proportion, a measure defined by Rinaldo et al. (1999a) as the ratio of channelised area A_{ch} to the total sub-basin area A_{tot} is used. However, applying this measure requires the prior identification of the basin boundaries as well as tidal network skeleton for every tidal sub-basin considered as in Figure 3.3.

To delineate the tidal sub-basin, divides were manually traced midway between adjacent channel borders (cf. Steel and Pye, 1997). The assumption of equidistant divides from the neighbouring channels also forms the basis of the hydrodynamic model of Rinaldo et al. (1999a). In fact, only when the catchment reaches artificial structures such as embankments or any other rising topographic features that the divides follows them.

The extraction of the skeleton of the tidal network was conducted following the automatic procedure developed by Fagherazzi et al. (1999). This technique consists of applying to the original digital terrain maps an elevation and surface curvature criteria to partition the planar domain containing the topographic data into two subsets: one including the pixels belonging to the tidal network and the other including the pixels belonging to the marsh platform. This method relies on the assumption that low elevation points should represent channels, and so applying an elevation threshold below which all points are assigned to the channel subset can allow delineating these low grid points and thus detect the location of the network course. This elevation threshold is then combined with a surface curvature threshold to better capture all connectivity elements of the network (i.e., bifurcations) especially at the finer scales. The identification of the values of these geomorphic thresholds is based upon the reading of the respective hypsometric curve and cumulative distribution function of surface curvatures in the catchment.

Finally, upon the delineation of the network basin and the extraction of the tidal network skeleton, the channel area proportion can be derived and the conventional drainage area can be computed by subtracting the channelized area from the total sub-basin area. Moreover, except for the stream Strahler order, the present study abstains from applying the traditional Hortonian topological metrics such as Horton's bifurcation and length ratios or Tokunaga's cyclicity due to their inability to distinguish differences between network structures (Kirchner, 1993; Rinaldo et al., 1998).

3.3.4 Statistical analysis

In total, 26 explanatory variables were considered in this study. Following the data acquisition, a statistical analysis was performed to explore first the overall variability of the data set and to progressively assess the factor(s) being able to characterise and discriminate the network patterns investigated.

Principal Component Analysis

Principal Component Analysis (PCA) was performed using XLSTAT v4.01 to explore the global variability of the data set, and to understand its underlying structure in relation to the embedded data classes (i.e., network types). 2 PCAs were conducted to account for the 26 explanatory variables (Table 3.2). As PCA works on ratio and ordinal measurement scales, corresponding categorical variables were first ranked according to their underlying gradient. For instance, marsh physiographic settings were ranked based on the increasing level of shelter / reduction of marine energy (i.e., tidal and wave energy). Similarly, sediment characteristics were classified from coarsest to finest-grained materials, etc. Normalized PCA based on Spearman's rank correlation matrix was applied to cancel out non-normality and differences in data units and measurement scales specific to the data set (Lehmann, 1975). The generated correlation matrix was also used as a support to study relationships between the explanatory variables.

Eigenvectors having high eigenvalues ($\lambda > 1$) and accounting altogether for at least 50% of the total cumulative variance in the data set were retained as Principal Components (PCs). Further reading of the break-in-slope in the corresponding scree plot introduced by Cattell (1966) helped to determine the number of relevant PCs. The interpretation of the PCs was based on the identification of the explanatory variables with factor loadings > 0.7 or < -0.7, indicative of a strongly positive or negative relationship respectively, and supported secondly by the variables with factor loadings comprised between 0.6 and 0.7 or -0.6 and -0.7. Eventually, a two dimensional scatterplot with the two axes representing the two PCs was generated to better visualise the position of the observation points and their possible aggregation into groups based on the respective classes.

ANOVA and Kruskal Wallis

Following the exploration of data variability of the data set, ANOVA and the equivalent non-parametric Kruskal Wallis statistical tests were conducted in XLSTAT to assess

Table 3.2: Feature themes and corresponding explanatory variables as inputs to Principal Component Analysis.

Feature themes		**Explanatory variables**
Marsh environmental characteristics	Hydrodynamics	Spring tidal range (m)
		Relative sea-level rise (mm/year)
	Sedimentology	Sediment composition
	Marsh eco-geomorphology	Marsh physiographic setting
		Median marsh elevation (m O.D.)
		Marsh depth below HAT (m O.D.)
		Marsh slope
		Vegetation area proportion
Network morphometric characteristics	Channel/network hydraulic geometry	Mouth cross-sectional shape
		Mouth cross-sectional area (m^2)
		Mouth aspect ratio
		Mouth width (m)
		Mouth depth (m)
		Max depth (m)
		Median width (m)
		Median depth (m)
		Network length (m)
		Network slope
		Network bed profile
		Main channel length (m)
		Main channel slope
		Main channel sinuosity
	Network topology	Channel area proportion
		Drainage area (ha)
		Total network basin area (ha)
		Strahler stream order

whether significant differences arose among the classes according to the factor variable considered (i.e., explanatory variable).

Therefore, ANOVA test, and when necessary Kruskal Wallis test, were successively applied to every of the 26 factor variables, with a significance level $\alpha = 0.05$. Whether the tests would point to a statistically significant result, that is $p < 0.05$, this would mean that at least one class would be different from the others. To identify this particular class, *post hoc* analyses consisting of multiple comparison tests were conducted subsequently. Thus, one-way ANOVA tests were followed by a Tukey's test while Kruskal Wallis tests were followed by a Dunn's procedure with Bonferroni correction correspondingly, if the tested factor variable showed statistical significance.

In this way, it was possible to detect which factor variables separate each class, and therefore use them to describe the properties of the classes. However, distinguishing which of these environmental and/or morphological characteristics has the highest discriminating power on the network types may not be easily readable at first glance since the inter comparison of ANOVA F-scores and Kruskal Wallis K-scores is not possible, both statistical scores being based on different computations. A Discriminant Analysis (DA) was conducted to this end.

Discriminant Analysis

DA has similarities with multiple linear regression which is limited to cases where the dependent variable is of interval scale. However, DA can predict a dependent variable of categorical scale based on a combination of interval and nominal scale predictor variables (Burns and Burns, 2008). DA classifies samples into groups which are a priori known, but is also used to investigate differences into classes on the basis of the combination of these predictor variables, and indicate which predictor(s) clearly discriminate between groups. Thus, DA is both a predictive and descriptive method. The descriptive DA is closely related to PCA as it identifies linear combination of factor variables, yet these so-called canonical Discriminant Functions (DFs) contribute maximally to group separation whereas PCs in PCA seek to maximise the variance in the entire data set (Martínez and Kak, 2001).

This study makes use of these two aspects of DA. Firstly, a DA was performed using XLSTAT on the combination of the factor variables showing individually statistical significance upon the results of the ANOVA and Kruskal Wallis tests to determine which factor variable contributed the most to group separation. Strictly speaking, the DA was built on a linear model due to the equality of the covariance matrices. Selection

and interpretation of the resulting DFs followed the same procedure as for the PCs in the PCA. Eventually, the predictor with the highest correlation (i.e., factor loading) on every DF constitutes the highest discriminant factor. In parallel, a two dimensional scatterplot with the two axes representing the 2 DFs was generated to see if the classes to which the observations belong were distinct. This DA was also carried out secondly to test whether observations were classified as predicted, in a way to validate the network pattern driven site selection and classification. To this end, cross-validated classification was applied to determine the probability that an observation belongs to a certain class.

3.4 Results

The results are presented in two sections: the first one explores the overall variability in the environmental and morphological properties of the observations making up the data set, the second one centres on the investigation of the factor variables contributing to network characterisation and differentiation.

3.4.1 Variability in network environmental and morphological characteristics

PCA was applied first to look at the marsh environmental characteristics embodying hydrodynamic, sedimentological and eco-geomorphological features, and secondly, to explore the variability in network morphometric characteristics by combining channel/network hydraulic geometrical and topological aspects (see Table 3.2).

Variability of marsh environmental characteristics

The normalised PCA on marsh environmental characteristics produced 3 PCs with eigenvalues greater than 1, explaining 70.09% of the total variance. The first 2 PCs account for 55.39% of cumulative total variance and the corresponding scree plot suggests that PC1 and PC2 explain the majority of data variability. PC1 describes a gradient of increasing tidal range and median marsh elevation of the corresponding network basin whereas PC2 expresses a gradient of increasing marsh depth below HAT (hence a decrease in marsh relative age) and, to a lesser extent, an increasing degree of shelter provided by the marsh physiographic setting and vegetation cover (see Table 3.3).

The two dimensional scatter plot made up of PC1 and PC2 and the corresponding factor scores of every observation is displayed in Figure 3.6. Along the axis of PC2, one

Table 3.3: Marsh environmental characteristics PCA: Eigenvalues, PCs and Factor loadings on the main PCs (factor loadings > 0.7 or < -0.7 are emboldened; factor loadings between 0.6 and 0.7 or -0.6 and 0.7 are underlined).

	PC1	PC2	PC3
Eigenvalue	2.69	1.75	1.18
Variability (%)	33.53	21.86	14.70
Cumulative %	33.53	55.39	70.09
Factor loadings	PC1	PC2	PC3
Spring tidal range (m)	**0.93**	0.00	0.11
RSLR (mm/yr)	0.40	0.28	0.8
Soil sediment composition	0.56	-0.37	-0.57
Marsh physiographic setting	-0.41	0.65	0.02
Marsh depth below HAT (m O.D.)	0.18	**0.70**	-0.34
Median marsh elevation (m O.D.)	**0.93**	-0.17	0.11
Marsh slope	0.31	0.47	-0.26
Vegetation area proportion	0.40	0.60	-0.11

might discern a slight gradient from linear / linear-dendritic to meandering networks transcribing a progressive deepening of the marsh platform below HAT associated with an increasing degree of shelter given by the marsh physiographic setting and an increase in vegetation cover. Nevertheless, Figure 3.6 primarily shows a relatively broad scatter, even for observations depicting similar network types and particularly for those located in the west coast of the UK. On overall, the variability in marsh environmental features captured by the PCA does not coincide with the variability in network patterns.

Variability of network morphometric characteristics

Multicolinearity between the morphometric variables was disregarded as one of the primary functions of PCA is to reduce the dimensionality of a data set by transforming a set of correlated variables into a new set of uncorrelated (orthogonal) variables, namely the PCs. The normalised PCA on network morphometric characteristics generated 5 PCs with eigenvalues greater than 1 and which amount to 85.71% of the total cumulative variance. However, the reading of the scree plot indicates that the first 2 PCs encompass the majority of the variability in the input data, both accounting for 58.73% of total variance, of which 44.82% is explained by PC1 itself. PC1 transcribes an increase in network size and complexity as well as in sub-basin size which is materialised by the high positive factor loadings for the majority of the channel/network hydraulic geometrical and topological variables. Moreover, PC2 sensibly describes an increase in network slope as seen in Table 3.4.

Table 3.4: Network morphometric characteristics PCA: Eigenvalues and Factor loadings on the main PCs (factor loadings > 0.7 or < -0.7 are emboldened; factor loadings between 0.6 and 0.7 or -0.6 and 0.7 are underlined).

	PC1	PC2	PC3	PC4	PC5
Eigenvalue	8.07	2.50	2.11	1.66	1.08
Variability (%)	44.82	13.90	11.72	9.25	6.02
Cumulative %	44.82	58.73	70.45	79.70	85.71
Factor loadings	PC1	PC2	PC3	PC4	PC5
Mouth cross-sectional shape	-0.63	-0.15	-0.44	0.12	0.12
Mouth cross-sectional area (m^2)	**0.81**	0.50	-0.04	-0.06	0.01
Max depth (m)	**0.82**	0.10	-0.41	0.17	-0.16
Mouth aspect ratio	0.53	0.12	0.73	-0.14	0.23
Mouth width (m)	**0.82**	0.47	0.21	-0.08	0.10
Mouth depth (m)	**0.73**	0.46	-0.38	-0.06	-0.10
Median width (m)	**0.88**	0.39	0.18	-0.06	0.00
Median depth (m)	**0.80**	0.17	-0.41	0.17	-0.22
Network length (m)	**0.85**	-0.40	-0.14	-0.02	-0.02
Network slope (m)	-0.50	0.67	0.14	-0.25	0.18
Network bed longitudinal profile	0.27	-0.072	0.76	0.34	-0.15
Main channel length (m)	0.64	-0.48	0.09	0.23	0.26
Main channel slope	-0.48	0.60	-0.24	-0.24	0.23
Main channel sinuosity	0.25	-0.06	-0.20	0.26	0.85
Channel area proportion	-0.03	0.25	-0.13	0.89	0.03
Drainage area (ha)	**0.76**	-0.38	-0.13	-0.40	0.07
Stream Strahler order	**0.74**	0.08	0.06	0.27	0.00
Total network basin area (ha)	**0.74**	-0.40	-0.18	-0.41	0.10

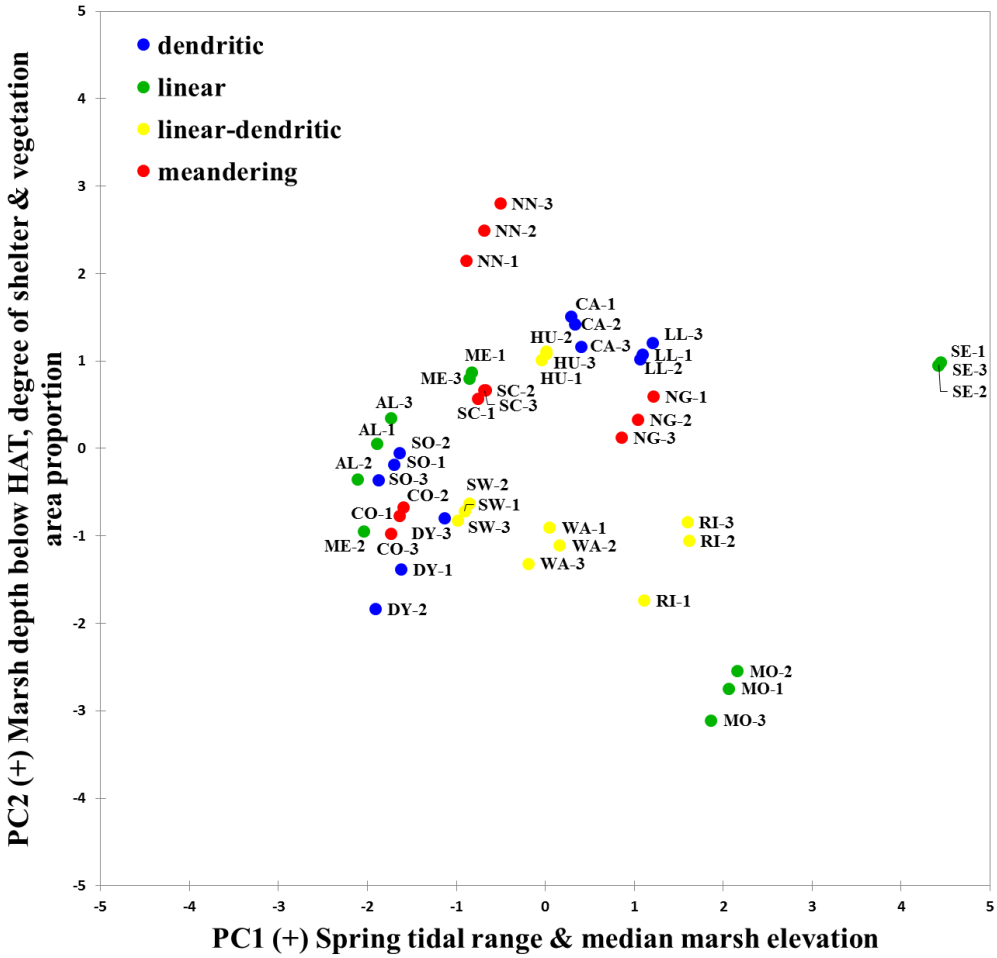

Figure 3.6: Scatter plot of PC1 vs PC2 derived from the marsh environmental characteristics PCA with network types and observation labels[1].

Factor scores of PC1 and PC2 are given in Figure 3.7, and despite a degree of scatter, gives rise to distinctions between network types. For instance, linear-type networks are clearly characterised by small network and sub-basin sizes as well as low level of network complexity (i.e., low stream Strahler order), whereas differentiation among the 3 other network types is less evident although linear-dendritic networks look smaller in network and sub-basin sizes with respect to their dendritic and meandering counterparts.

[1]MO: Morecambe bay; RI: Ribble estuary; DY: Dyfi estuary; LL: Loughor estuary- Llanelli; NG: Loughor estuary - North Gower; SE: Severn estuary - Cardiff; CA: Camel estuary; SO: Solent estuary; ME: Medway estuary; SW: Swale estuary; CO: Colne estuary; AL: Alde estuary; NN: North Norfolk - Blakeney point; SC: North Norfolk - Scolt Head island; WA: The Wash; HU: Humber estuary. The numbers identify the specific network replicate.

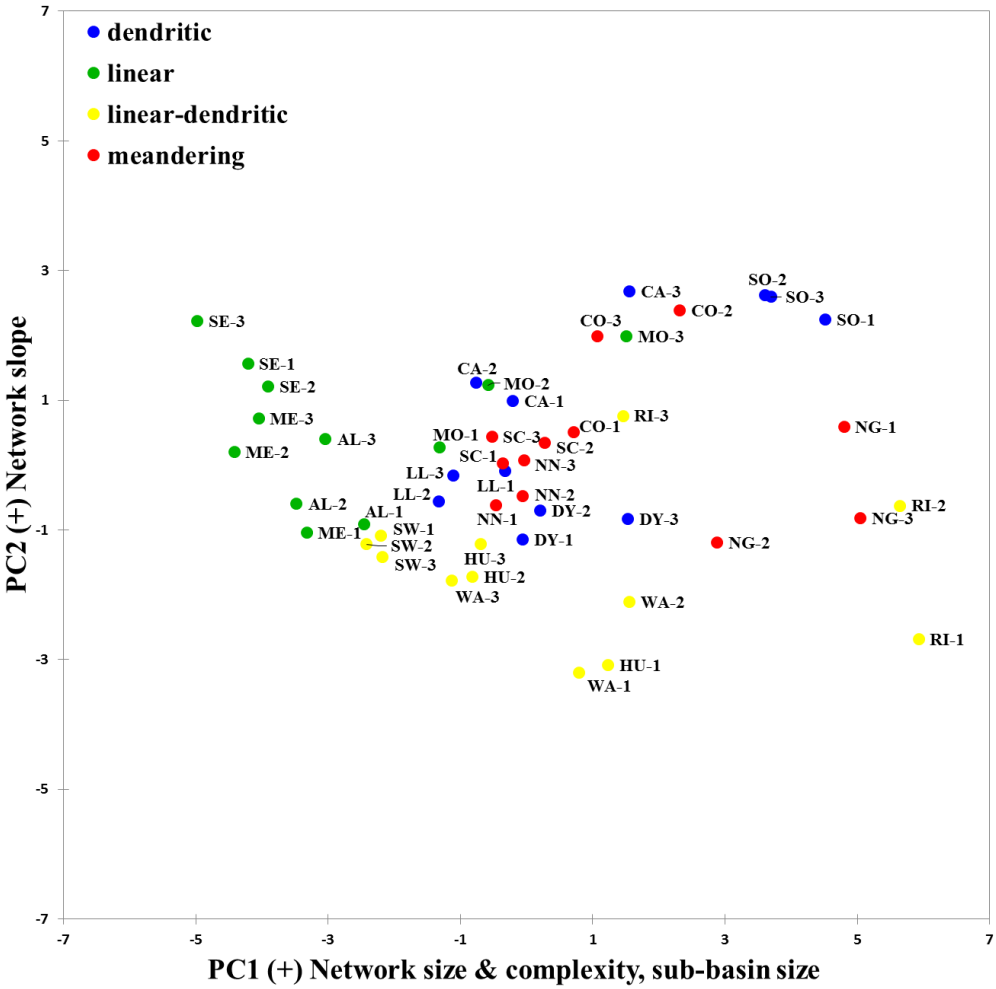

Figure 3.7: Scatter plot of PC1 vs PC2 derived from the network morphometric characteristics PCA with network type and observation labels[1].

Furthermore, along the axis of the second PC, linear-dendritic networks seem to depict gentle slopes in comparison with the other network types, particularly with the linear type which looks steeper. Therefore, in view of the previous observations, it appears that linear networks, and to a lesser extent linear-dendritic, portray distinct geometrical and topological properties whereas dendritic and meandering networks show a relative degree of similarity as regards their morphometric characteristics. As a note, intra-site variability materialises linear-dendritic, dendritic and meandering networks, particularly for the sites located in the west coast of the UK, similarly with Figure 3.7.

3.4.2 Identification of network type discriminant factors

One-way ANOVA and Kruskal Wallis statistical tests were performed on every explanatory variables to identify which ones were statistically significant. Then, a DA was applied on all significant variables to determine which was the most effective in discriminating network types.

ANOVA and Kruskal Wallis tests on explanatory variables

4 out of 26 explanatory variables depicted a Gaussian distribution. These 4 factor variables also satisfied the assumption of variance homogeneity. ANOVA test was therefore applied on each of these 4 factor variables while Kruskal Wallis test was individually performed on the remaining ones. 21 out of 26 factor variables were statistically significant ($p < 0.05$) and were followed by multiple comparison tests to identify which class(es) were significantly different from each other. Both statistical tests had 3 degrees of freedom. Results are listed in Table 3.5.

Results from Table 3.5 indicate that 6 factor variables are highly significant with $p < 0.0001$ (see emboldened variables), and of which the successive applied multiple pairwise comparison tests have identified 3 out of 4 network types being significantly different from one another, except for Stream Strahler order. Corresponding boxplots are displayed in Figure 2.8. Therefore, despite the relatively high number of resulting significant factor variables, no one itself is able to statistically discriminate between the 4 network types investigated. Except for the marsh physiographic setting, all these highly significant factor variables relate to network size or complexity.

On the whole, the reading of the results shows that linear networks are the steepest while meandering and above all linear-dendritic networks are the gentlest which is illustrated in Figure 3.8d. Although the distinction with meandering and dendritic networks is not statistically significant, linear-dendritic networks appear to be the longest, especially compared to the linear ones (which can be seen in Figure 3.8e). A similar trend is depicted for the drainage and total sub-basin areas. Dendritic and meandering networks are respectively the widest and deepest tidal networks as opposed to linear networks and to a lesser extent linear-dendritic networks. The boxplots of mouth and median depth in Figure 3.8a and b and median width in Figure 3.8c illustrate this. Consequently, the mouth cross-sectional area of meandering and dendritic networks is the largest whereas it is the smallest for their linear counterparts. Similarly, the highest aspect ratio occurs for dendritic networks and the lowest for meandering networks. Moreover, meandering networks exhibit the highest degree of complexity as

Table 3.5: Detailed statistical results of the 21 factor variables showing significant differences. (A) ANOVA and Tukey's tests; (B) Kruskal Wallis and Dunn's procedure with Bonferroni correction. Factor variables are ranked per network type significance.

(A) Factor variables	p-value	ANOVA F-score	Tukey's test[1] (critical value = 3.776)
Max depth	0.001	6.699	Meandering > Linear-dendritic, Linear
Mouth depth	**<0.0001**	**12.649**	Meandering > Linear-dendritic, Dendritic ; Meandering ≫ Linear
Median depth	**<0.0001**	**15.201**	Meandering > Linear-dendritic, Dendritic ; Meandering ≫ Linear
Channel area proportion	0.000	8.081	Meandering > Dendritic, Linear-dendritic, Linear
(B) Factor variables	**p-value**	**K.W. K-score[2]**	**Dunn's procedure with Bonferroni correction[1] (significance level = 0.0083)**
RSLR	0.022	9.618	Linear > Dendritic
Network slope	**<0.0001**	**23.619**	Linear > Meandering ; Linear ≫ Linear-dendritic
Main channel slope	0.012	11.042	Linear > Linear-dendritic
Marsh slope	0.027	9.196	Linear, Dendritic, Linear-dendritic, Meandering
Network length	**<0.0001**	**27.86**	Linear-dendritic, Meandering, Dendritic > Linear
Main channel length	0.003	13.817	Linear-dendritic, Meandering > Linear
Drainage area	0.001	15.455	Linear-dendritic > Linear
Total network basin area	0.002	15.069	Linear-dendritic > Linear
Sediment composition	0.02	9.805	Dendritic > Meandering
Marsh depth below HAT	0.048	7.886	Dendritic > Linear
Mouth aspect ratio	0.001	16.301	Dendritic > Linear, Meandering
Mouth width	0.004	13.228	Dendritic > Linear-dendritic, Linear
Median width	0.002	14.931	Dendritic, Meandering > Linear
Marsh physiographic setting	**<0.0001**	**21.752**	Meandering > Linear ; Meandering ≫ Linear-dendritic
Mouth cross-sectional area	0.004	13.459	Meandering, Dendritic > Linear
Main channel sinuosity	0.012	10.924	Meandering > Dendritic, Linear-dendritic
Stream Strahler order	**<0.0001**	**31.387**	Meandering, Dendritic, Linear-dendritic > Linear

[1] > means significantly different than, ≫ means highly significantly different than (in case of three distinct classes); otherwise, network types are ordered by their mean scores from the highest to the lowest value

[2] K-threshold value = 7.815

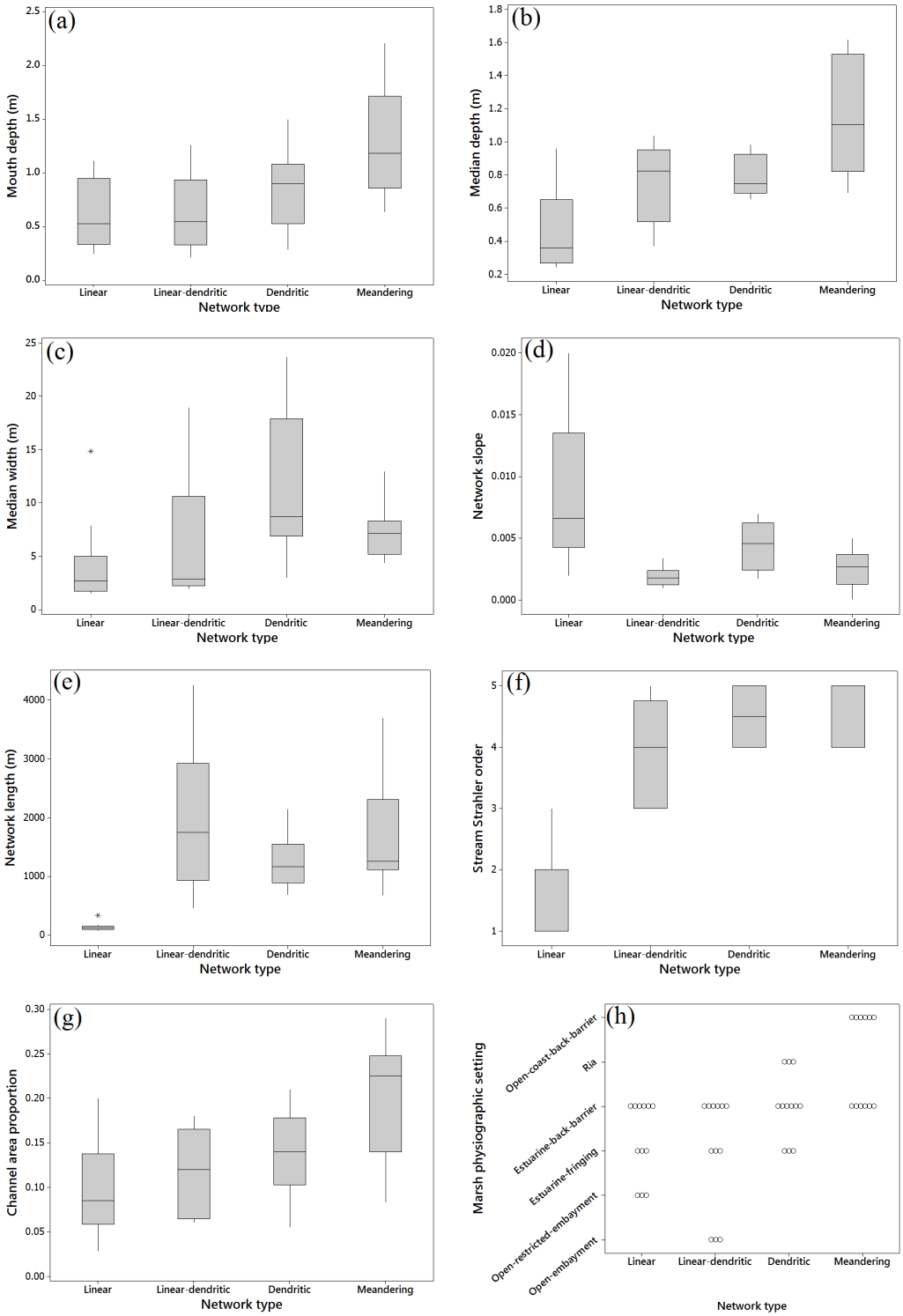

Figure 3.8: Box and individual plots of the 6 highly significant factor variables supplemented with the boxplots of median width and channel area proportion.

a result of their high stream Strahler order and channel area proportion (see Figure 3.8f and g) compared with linear networks and also due to their high main channel sinuosity with respect to linear-dendritic networks (see Table 3.5). In addition, meandering networks occur in sheltered marsh systems (e.g., spit enclosed estuarine systems) and therefore experiencing low input marine energy with regard to linear and linear-dendritic networks taking place in more exposed environments (e.g., embayments) and thereby involving higher input marine energy which is highlighted in Figure 3.8h.

Discriminant Analysis on significant factor variables

A DA was applied on the 21 statistically significant variables. Although some variables are not strictly normally distributed, they were still included in the DA as this multivariate statistical test is relatively robust facing violations of normality (Lachenbruch, 1975). Two Box's tests (with χ^2 and Fisher's F asymptotic approximations) indicated that the assumption of equality of covariances between the classes was observed. Significant mean differences were also observed for all the predictors. The DA produced two discriminant functions cumulating 83.43% of the total discrimination in the data set. Statistical significance of the corresponding DFs was confirmed through Wilks' test. Closer analysis of the factor correlations (i.e., factor loadings) as well as standardised canonical DF coefficients revealed two main significant predictors, namely Stream Strahler order on DF1 and Median depth on DF2 as displayed in Table 3.6.

Stream Strahler order and median depth, reflecting network complexity and size respectively, provides the greatest discrimination between network types and support the findings of the tests on variable significance (i.e., ANOVA and Kruskal Wallis tests) and the PCA on network characteristics.

Figure 3.9 represents the observations plotted on a two dimensional chart in which the two discriminant axes are formed by the respective discriminant functions. It allows to see whether the classes to which the observations belong are clearly distinct. Figure 3.9 confirms that the sites are well discriminated on the corresponding discriminant functions extracted from the original explanatory variables.

The predictive DA was also used to classify the observations into classes by means of the cross-validation technique and the classification matrix, or confusion matrix (Burns and Burns, 2008), is summarised in Table 3.7. Rows of the matrix are the observed categories (i.e., the former known classification) and columns are the predicted categories. When prediction perfectly matches the original classification, all observation counts will lie on the diagonal.

Table 3.6: DA on the 21 significant variables: Eigenvalues and factor correlations on the main DFs.

	DF1	DF2	DF3
Eigenvalue	60.21	36.60	19.22
Discrimination (%)	51.89	31.54	16.57
Cumulative %	51.89	83.43	100
Factor correlations	DF1	DF2	DF3
RSLR (mm/yr)	0.31	-0.14	0.46
Depth below HAT (m O.D.)	-0.24	0.34	0.00
Marsh slope	0.35	-0.19	-0.37
Mouth cross-sectional area (m^2)	-0.15	0.36	-0.13
Max depth (m)	-0.35	0.47	0.37
Mouth aspect ratio	-0.29	0.07	-0.49
Mouth width (m)	-0.19	0.25	-0.32
Mouth depth (m)	-0.02	0.54	0.17
Median width (m)	-0.29	0.29	-0.28
Median depth (m)	-0.27	**0.60**	0.30
Network length (m)	-0.58	0.16	0.32
Network slope (m)	0.56	-0.21	-0.32
Main channel length (m)	-0.42	-0.05	0.31
Main channel slope	0.51	-0.24	-0.12
Main channel sinuosity	0.10	0.45	0.35
Channel area proportion	-0.06	0.56	0.23
Drainage area (ha)	-0.38	-0.12	0.25
Stream Strahler order	**-0.67**	0.59	0.06
Total basin area (ha)	-0.35	-0.20	0.25
Soil sediment composition-Sand	0.402	-0.21	-0.07
Soil sediment composition-Sandy silt	-0.32	0.19	-0.18
Soil sediment composition-Clayey silt	-0.043	-0.23	-0.16
Soil sediment composition-Silt	-0.18	0.12	-0.40
Soil sediment composition-Silty clay	0.53	-0.03	0.07
Soil sediment composition-Silty Clay	-0.24	0.10	0.53
Physiographic setting-Restricted-entrance embayment	0.39	-0.21	-0.07
Physiographic setting-Estuarine fringing	0.08	-0.36	0.10
Physiographic setting-Estuarine back-barrier	-0.09	0.06	-0.20
Physiographic setting-Ria	-0.18	0.12	-0.40
Physiographic setting-Open coast back-barrier	0.10	0.54	0.38
Physiographic setting-Open embayment	-0.28	-0.28	0.21

Table 3.7: Confusion matrix for the cross-validated classification.

from / to	Dendritic	Linear	Linear-dendritic	Meandering	Total	% correct
Dendritic	12	0	0	0	12	100.00%
Linear	0	12	0	0	12	100.00%
Linear-dendritic	2	0	10	0	12	83.33%
Meandering	0	0	0	12	12	100.00%
Total	14	12	10	12	48	95.83%

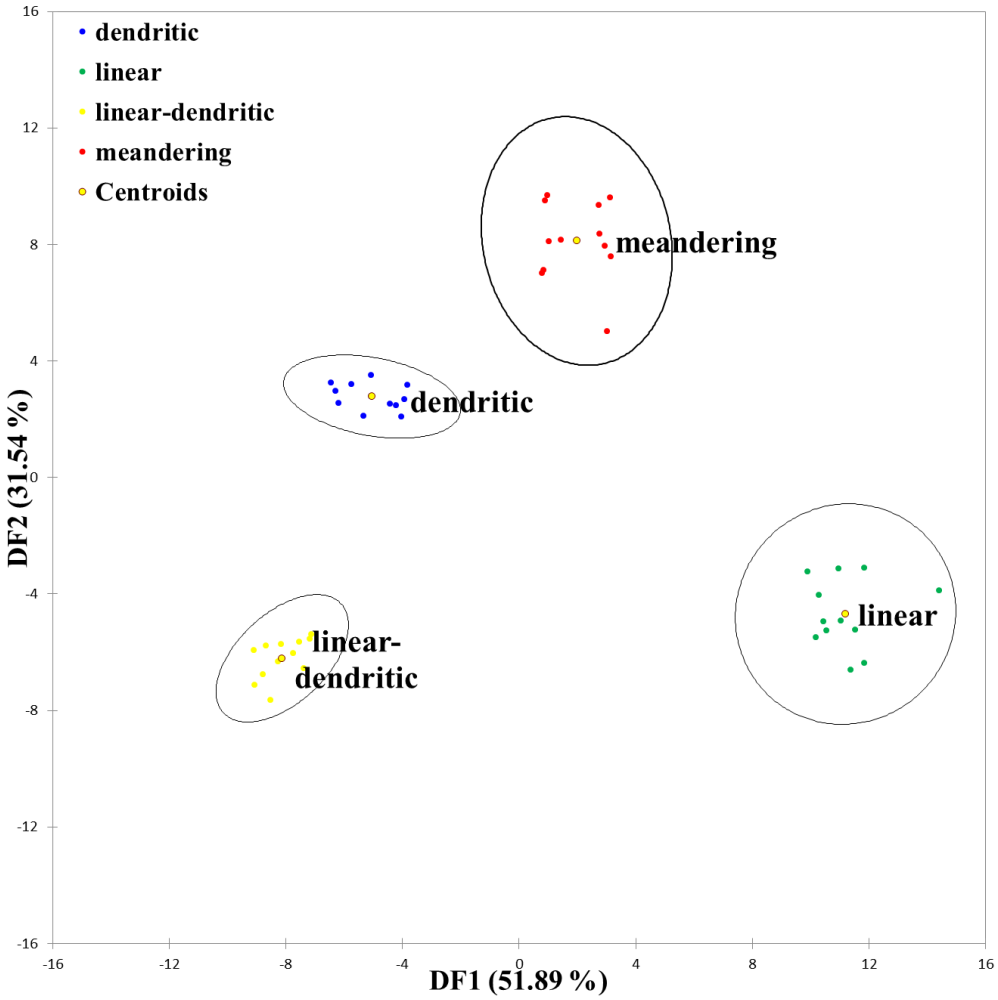

Figure 3.9: Two dimensional observation chart displaying the different classes with corresponding centroids and confidence ellipses.

The DA model reveals that 95.83% of the observations were correctly classified and only two cases were reclassified in the model (from linear-dendritic to dendritic network type). Such a result validates the site selection based on the classification of Pye and French (1993). It also approves for the choice of the explanatory variables to explain the variability in network patterns.

3.5 Discussion

3.5.1 Characterisation of tidal network patterns

ANOVA and Kruskal Wallis inferential statistical tests revealed that every network pattern can be distinguished based on its geometrical aspect. Thus, linear networks are the steepest and the shortest. Conversely, linear-dendritic networks are long and have the gentlest slope, resulting in the largest drainage areas. Dendritic networks are the widest, depicting the highest mouth aspect ratio, whereas meandering networks are the deepest, with the lowest mouth aspect ratio. Moreover, meandering networks are the most elaborated due to their high stream Strahler order, sinuosity and channel area proportion, which are followed by dendritic, linear-dendritic and lastly linear networks. Such results indicate that network size and complexity constitute properties upon which differentiation in network pattern can occur.

DA identifies stream Strahler order and median depth, measures of network complexity and size, as the two best predictors in allocating tidal network samples to the different classes. Likewise, this suggests that an increase in network size corresponds to an increase in network complexity as reported in Yapp et al. (1917) and Pethick (1969). However, despite a high correlation in the second DF, the median depth should be treated as equally significant as the stream Strahler order in contributing to network pattern segregation. As a matter of fact, multiple pairwise comparisons have shown that the median depth itself was able to show statistical significance between 3 network types whereas the stream Strahler order was only able to distinguish between 2 network types, its large K-score (see Table 3.5) eventually contributing to its high discriminating weight. In addition, the non-normality of the latter variable justifies the caution in interpreting the results. In fact, another DA was performed on the same factor variables but excluding the stream Strahler order in which the median depth resulted as the highest discriminant factor.

As a follow-up from the multivariate statistical analysis, possible variable relationships with median depth were assessed by looking at the Spearman's rank correlation

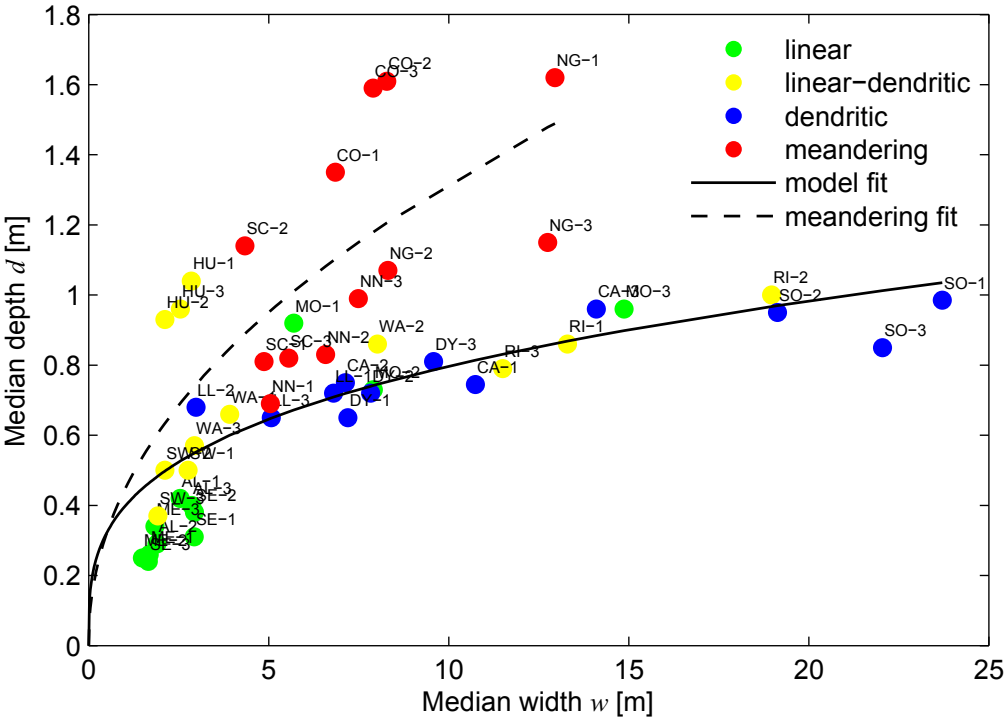

Figure 3.10: Median depth d versus median width w for the surveyed tidal network replicates with observation labels[1] and supplemented with regression fits. Colours indicate the different network types. Solid line represents the regression model of equation $d = 0.40w^{0.30}$ with $R^2 = 0.52$, applied to all network type replicates except for the meandering ones which are fitted with the dashed regression line of equation $d = 0.44w^{0.47}$ with $R^2 = 0.35$.

matrix produced on the 26 explanatory variables during the application of the two normalised PCAs. Following the computation of the correlation matrix and ignoring the multicolinear variables, median depth showed the highest correlation with the median width ($\rho = 0.675$, significant at 95% confidence interval). A scatter plot of channel median depth d against channel median width w was generated accordingly (Figure 3.10).

Correspondingly, figure 3.10 yields information on the median width-to-depth ratio $\beta = w/d$ in the main channel of every surveyed tidal network. The median β for all surveyed tidal networks equals to 7.4 which is consistent with the range $5 < \beta < 8$ for salt marsh creeks as reported in Marani et al. (2002) (see Figure 2.7 in Chapter 2). However, Figure 3.10 supplements Figure 2.7 in that it distinguishes β on the basis of the network types considered. Thus, although important fluctuations occur, the overall disposition of linear, linear-dendritic and dendritic networks seems to transcribe

a certain degree of relationship. As an exercise, these respective samples were fitted with a regression model (solid line in Figure 3.10), which showed that this trend can be approximated by a power law function. This spatial arrangement also suggests a transitional gradient from one network type to another although geomorphic thresholds are not clearly defined, and that these corresponding network types are seen to respond to similar erosional processes, with a progressive increase in β values. However, despite again a strong intra- and inter-site variability, meandering networks clearly depart from this relationship, which is materialised by the corresponding regression fit (dashed line in Figure 3.10), yielding a different slope. This difference in β values between the meandering networks and the other surveyed network types alludes to different erosional processes at work, resulting in different incisions.

3.5.2 Relation to environmental controls

In sum, morphometric measures of network size and complexity appear to be the best factors to characterise a particular network pattern. One may ask then whether these factors respond to environmental conditions. As mentioned previously, the PCA on marsh environmental characteristics has revealed that the maximum data variability does not necessarily match with the diversity of network patterns investigated. However, the statistical significance found for several marsh environmental variables may allude to the presence of environmental controls. Among them, marsh physiographic setting has shown to be significantly different between the network types (see Table 3.5). Results have demonstrated that linear and linear-dendritic networks were frequently located in well-exposed estuarine environments such as embayments, open-restricted embayments and estuarine fringing settings. To the contrary, dendritic and particularly meandering networks were mostly located in sheltered estuarine systems such as estuarine back-barrier, ria and open coast back-barrier settings (see Figure 3.8h), characterised by their confinement (e.g., ria) and the presence of protective spit(s) backed by extensive tidal lagoons (see Chapter 2). Thus, the sequence from linear to meandering networks transcribes a gradient from highly exposed to highly sheltered physiographic settings. This gradient also translates a progressive decrease in input marine energy from embayment estuarine types typically characterised by a wide mouth open to large wave and tidal effects to open coast back-barrier systems where beach barriers constrain the inlet of the estuarine channel and therefore reduce the input wave and tidal energy (EstSim Consortium, 2007). Several auhtors have reported the presence of linear networks in tidal environments experiencing large tidal range or storm surges

(e.g., Eisma, 1998; Hughes, 2012), corroborating thus with these observations. Putting this consideration in line with the observed increase in network size and complexity associated with the sequence from linear, linear-dendritic, dendritic to meandering networks, marsh physiographic settings seem to emerge as an environmental control on tidal network morphometrics, hence on the occurrence of a particular network pattern.

The rationale behind this concept can be explained as follows: a tidal network developing in a sheltered setting with a low-input marine energy must elaborate itself in order to drain the tidal basin effectively. In other words, to flood and drain its marsh platform, given the low hydrodynamics and the rather flat topography characterising these estuarine configurations, the tidal network must portray high size, density and complexity. These morphometric aspects have shown to characterise dendritic and above all meandering networks through this analysis (see Table 3.5). To the opposite, a tidal network developing in an exposed setting with a higher-input marine energy may only develop a linear pattern which is sufficient to drain effectively its tidal basin. As a matter of fact, due to the high depositional regime of these estuarine environments, relatively steep topographic profiles may characterise the tidal wetlands, favouring the possibility of topographically-driven tidal flows. Moreover, the associated high-input tidal and wave energy may be subject to large water volumes transported as sheet flow directly from the marsh seaward edge rather than as tidal flows routed via the tidal network (Temmerman et al., 2005a). As a consequence, the network may only feature a simplistic structure.

In truth, considering the marsh physiographic setting as a "master variable" that controls tidal network pattern also reveals the linkage between network morphology and the overall morphodynamic regime of the marsh system. Indeed, in coastal and estuarine environments, wetlands exist in a dynamic equilibrium between erosional and depositional forces (Day Jr et al., 1999), so much that most of the morphodynamic work occurs for this purpose. Therefore, in addition to a better drainage, the tendency for the development of elaborated tidal networks within sheltered physiographic settings may be a response to the limited sediment supply as dendritic and particularly meandering networks allow for a more effective transport and delivery of fine sediments, uniformly onto the marsh platform, so that it can maintain its equilibrium profile.

Marsh sediment composition has appeared to be a significant variable, but its control on tidal network pattern is not evident as it was only able to discriminate between dendritic and meandering networks. Results have shown that dendritic networks frequently occur on silty sediments whereas meandering networks develop over more clayey sedi-

ments (see Table 3.1 and Table 3.5). Such a difference in sediment characteristics may explain why meandering networks are deeper, and have a lower width-to-depth ratio than dendritic ones as displayed in Figure 3.10, since finer-grained materials favour steeper banks than sander sediments (Steel and Pye, 1997; Allen, 2000).

Lastly, intra-site variability may emerge when investigating network morphometric properties as seen in the corresponding PCA (see Figure 3.7) and looking at the scatter plot of median depth vs median width (see Figure 3.10). Such a variability is ascribed to local competing dynamic processes, which explain the lack of scale invariance features peculiar to tidal networks. Moreover, a relatively wide scatter in marsh environmental characteristics portray marshes located in the West coast of the UK with respect to their eastern counterparts. This reflects the broad range of environmental conditions found in the western coast regarding the hydrodynamics, topography and geology as compared with the eastern coast of Britain (Bird and Bird, 2000).

Chapter 4

Assessing the bio-physical controls on tidal network ontogeny

This chapter discusses on the processes driving tidal network ontogeny, particularly channel formation and early development. A review on the current state of the art regarding this field of research along with the advances and challenges in transcribing the knowledge in a mathematical modelling perspective will constitute the introductory chapter. Then, the main core of the chapter will comprise the description and test of the developed modelling framework aiming to bring further insights into the main mechanisms governing tidal network ontogeny.

4.1 Channel formation and early development: theories and modelling transcription

4.1.1 Conceptual models of tidal channel development

Channel formation and early development is undoubtedly a complex field of study and the actual lack of consensus within the scientific community regarding the providence of a clear and detailed description of tidal network ontogeny constitutes its best testimony. Improving our understanding on the chief channel-forming processes is yet essential due to the primary role of the tidal network in providing a broad range of ecosystem services within the tidal wetland landscape (Barbier et al., 2011). Although tidal course networks have been little studied in comparison with their fluvial counterparts, this intriguing problem has become a subject of great scientific interest especially over the last decades and a large body of literature have consequently emerged, describing tidal

channel initiation and further evolution (De Swart and Zimmerman, 2009; Fagherazzi and Overeem, 2007; Fagherazzi et al., 2012; Coco et al., 2013; Hughes, 2012).

Tidal creeks, channels and by extension networks, are believed to experience three main evolutionary (or ontogenic) stages namely initiation, elaboration and integration (or reduction) (Steel and Pye, 1997; Allen, 2000). Conventionally, while channel initiation and integration clearly represent the respective initial and final channel development stages, sometimes the elaboration stage constitutes itself a phase or a manifestation of a more global intermediate stage including also the elongation and extension phases as in Glock (1931).

Channel initiation can be primarily attributed to channel incision. Fundamentally, tidal channels usually develop onto tidal flats, particularly mud flats and to a lesser extent sand flats (Allen, 2000). These landforms are characterised by topographic perturbations which concentrate the tidal sheet flow into local depressions, producing scours where the local shear stress exceeds a threshold value for erosion. The resulting incised patterns favours a further flux concentration due to their expanding cross-sectional areas associated with the decreasing flow resistance as the forming course deepens (e.g., Fagherazzi and Furbish, 2001), which results in higher bed shear stress and therefore further erosion. Clearly, the concomitant actions of course deepening and net erosion translate a positive feedback mechanism between erosion and channel formation, defining the concept of headward erosion (e.g., D'Alpaos et al., 2005). Figure 4.1 illustrates this erosional channel formation process. This erosional channel initiation mechanism has been observed in numerous locations such as in the barrier and estuarine coasts of the Netherlands (Beeftink, 1966), and in the North-Norfolk barrier coast, UK (French and Stoddart, 1992) and constitutes the dominant paradigm to explain the formation of tidal channels.

Perillo et al. (1996) describes another conceptual model of channel initiation through the interconnection of a series of ponds as a result of the combined action of wind/wave erosion (see Figure 4.2). Firstly, waves enlarge the pond walls (Figure 4.2d) which provoke inevitably the ponds to merge and to form ill-defined creeks (Figure 4.2c). These incipient creeks are then connected to existing channel via ebbing-water cascade, which takes place at first order channel tips, combined with seaward flooding water erosion which penetrates the ponds. Channel maintenance becomes then a function of water exchange intensity. This mechanism has been described in a particular marsh site located in southern Argentina where strong direction concentrated winds usually occur. Similar creek-forming process was also noticed by the same author in a freshwater

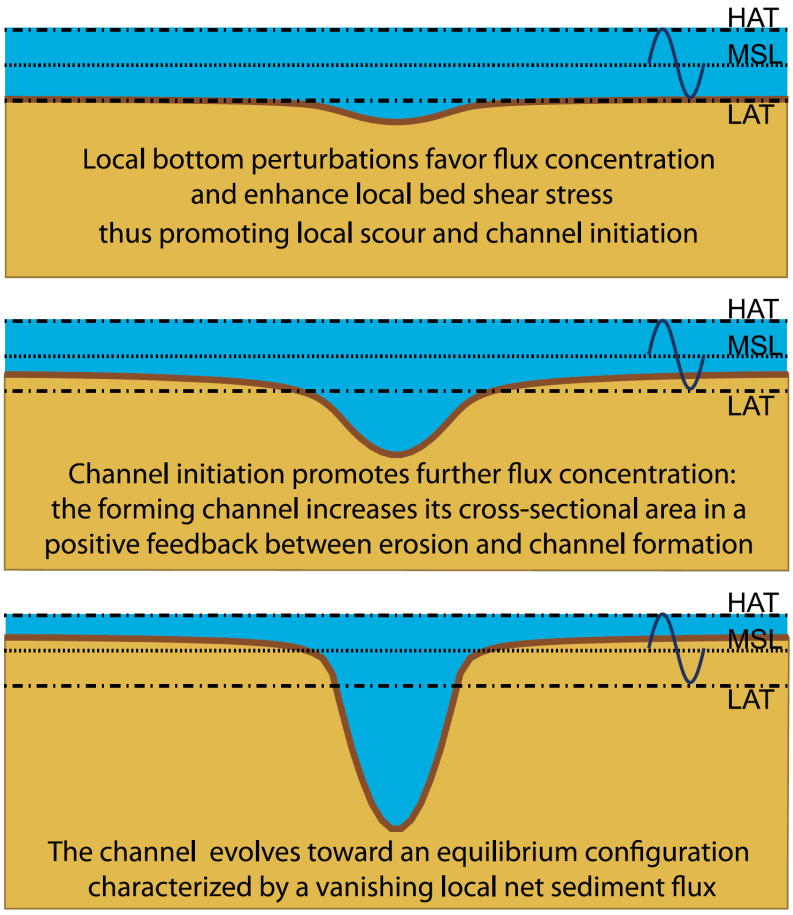

Figure 4.1: Sketch illustrating the process of channel initiation resulting from a negative feedback mechanism between net erosion and channel formation (from Fagherazzi et al. 2012).

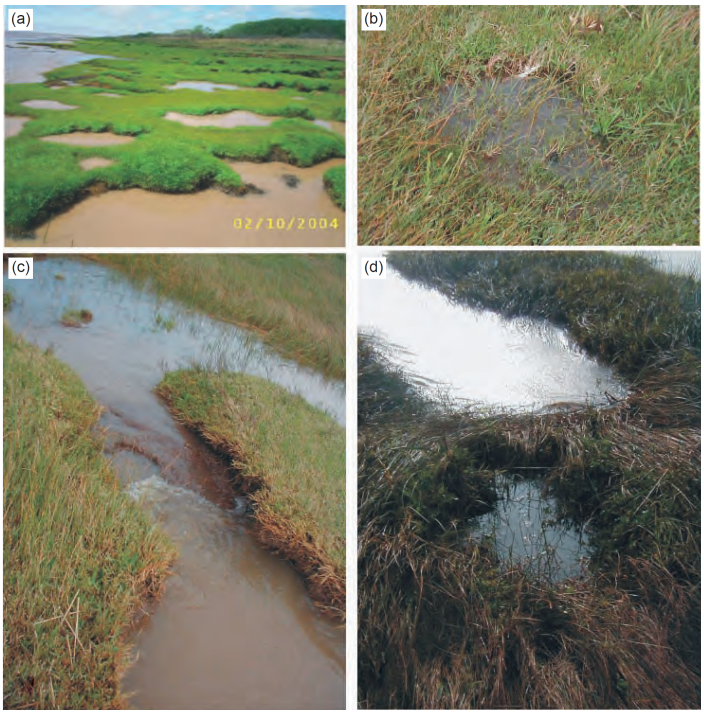

Figure 4.2: A set of photos transcribing the formation of channel as a result of the interconnection of ponds. (a) a series of ponds along the southern coast of the Rio de la Plata; (b) zoom in on a pond showing the plant ecology; (c) creek initiation following the cutting of the threshold (i.e., wall) between two ponds; (d) a threshold between two ponds (from Perillo 2009).

marsh on the southern coast of the Rio de la Plata estuary (Perillo and Iribarne, 2003b) (see Figure 4.2). Other sites located in open estuarine or coastal settings and exposed to the wind forcing may illustrate this proposed model as ponds constitute a relatively frequent morphological feature within the tidal landscape.

While these two above conceptual models of tidal channel initiation rely on interaction among physical processes, the following reflect the notable interplay between biotic and abiotic processes in controlling the morphological evolution of the intertidal landscape. Particularly, biological processes such as vegetation and microphytobenthos colonization strongly influence the dynamic response of the system.

For instance, Yapp et al. (1917) proposed a model for tidal channel initiation as a result of plant flow interaction. Typically, at the lowest intertidal elevations, soil colonisation by pioneer halophytic species is often manifested by the presence of low and flat hummocks. With time, these hummocks expand vertically and horizontally as the vegetation further traps sediments, reducing the area of the adjacent bare soil.

This favours the appearance of drainage patterns during ebb tide as the flow tends to be obstructed by the hummocks and therefore redirected in between where it soon starts cutting shallow, winding channels. These incipient channels progressively evolve towards more definite channels due to the further aggradation of the lateral hummocks combined with vegetation constriction. This mechanism of flow concentration and channel erosion between laterally expanding vegetation patches was first derived from observations in a floristic marshland located in the Dyfi estuary, west Wales (Yapp et al., 1917). Similar observations were also noticed later in a tidal flat encroached by hummocks located in the Westernschelde estuary, Netherlands (Temmerman et al., 2007). In truth, this conceptual model somehow complements the dominant paradigm for tidal channel formation as, similarly with topographic perturbations, hummocks constitute an additional factor driving flow concentration into preferential locations.

Another conceptual model for tidal channel formation is associated with groundwater and tidal actions mediated by bioturbation effects due to crab-plant interactions, which was described in the particular environment of the Bahía Blanca estuary (Perillo and Iribarne, 2003a,b). At first, crabs (*Neohelice granulatus*) interact with a halophytic plant (*Sarcocornia perennis*) producing a high number of burrows. These burrows are all disposed in the centre of circles where plants occupy the outer edge forming rings of width typically ranging from 0.5m to 1.5m (Perillo et al., 2005). The high density of crab burrows trigger soil alteration characterised by less cohesive and more loosely sediments. As a result, water starts migrating within the holes breaking the walls and creating caves. Later, soil surface fails due to the combined action of groundwater and tidal flows and ultimately a channel starts initiating with at first intercave flanks being progressively smoothed out with successive tides (Perillo and Iribarne, 2003b). A somewhat analogous mechanism put forward by Hughes et al. (2009) explains the extension of tidal creeks in a salt marsh in South Carolina, USA, where intense crab-burrowing activity coupled with vegetation dieback produces depressions located at the creek head which become channelized eventually.

All the preceding conceptual models of tidal channel formation are said to be erosional models as they assume tidal channel initiation as a result of the erosive action of the involved processes. Indeed, the dominant paradigm and the Yapp model are primarily associated with tidal erosion, the pond model is linked with wind/wave erosion and the models based on crab burrowing activity are associated with groundwater and tidal erosion. To the contrary, Hood (2006) proposed a depositional model for tidal channel formation departing from this erosional origin. This new conceptual model

stems from observations in marshlands located in the Skagit River delta, Washington, USA. In this estuarine system, the accumulation of sediments along the river course form marsh islands separated by river distributaries which are eventually blocked by more sediments to become blind tidal channels. This sequence of events suggests that tidal channels are formed by sedimentation. Figure 4.3 depicts an example of such sequential events. Of course, in this context, the mechanism develops in a peculiar tidal environment dominated by river discharge. However, examples of tidal channel formation as a result of depositional processes have been noticed in other physiographic settings. Redfield (1972) was notably the first to allude to depositional tidal channel development following observations in a New England coastal prograding salt marsh sheltered by a long sand spit. Sediment inputs to this open coast back-barrier system were of marine origin, suggesting that depositional tidal channel development is not only driven by fluvial processes.

Nonetheless, marsh progradation appears to be a necessary condition for the development of depositional tidal channels. Indeed, the formation of marsh islands due to the accumulation of sediments which further splinter the river into distributaries refers to the process of differential deposition which results from the spatial variability in sediment deposition: strong water fluxes within the channel induce erosion or channel maintenance as opposed to weak water fluxes in the adjacent rising ground which allow deposition fluxes to predominate. As a result, the soil aggrades vertically and progrades horizontally (D'Alpaos et al., 2009). Subsequent channel lengthening and narrowing described by Hood (2006) also translate the prograding nature of the adjacent surface, enhanced by the vegetation, and which diminishes channel gradient and stream power (see figure 4.3). Finally, channel segmentation and closure occur by local infilling through bridging of overhanging vegetation (Chapman, 1960; Pestrong, 1972; Collins et al., 1987). The above processes of differential deposition, channel elongation, gradient reduction and channel senescence towards the conversion to a blind tidal channel constitute manifestations a more global scale systemic depositional process of marsh progradation, therefore defining this conceptual model of depositional tidal channel development (Hood, 2006).

Globally, the presented conceptual models for tidal channel initiation and early development support the concept of inheritance of the major features of the channelized patterns, either from antecedent river distributary networks (e.g., Hood, 2006), or from tidal flat characteristics particularly regarding their morphology or sedimentology (e.g., Allen, 2000; Friedrichs and Perry, 2001; Marani et al., 2003).

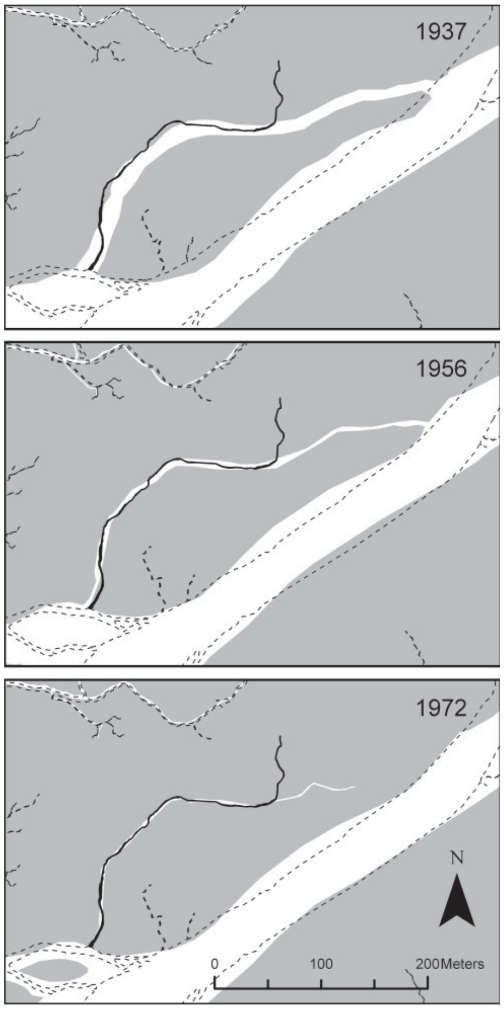

Figure 4.3: A sequence of historical images showing the scenescent aspects experienced progressively by a distributary from course narrowing in 1956 towards course segmentation with the resulting creation of a blind tidal channel in 1972. The superimposed solid black line represents the course of the blind tidal channel in 2004 whereas dashed lines are marsh boundaries in 2004 (from Hood 2006).

Compared to channel initiation, subsequent channel elaboration is agreed to take place over longer time scales (D'Alpaos et al., 2005). The progressive elaboration of the tidal networks is primarily manifested by channel deepening, extension, densification leading to an increase in network complexity and sees the channel with their longest and densest aspects. Indeed, as the marsh increases in surface extent through its youthful stage, the main channels elongate and new first order tributaries start initiating. While the initiation of these tributaries can be attributed to headward erosion, which can amount to several meters per year (e.g., Steers, 1939; Beeftink, 1966; Pethick, 1969; Allen, 2000), the increasing depth of the main channels can be either controlled by differential deposition as observed in the Dyfi estuary (Yapp et al., 1917; Beeftink and Rozema, 1988) or through channel incision as prevailing in a majority of tidal environments such as in the North-Norfolk barrier coast (Chapman, 1960; French and Stoddart, 1992).

Another aspect of channel elaboration is channel meandering. Usually, channels feature linear patterns during early development, which however become increasingly sinuous in time, with notably the formation of meanders depicting a high degree of sinuosity even within distances of a few hundred meters (Marani et al., 2002). Although, tidal meanders appear geometrically similar to their fluvial counterparts (Marani et al., 2002; Solari et al., 2002; Fagherazzi et al., 2004), yet their formation and evolution remain poorly understood. In analogy to fluvial meanders, the formation of tidal meander bends is related to the redistribution of flow momentum due to channel curvature, triggering sediment transport in which erosion plays a dominant role (Solari et al., 2002). In contrast, Hood (2006) described a depositional mechanism for tidal meander formation in the Skagit River delta marshes following a developmental sequence from the formation of a sand bar at the confluence of a tidal channel with a delta distributary that evolves into a vegetated island and eventually triggers the formation of a meander during island coalescence with marsh mainland. This mechanism occurs concurrently with delta progradation and its manifestations towards the formation of blind tidal channels as described earlier.

The phase of network elaboration persists until the channels have reached the catchment boundaries, prior to assisting to network regression. This new evolutionary stage characteristic of old marshes is materialised by a series of channel senescence aspects such as retrogradation of low-order channels, narrowing of main channels and even channel segmentation due to local infilling as a result of bridging by overhanging vegetation or obstruction by collapsed silt blocks or woody debris (Yapp et al., 1917;

Chapman, 1960; Pestrong, 1972; Collins et al., 1987; Hood, 2006).

In the end, from the previous remarks, it seems that, within the frame of tidal channel development, vegetation has a dual role. Indeed, vegetation can promote channel incision as illustrated by the model of vegetation hummocks from Yapp et al. (1917). However, it can stabilise channel banks and therefore confine channels in definite limits. Likewise, vegetation tends to control the degree and rate of channel lateral migration and meandering (Garofalo, 1980). Finally, as just mentioned, vegetation can enhance channel senescence due to its contribution to marsh aggradation and progradation, therefore augmenting channel narrowing and closure, a role contrasting with the very first listed. In fact, each of these contributions seems to take place over a particular channel ontogenic stage.

4.1.2 Advances and challenges in mathematical models of tidal channel morphodynamics

Towards the global necessity to understand the physics lying behind marsh formation and its dynamic response facing threats such as climate change and human pressure, a number of analytical and numerical models simulating the morphogenesis and long-term morphological evolution of tidal networks and their intrinsic channels have emerged during the past decade.

Simplified one dimensional morphodynamic models typically simulating the evolution of the longitudinal estuary/channel bed profile have brought first notable insights into the morphodynamic equilibrium of tidal channels. For instance, Schuttelaars and de Swart (2000) demonstrated that a unique equilibrium profile exists for all embayment or channel lengths shorter than the frictional length scale of the tidal wave. Additionally, Lanzoni and Seminara (2002) showed that equilibrium configurations can be reached asymptotically, ensuring a vanishing net along-channel sediment transport. Likewise, both studies have proven that this equilibrium bed profile is characterised by a certain degree of concavity based on estuary or channel characteristic length. Toffolon and Lanzoni (2010) revealed as well that this equilibrium profile involves a series of extrinsic factors, namely, the amplitude and the period of the forcing tide as well as the critical velocity for sediment erosion. In parallel, other numerical models have looked at the morphological evolution of channel cross-sections. Fagherazzi and Furbish (2001) found that the relatively short duration of the peak spring tidal discharge associated with the corresponding erosion rates and the autoconsolidation of cohesive sediments contribute to the widening of channel cross-sections. This numerical study

was later reconsidered by D'Alpaos et al. (2006) accounting for the vertical growth of the adjacent platform and colonisation by halophytic plants. Results have shown that channel cross-sections tend to adapt to changing flow conditions resulting from the inclusion of the two above processes.

As two-dimensional channel patterns represent key morphological characteristics, and can be used to identify tidal networks, lately, a rapid growing number of intricate 2D simulations capable of reproducing the landscape evolution have been proposed, succeeding the preceding 1D models. The majority of these 2D models fall within two different modelling approaches referred to as "explicit numerical reductionism" and "exploratory modelling" (Murray, 2003).

The "explicit numerical reductionism" approach relates to modelling long-term landscape evolution by means of solving variables at the fastest and smallest scales. By doing so, one seeks to provide a full detailed picture of the landscape morphodynamics and such modelling studies are useful in demonstrating some physical principles. However, adopting such an approach where the emphasis is placed on the fast and small scale processes can lead to challenges in appreciating the effect of a particular factor on the long-term and large scale dynamic response of the system, not to forget the tendency of increasing errors while upscaling the solution of the system (Coco et al., 2013). Examples of 2D long-term morphodynamic models based on fast and detailed scale variables include notably the numerical experiment of Marciano et al. (2005) who was one of the first to use a detailed numerical model based on the Delft3D software system to simulate the long-term development of tidal networks. The solver comprising the classic 2D depth-integrated shallow water and advection-dispersion equations was used to simulate the respective hydrodynamics and sediment transport whereas the morphological change was solved by means of the sediment continuity equation. Results have shown that the model is able to predict key properties of branching channel patterns similar to field observations in the Wadden Sea basins. However, these branching structures seem to develop only when the initial bottom hypsometry is not too far from equilibrium. van Maanen et al. (2013) using a different solver, explored the sensitivity of the development of tidal networks to varying tidal range and initial platform sloping degrees. Results show that a large variability in morphology could be observed, indicative of the crucial role that initial bathymetry and tidal conditions play in the large scale evolution of tidal embayments. For instance, the formation of tidal channels was enhanced when the initial depth of the basin decreased and/or the tidal range increased.

Using such detailed hydrodynamic and morphodynamic solvers leads to time-costly computations and therefore reveal to be ineffective to study long-term morphodynamics. Such a modelling application can be possible only if a computational technique is applied to accelerate the morphological evolution in time. Accordingly, several simulation studies adopt a so-called "morphological factor" M which multiplies the bed level change to artificially enhance the morphological evolution (e.g., Marciano et al., 2005; van Maanen et al., 2013; Schwarz et al., 2014). Several approaches, listed notably in Roelvink (2006) exist, however applying such a technique generates some approximations which can be minimised by means of sensitivity analyses which are yet complex, therefore leading often to an *a priori* choice for the value of the morphological factor.

To the opposite line lies the "exploratory modelling" approach which consists of the high simplification or even possible exclusion of certain factors to better retain and focus on the key feedback interactions governing the system at the scale of interest (Murray, 2003; Coco et al., 2013). As its name indicates, adopting such an approach suggests an exploratory manner of tackling the problem rather than a precise quantitative manner, and prove to be somewhat more effective in gaining insights into the effect of a particular factor on the long-term response of the overall system. Accordingly, Fagherazzi and Sun (2004); D'Alpaos et al. (2005, 2007a,b); Kirwan and Murray (2007) used process-oriented models, addressing tidal channel morphogenesis and further evolution, based on a simplified hydrodynamic model, usually referred to as the Poisson model and developed by Rinaldo et al. (1999a). The Poisson hydrodynamic model relies on several assumptions among which it is assumed that the tidal propagation on the marsh platform flanking the channels is frictionally dominated and is instantaneous through the tidal network. These assumptions imply that a balance holds between frictional terms and water surface slope (pressure term) in the momentum equation, while the flow velocities are very negligible. The simplified momentum equation coupled with the continuity equation therefore leads to a Poisson boundary value problem of the form:

$$\nabla^2 \eta_1 = \frac{\Lambda}{D_0^2} \frac{\partial \eta_0}{\partial t} \tag{4.1.1}$$

where η_1 is the local deviation of the free surface elevation from its instantaneous average value η_0, Λ is the bottom friction coefficient and D_0 is the average water depth above the marsh platform.

The stochastic model of Fagherazzi and Sun (2004) suggests that local heterogeneities in sediment substrate are important for the development of the small tidal

channels, thus influencing the small scale of the network, whereas the development of large channels is controlled by the critical shear stress for erosion. The numerical model of D'Alpaos et al. (2005) shows that large values of the shear stress is located at channel tips and pronounced bends suggesting that headward growth, driven by the exceedance of a critical shear stress controlled by surface water gradient is the chief process for tidal network development, therefore corroborating the findings from Fagherazzi and Sun (2004). In a later contribution, D'Alpaos et al. (2007a) used the same modelling framework in an attempt to reproduce the formation of small creek networks in an artificial salt marsh in the Venice lagoon. Results revealed a close match between the inception locations of the synthetic and actual creeks, thereby confirming the assumption of the substantial control exerted by the water surface gradients and the resulted shear stress in driving the process of channel incision. Di Silvio et al. (2010) also used the Poisson hydrodynamic model embodied in a morphodynamic model to simulate the overall evolution of a tidal lagoon. Results also evoke a rapid tidal network initiation stage followed by a slower elaboration stage when the system is approaching an equilibrium state. A particularity of the model resides in the combination of processes solved at different temporal scales. Indeed, the solver comprises both fast scale hydrodynamic variables with slower scale sediment transport variables expressed as the difference between the local transport concentration and long-term equilibrium concentration. Therefore, this model is better referred to as a "hybrid" model conventionally (Coco et al., 2013).

In line with the different conceptual models of tidal network ontogeny described in the previous section, mostly mathematical models do not reflect the diversity of tidal channel formation processes. As a matter of fact, all the previously listed models assume that the key mechanism for channel development is headward growth (Hood, 2006). Besides, the majority of these models do not include biotic processes such as halophytic vegetation productivity and the related feedbacks with the hydrodynamics and sediment transport. However, several exceptions exist. For instance, the conceptual model of tidal channel formation linked to crab burrowing activity following observations in the Bahía Blanca estuary has been tested by means of a simplified cellular automata model (Minkoff et al., 2006), considering this bioturbation effect linked to the crab/plant interactions existing in the marsh. Results reveal that in such a setting, these interactions play a substantial role in driving the development of tidal creeks, prevailing over the impact of water surface gradient and its related shear stress.

Temmerman et al. (2005b) developed a fast and small scale numerical model

based on the Deflt3D modelling system to simulate the coupled morphodynamics and vegetation dynamics of a tidal marsh in an attempt to explain observed tidal channel development resulting from the coalescence of vegetation patches in the Westernschelde estuary. The model suggests that vegetation favours channel erosion by rerouting the flow between the dense hummocks, recalling the plant/flow interaction conceptual model derived from the observations of Yapp et al. (1917). This modelling framework was later extended by Schwarz et al. (2014) in order to investigate the conditions in which vegetation favours either channel erosion or channel stabilisation. Results argue that such a balance between erosional and stabilizing properties depends on the degree of channel elaboration and the presence or absence of vegetation during the short time span in which channel incision occurs. These two modelling studies account for a highly detailed representation of the vegetation characteristics and its influence on flow and turbulence. However, other eco-geomorphic processes are neglected such as sediment particle capture by plant stems and leaves as well as sediment organic production. Surprisingly, marsh accretion never occurred in the different simulations as the initial mudflat never experienced gain in elevation throughout the simulation period; only channel incision took place.

D'Alpaos et al. (2007b) and Kirwan and Murray (2007) developed two other fairly similar bio-morphodynamic modelling frameworks. These two exploratory models simulate the long-term coevolution of both the marsh platform and the vegetation colonising it with the intertwined tidal network under conditions of sea level rise. D'Alpaos et al. (2007b) assume the evolution of tidal networks in an implicit manner through relationships describing channel geometry, and demonstrated that tidal network geometrical variables such as width and depth are highly influenced by the changing tidal prism resulted from sea level rise. Kirwan and Murray (2007) on the other hand explicitly modelled the 2D expansion of tidal networks. The numerical experiments notably show that the aggrading and prograding marsh platform together with the vegetation colonization constrict the existing channels into a fewer deeper channels with greater discharge, being manifestations of channel elaboration as a result of depositional processes. However, the model does not treat tidal network initiation as the initial topography consists of a radial tidal network, constituting a sort of inlet where the flow is exchanged in and out of the tidal basin, similarly with D'Alpaos et al. (2005). Moreover, the parameterisation of some of the processes may be called into question. Indeed, while the model uses the water surface gradients obtained from the Poisson boundary value problem of Rinaldo et al. (1999a) to represent flow routing

across the marsh surface, the treatment of the sediment transport reveals to be rather simplified. Indeed, deposition rates are not linked to hydrodynamic shear stress but simply proportional to above-ground biomass while the sediment concentration is assumed to be uniform across the domain. Likewise, no eco-geomorphic processes are accounted for in the model.

4.2 Objectives

As pointed out in Section 4.1.2, this diversity of channel forming processes is not reflected in mathematical models of tidal channel morphodynamics as, except for a few cases (e.g., Kirwan and Murray, 2007), they mostly assume an erosional channel formation, notably through the mechanism of headward growth. In this regard, several modelling studies have investigated the role of forcing factors inducing channel erosion such as tidal range (e.g., van Maanen et al., 2013) and relative sea level rise (e.g., D'Alpaos et al., 2007b; Van Maanen et al., 2013). However, despite its potential implication in tidal channel formation (Hood, 2006), the role of sediment supply has not been explored individually from a modelling perspective. Accordingly, we develop a modelling framework to investigate this control on tidal channel morphodynamics. On a second stage, the analysis is extended to the exploration of the role of the initial topography in driving the dynamic response of the system, by considering random initial topographic perturbations with different scenarios of amplitudes and degrees of smoothness.

As tidal networks are tightly coupled with the tidal flat and the salt marsh settings onto which they develop, a holistic approach is adopted by simulating the co-evolution of the marsh platform with the embedded tidal networks similarly to Kirwan and Murray (2007). However, a typical challenge when attempting to model the coupled evolution of the marsh platform and the tidal network regards the inclusion of biotic processes and their related feedbacks with hydrodynamics and sediment transport. Albeit the majority of models of tidal channel evolution do not incorporate these components, recent modelling efforts have tried to meet this challenge by parametrizing certain of these bio-physical processes with different degrees of complexity (e.g., Minkoff et al., 2006; D'Alpaos et al., 2006, 2007b; Kirwan and Murray, 2007; Temmerman et al., 2005b; Schwarz et al., 2014). In the present case, a morphodynamic model which was developed by Defina (2000) and later extended by Carniello et al. (2005, 2011, 2012) is adopted, and is then coupled with the development of an ecological module simulating

vegetation growth, using two distinct mathematical parameterisations, and related eco-geomorphic processes. While the hydrodynamic and morphodynamic modules solve fast and detailed scale variables, the ecological module is seen as a process-based model incorporating a simplified mathematical description of the vegetation dynamics which is based on long-term assumptions, therefore making the modelling framework a "hybrid" tool.

Through this modelling framework, our motivation is globally to bring further insights into the mechanisms governing the formation and evolution of tidal networks. Particularly, the emphasis is placed on the investigation of i) how tidal networks form and evolve in different sedimentary contexts, ii) how they form and evolve starting from different initial tidal flat bathymetric configurations and iii) how they respond to eco-geomorphic feedbacks involving different ecological scenarios and mathematical parameterisations.

4.3 The modelling framework

The evolution of the salt-marsh landscape is studied on the basis of the eco-morphodynamic approach, i.e. the modelling framework considers interactions and feedbacks between processes (tidal currents and wind waves) and morphology, driven by sediment transport and mediated by vegetation growth through related eco-geomorphic processes. In the following will be described these different constituents prior to discussing on the numerical settings.

4.3.1 Model description

The hydrodynamic module

The mechanical interaction of tidal currents and waves with sediments is described on the basis of the two-dimensional model originally developed by Defina (2000) with the inclusion of the WWTM (Wind Wave Tidal Model) developed by Carniello et al. (2005, 2011).

The hydrodynamic model was specifically designed to study the morphodynamics of very-shallow tidal basins, this specificity being notably embodied in the mathematical formulation of the hydrodynamics. Indeed, estuarine environments such as salt marshes and tidal flats present very shallow flows with wide portions of the ground surface being subject to repetitive wetting and drying processes. To deal with flows in highly irregular topography, the Shallow Water Equations are modified in order to account

for partially wet domains: a phase-averaging procedure is first applied to the original Reynolds equations prior to integrating the resulting equations over the depth. We refer the reader to Defina (2000) for the complete derivation of the set of shallow water equations for partially dry areas. Here, we only report the resulted momentum and continuity equations once the phase averaging and the depth integration have been applied, yielding:

Momentum equations in the two horizontal directions:

$$\Phi\left\{\left[\frac{\partial\eta}{\partial x}+\left(\frac{u}{g}\frac{\partial u}{\partial x}+\frac{v}{g}\frac{\partial u}{\partial y}\right)-\frac{q_x}{gY^2}\frac{\partial\eta}{\partial t}+\frac{1}{gY}\frac{\partial q_x}{\partial t}-\frac{1}{g}\left(\frac{\partial R_{xx}}{\partial x}+\frac{\partial R_{xy}}{\partial x}\right)\right]+J_x-\frac{\tau_{sx}}{\gamma}-\frac{S}{gY\Phi}U_{x|z=\eta}\right\}=0 \quad (4.3.1)$$

$$\Phi\left\{\left[\frac{\partial\eta}{\partial y}+\left(\frac{u}{g}\frac{\partial v}{\partial x}+\frac{v}{g}\frac{\partial v}{\partial y}\right)-\frac{q_y}{gY^2}\frac{\partial\eta}{\partial t}+\frac{1}{gY}\frac{\partial q_y}{\partial t}-\frac{1}{g}\left(\frac{\partial R_{xy}}{\partial x}+\frac{\partial R_{yy}}{\partial x}\right)\right]+J_y-\frac{\tau_{sy}}{\gamma}-\frac{S}{gY\Phi}U_{y|z=\eta}\right\}=0 \quad (4.3.2)$$

Continuity equation:

$$\Phi\frac{\partial\eta}{\partial t}+\frac{\partial q_x}{\partial x}+\frac{\partial q_y}{\partial y}=0\,, \quad (4.3.3)$$

where η is the free surface elevation [m]; u and v are the flow velocity components in the x- and y-directions respectively [ms^{-1}]; $q_x = uY$ and $q_y = vY$ are the corresponding depth-integrated phase-averaged velocities (discharges per unit width) [m^{2}s^{-1}]; R_{xx} and R_{yy} are the horizontal Reynolds stresses; τ_{sx} and τ_{sy} are the two components of the shear stress exerted at the free surface [N.m^{-2}]; S is a source term being the phase-averaged vertical flow rate per unit area which accounts for possible water inflows [ms^{-1}]; $\gamma = \rho_w g$ is the specific weight of water [N.m^{-3}]; $U_{x|z=\eta}$ and $U_{y|z=\eta}$ are the phase-averaged velocities at the free surface and finally J_x and J_y are the x- and y-components of the Energy slope. The variable Φ and Y appearing in both momentum and continuity equations result from the phase-averaging procedure. Φ is expressed as follows:

$$\Phi = \vartheta(x,y,\eta)\,, \qquad \text{with} \qquad \vartheta = \langle\varphi(\mathbf{x})\rangle\,, \quad (4.3.4)$$

where $\mathbf{x} = (x,y,z)$ denotes the vector of spatial coordinates. From equation (4.3.4), Φ

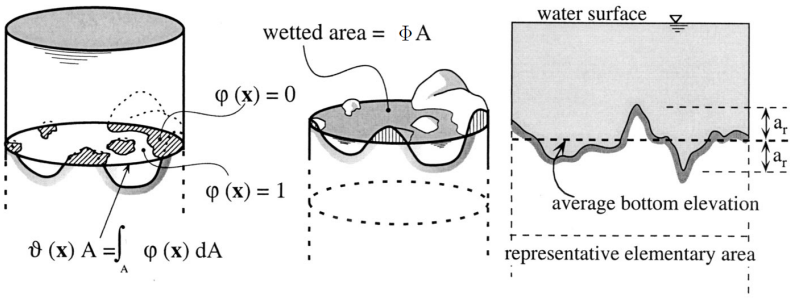

Figure 4.4: Definition sketch of φ, ϑ, Φ and a_r (adapted from Defina 2000).

is related to the function ϑ which can be expressed statistically as the probability that the local bottom elevation ζ, within a representative elementary area A being typically of the size of a computational element, does not exceeds the generic elevation z. In other words, ϑ represents the fraction of A lying above the ground surface; Φ constitutes its wet fraction and $\varphi(\mathbf{x})$ is a phase function detecting the bottom surface correspondingly (Figure 4.4).

Y is the water volume per unit area representing an effective water depth [m], reading:

$$Y = \int_{-\infty}^{\eta} \vartheta dz \,, \tag{4.3.5}$$

Judging by figure 4.4, $\vartheta(\mathbf{x})$ depends in fact on the statistical distribution of bottom elevation within each representative elementary area used to discretize the flow domain. Under the assumption that, as a first approximation, the probability density function of bed elevations distributed around the mean bed elevation is Gaussian, the function $\vartheta(\mathbf{x})$ can be expressed analytically through the following equation:

$$\vartheta(\mathbf{x}) = \frac{1}{2}\left[1 + \mathrm{erf}\left(2\frac{(z-\bar{\zeta})}{a_r}\right)\right] \,, \tag{4.3.6}$$

where $\mathrm{erf}()$ is the error function, $\bar{\zeta}$ is the mean bed elevation and a_r represents the amplitude of ground irregularities (see figure 4.4). Similarly, Φ and Y can be expressed as follows:

$$\Phi(\mathbf{x}) = \frac{1}{2}\left[1 + \mathrm{erf}\left(2\frac{(\eta-\bar{\zeta})}{a_r}\right)\right] \,, \tag{4.3.7}$$

and

$$Y = a_r \left\{ \Phi \frac{\eta - \bar{\zeta}}{a_r} + \frac{1}{4\sqrt{\pi}} \exp\left[-4 \left(\frac{\eta - \bar{\zeta}}{a_r} \right)^2 \right] \right\} , \tag{4.3.8}$$

The phase-averaging procedure offers clear advantages for treating flows over partially dry areas (wetting and drying). First, it is easily recognisable that when the amplitude of ground irregularities a_r is much lower than the water depth, the classical 2D depth-averaged shallow water equation can be recovered from equations (4.3.1), (4.3.2) and (4.3.3). Indeed, suppose a water depth D being defined as the difference between the free surface elevation η and the mean bottom elevation $\bar{\zeta}$. If $a_r \ll D$, the area A becomes completely wet and $\Phi = 1$. Therefore $Y = D$ and all the parameters in the momentum equations reduce to the usual expressions (Defina, 2000). As a consequence, this weighting and drying method holds indifferently for wet and partially wet elements and does not require a prior identification of partially wet elements, making this method applicable to classic numerical schemes without any *ad hoc* modifications (D'Alpaos et al., 2007b).

However, when $a_r \gg D$, a completely different picture of the flow field holds. Indeed, the resulted high bottom irregularities strongly affect the free surface elevation, and the assumption of smoothed water surface cannot remain. The bottom irregularities induce water flux concentrations following sinuous paths giving the appearance of a shallow-braided channel patterns (Defina, 2000). Despite the resulted drawbacks, the proposed method is still successful in inhibiting any spurious velocities or any numerical instabilities related to the flow field which typically arise when dealing with very shallow flows.

For the case of turbulent flow over a rough wall, the magnitude of the components of the Energy slope J_x and J_y in equations (4.3.1) and (4.3.2) respectively yields:

$$J = \frac{\tau}{\gamma Y} = \frac{\mathbf{q}^2}{K_s^2 H^{10/3}} , \tag{4.3.9}$$

where τ is the total shear stress [N.m^{-2}], $\mathbf{q} = (q_x, q_y)$ is the magnitude of the flow rate per unit width $\mathbf{q} = \sqrt{q_x^2 + q_y^2}$ [m^{2}s^{-1}], K_s is the hydrodynamic Gauckler Strickler's roughness coefficient [m$^{1/3}$s^{-1}] and H is an equivalent water depth.

The bed shear stress depending on the sediment grains (i.e., skin friction) is expressed as follows:

$$\tau_g = \frac{\rho_w g \mathbf{q}^2}{K_{s_g}^2 Y^{7/3}} , \tag{4.3.10}$$

where ρ_w is the density of water [kg.m^{-3}], g is the gravitational acceleration [ms^{-2}] and K_{s_g} is the grain (or surface) Strickler's roughness coefficient [m$^{1/3}$s^{-1}].

In order to solve the closure of the Reynolds stresses which appear in equations (4.3.1) and (4.3.2), as customary, a suitable eddy viscosity is introduced and evaluated by means of a Smagorinski model. The horizontal component of the Reynolds stresses then read:

$$R_{xx} = 2\nu_e \left(\frac{\partial q_x}{\partial x} \right) , \qquad R_{xy} = \nu_e \left(\frac{\partial q_x}{\partial y} + \frac{\partial q_y}{\partial x} \right) , \tag{4.3.11}$$

In reality, the eddy viscosity ν_e in equation (4.3.11) differs from the standard one as it also encloses the contribution from the stresses produced by the subgrid momentum exchange, $-\rho\varphi\langle\tilde{u}\tilde{\mathbf{v}}\rangle$ and $-\rho\varphi\langle\tilde{v}\tilde{\mathbf{v}}\rangle$ which are yet difficult to evaluate owing to their dependence on the full three-dimensional morphology of the ground surface (Defina, 2000).

The sediment transport and bed evolution module

The morphodynamic model, which encompasses the coupled sediment transport and bed evolution modules is grouped in the STABEM (Sediment Transport And Bed Evolution Model) developed by Carniello et al. (2012). This model has been designed to simulate the resuspension, deposition and transport of sediments by wind waves and tidal currents offering the possibility to include a two size-class mixture of sediments, which makes feasible to model the simultaneous presence of cohesive and non-cohesive sediments as well as their mutual interactions (Carniello et al., 2012). In the present study, emphasis is placed on the evolution of tidal channels and salt marshes in a sediment rich context which can characterize the innermost areas of tidal environments. For this reason, consistently with field observations, only one sedimentological class of cohesive material is considered and the wind-wave effect is neglected in view of the highly limited fetch characterizing these areas. The reader is invited to (Carniello et al., 2012) for a full description of the morphodynamic module with its full potential.

Since cohesive sediments are usually transported in suspension, the role of advection cannot be neglected. Under the assumption of turbulent flow and in accordance with the dimensions considered to describe the problem, this mode of transport takes the form of a 2D depth-averaged advection-dispersion equation, yielding:

$$\frac{\partial(CY)}{\partial t} + \nabla\mathbf{q}C - \nabla\left(\mathbf{D}Y\nabla C\right) = Q_e - Q_d \,, \tag{4.3.12}$$

where $C(\mathbf{x}, t)$ is the depth averaged volumetric sediment concentration, $\mathbf{D}$ is the two dimensional diffusion tensor, and Q_e and Q_d are the respective erosion and deposition fluxes. Equation (4.3.12) can be further simplified by assuming that the dispersion can be neglected compared to advection (Pritchard and Hogg, 2003).

The evolution of bed topography results from mass conservation, which considering a single size of sediment particles reads:

$$(1-p)\frac{\partial \zeta}{\partial t} = Q_d - Q_e \,, \tag{4.3.13}$$

where ζ is the local bottom elevation and p is the bed porosity which is assumed constant in our analyses, thus neglecting compaction processes. Equation (4.3.13) stipulates that the morphological changes derive directly from the net balance between erosion, Q_e, and deposition, Q_d, rates.

The erosion flux Q_e can be expressed by means of the following formula reading:

$$Q_e = M_m T \quad \text{with} \quad T = -1\left[1 + \left(\frac{\tau_g}{\tau_{cr,e}}\right)^2\right]^{1/2} , \tag{4.3.14}$$

where M_m is the specific entrainment for pure mud, T is the transport parameter and $\tau_{cr,e}$ is the critical shear stress for erosion. In fact, equation (4.3.14) slightly departs from the classic erosion formulation from Partheniades (1965) which evaluates the transport parameter T as follows:

$$T = \max\left[0; \left(\frac{\tau_g}{\tau_{cr,e}} - 1\right)\right] , \tag{4.3.15}$$

In fact, the transport parameter T calculated in equation (4.3.14) is based on the assumption that both the bed shear stress and critical shear stress are random and distributed according to a log-normal probability density function (Grass, 1970; Bridge and Bennett, 1992). As a matter of fact, due to factors such as turbulence, non-uniform flow velocity and irregular bottom topography, the bottom shear stress is very unsteady and non-uniform. Similarly, this non-uniformity characterises the critical shear stress notably as a result of the random grain exposure and bed composition in time and space (Carniello et al., 2012). The effect of adopting such a stochastic approach is therefore to smooth out the transition between $T = 0$ and $T = (\tau_g - \tau_{cr,e})/\tau_{cr,e}$ which appears to be rather sharp when using equation (4.3.15), especially in the case of shallow micro-tidal basins close to equilibrium where bed shear stress and critical shear stress are very close (Carniello et al., 2012). The erosion flux Q_e can be also influenced in line with some

eco-geomorphic mechanisms coming into play as soon as vegetation starts colonising portions of the tidal domain and will be reviewed in Section 4.3.1.

The presence of vegetation can influence also the deposition flux Q_d, which is therefore made up of three contributions as follows:

$$Q_d = Q_{dt} + Q_{db} + Q_{ds}\,, \tag{4.3.16}$$

where Q_{dt} is the rate of particle capture by plant stems, Q_{db} is the production of organic sediments due to the presence of vegetation, and Q_{ds} is the settling rate of suspended sediments possibly enhanced due to plant drag. These eco-sedimentary processes will be described in Section 4.3.1 in further detail. Obviously, if the marsh is not vegetated, both Q_{dt} and Q_{db} vanish, whereas Q_{ds} only depends on physical processes (settling of sediments) evaluated by the formula proposed by Krone (1962):

$$Q_{ds} = w_s\, C\, \max\left[0; \left(1 - \frac{\tau_g}{\tau_{cr,d}}\right)\right]\,, \tag{4.3.17}$$

where w_s is the settling velocity in still water [ms^{-1}], and $\tau_{cr,d}$ is a critical shear stress for deposition, i.e., below which all the suspended sediments deposit. Such an empirical description usually characterises the deposition of cohesive sediments in coastal environments Krone (1987).

Once sediment fluxes have been evaluated, the evolution of bed topography results from mass conservation, which considering a single size class of sediments, reads:

The ecological module

The halophytic vegetation colonising the marsh platform dissected by the tidal networks is often termed as an "ecosystem engineer" (Jones et al., 1994), capable of tuning the landscape topography to elevation ranges offering more favourable conditions for its growth (e.g., Marani et al., 2013). This contribution to the overall landscape morphological evolution is possible through a range of eco-geomorphic processes. Indeed, vegetation productivity contributes to sedimentation on the marsh platform by means of three processes: the capture of sediments by plant stems through the canopy Q_{dt}, the production of organic sediments Q_{do}, and the enhanced settling of suspended sediments Q_{ds} due to plant drag leading to a reduction of the turbulence through the canopy (e.g., Mudd et al., 2010). Such mechanisms translate the coupling between biotic factors (e.g., plants) and physical processes, therefore depending on vegetation characteristics, and particularly on plant biomass which becomes necessary to evaluate.

As it will be further pointed out in Chapter 5, in a given estuary with relatively constant tidal amplitude, temperature, and sediment supply, marsh elevation becomes the dominant factor in determining plant biomass (Morris et al., 2002). The spatial distribution of the biomass density B is therefore described as a function of the local bottom elevation ζ:

$$B(\zeta) = b(\zeta)\, B_{max}\,, \tag{4.3.18}$$

where B_{max} is the maximum biomass density and $b(\zeta) \in (0, 1)$ represents the distribution of the dimensionless biomass density in the tidal frame.

The structure of equation (4.3.18) implies that biomass adapts instantaneously to elevation change. Of course, this assumption is not strictly valid (e.g., because of the seasonal variations) on a short time scale, but holds over medium-to-long temporal scales, when the analysis does not aim to reproduce the actual sequence of the vegetation colonization, but only the net results over a few years. As we will discuss later, this assumption is also consistent with the use of a relatively large morphological factor for accelerating the morphodynamic simulations. Nonetheless, this formulation provides a simple quantitative means for the representation of the well-documented feedback between salt marsh ecology (marsh vegetation) and geomorphology (marsh elevation) (Marani et al., 2007, 2010).

Different parameterizations can be adopted for the biomass-elevation relationship $b(\zeta)$ in equation (4.3.18). In particular, we consider two cases: a continuous relationship modified after Marani et al. (2013), and a simplified discontinuous linear relationship reported in D'Alpaos et al. (2007b). Referring, for sake of simplicit,y to the dimensionless biomass density $b(\zeta)$, we recast the Marani et al. (2013) continuous formulation as $b(\zeta) = B/B_{max} = f(\zeta)/f_{max}$, where

$$f(\zeta) = \frac{2}{\exp\left(\lambda_1\left(\zeta - \zeta_0\right)\right) + \exp\left(-\lambda_2\left(\zeta - \zeta_0\right)\right)}\,, \tag{4.3.19}$$

and f_{max} is its maximum value (in order to rescale the maximum of b to 1).

In equation (4.3.19), ζ_0 depends on the optimal elevation, namely the elevation at which the vegetation is the most productive ($b(\zeta_0) = 1$ if $\lambda_1 = \lambda_2$), and λ_1 and λ_2 are parameters controlling the rate at which the biomass B tends to zero away from its maximum and can be chosen to be equal or different in order to depict a symmetric or asymmetric function respectively.

In an attempt to investigate emergent geomorphic patterns in marshes characterized

by different ecology across the world, we include two vegetation scenarios following D'Alpaos et al. (2007b). The first scenario (hereinafter referred to vegetation type-1 scenario) portrays marshes colonized by pioneer species such as *Spartina alterniflora*, characterizing the marshes located in the Northern American East Coast, which typically appear as monospecific contexts. The second scenario (vegetation type-2 scenario) portrays marshes colonized by multiple species and characterizes the plant ecology of the majority of marshes worldwide.

Based on the findings of Morris et al. (2002), in the vegetation type-1 scenario (monospecific), the plant biomass depicts its maximum productivity in marsh regions situated near mean sea level. Vegetation rapidly dies back for lower marsh elevations due to increasing hypoxia conditions while the plant biomass progressively diminishes for higher elevations due to the reduction of the hydroperiod and frequency of flooding leading to higher rates of salinity in pore waters. We therefore transcribe this relationship in the discontinuous formulation as follows:

$$b(\zeta) = \begin{cases} 0 & \text{if} \quad \zeta < \zeta_{min} \\ \dfrac{\zeta_{max} - \zeta}{\zeta_{max} - \zeta_{min}} & \text{if} \quad \zeta_{min} \leq \zeta \leq \zeta_{max} \\ 0 & \text{if} \quad \zeta > \zeta_{max} \end{cases} \tag{4.3.20}$$

where ζ_{min} is the minimum elevation at which *Spartina alterniflora* starts colonizing the marsh platform and ζ_{max} is the maximum elevation that *Spartina alterniflora* can tolerate. In accordance with field observations (e.g. Frey and Basan, 1978), $\zeta_{min} =$ MSL (Mean Sea Level) and $\zeta_{max} =$ MHT (Mean High Tide).

On the contrary, field and remote sensing analyses of marshes covered by a variety of halophytic species provide evidence for the increase in vegetation richness and density, hence vegetation biomass with soil elevation (Silvestri et al., 2005).

In this respect, in the case of vegetation type-2 scenario (multiple species), a different equation can be used:

$$b(\zeta) = \begin{cases} 0 & \text{if} \quad \zeta < \zeta_{min} \\ \dfrac{\zeta - \zeta_{min}}{\zeta_{max} - \zeta_{min}} & \text{if} \quad \zeta_{min} \leq \zeta \leq \zeta_{max} \\ 1 & \text{if} \quad \zeta > \zeta_{max} \end{cases} \tag{4.3.21}$$

where we set $\zeta_{min} =$ MSL and $\zeta_{max} =$ MHT (D'Alpaos et al., 2007b).

To allow fair comparisons with the continuous formulation of equation (4.3.19), we set ζ_0 according to an optimal elevation equal to MSL and MHT for the vegetation

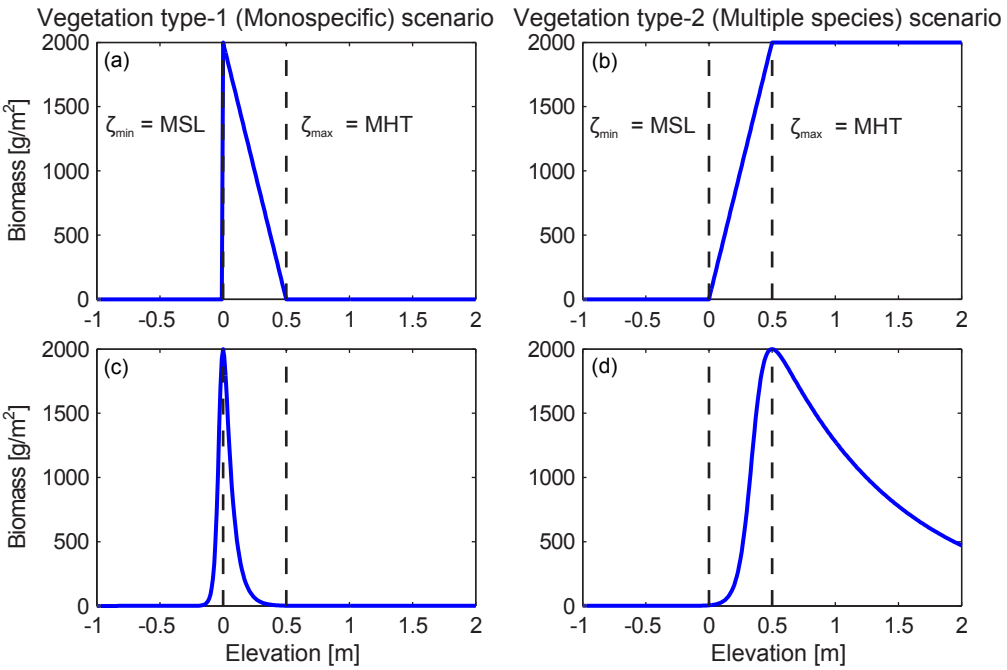

Figure 4.5: Halophyte biomass for the two ecological scenarios (left column: type-1, monospecific; right column, type-2, multiple species), evaluated using: the discontinuous formulation D'Alpaos et al. 2007b (first row); the continuous function, modified after Marani et al. 2013 (second row).

type-1 and type-2 scenarios respectively. Figure 4.5 graphically represents the biomass density as a function of marsh elevation according to the two ecological scenarios (type-1 and type-2) and evaluated mathematically by means of the two considered formulations (continuous and discontinuous). Vegetation dynamics in salt marshes will be further discussed in Chapter 5.

Other vegetation characteristics such as stem density n_s [m^{-2}], stem diameter d_s [m], stem averaged height h_s [m], and projected plant area per unit volume a_s [m^{-1}], come into play in some of the eco-geomorphic processes and need to be specified. For sake of simplicity, and considering the lack of empirical data, apart from the large dataset provided by Morris and Haskin (1990), they are assumed to be a function of the vegetation biomass B. On the basis of a long term record of *Spartina alterniflora* productivity in the North Inlet estuary, USA, (Morris and Haskin, 1990), Mudd et al. (2004, 2010) found that these variables follow power law distributions, namely:

$$n_s = \alpha_n B^{\beta_n}\,, \qquad h_s = \alpha_h B^{\beta_h}\,, \qquad d_s = \alpha_d B^{\beta_d}\,, \qquad a_s = \alpha_a B^{\beta_a}\,, \quad (4.3.22)$$

where α_n, β_n, α_h, β_h, α_d, β_d, α_a and β_a are empirical coefficients. Following D'Alpaos et al. (2007b), similar relationships are assumed to hold for the case of the marshes colonized by multiple species to allow a fair comparison between the two ecological scenarios.

Once the vegetation related variables have been evaluated, some of the eco-geomorphic processes, notably the eco-sedimentary processes induced by the presence of the halophytic vegetation can be formulated. Following the approach of Palmer et al. (2004), the particle capture process Q_{dt} reads:

$$Q_{dt} = C\,U\,\epsilon\,d_s\,n_s\,\min\left(h_s; Y\right)\,, \qquad \epsilon = \alpha_\epsilon \left(\frac{\mathbf{U} d_s}{\nu}\right)^{\beta_\epsilon} \left(\frac{d_{50}}{d_s}\right)^{\gamma_\epsilon}\,, \tag{4.3.23}$$

where U is the magnitude of the velocity [ms^{-1}], ϵ is a capture efficiency, describing the rate at which a particle in suspension is being trapped by plant stems, d_{50} is the particle size [m], ν is the water kinematic viscosity [m^2.s^{-1}], and α_ϵ, β_ϵ and γ_ϵ are empirical coefficients.

The second eco-sedimentary process considered in equation (4.3.16) concerns the production of organic sediments which can be related to the annually averaged aboveground plant dry biomass following the work of Randerson (1979). Thereby, similarly with D'Alpaos et al. (2007b), the formulation for the rate of organic sediment production Q_{db}, proposed by Mudd et al. (2004), reads:

$$Q_{db} = Q_{db,0}\,b\,, \tag{4.3.24}$$

where $Q_{db,0}$ [m.yr^{-1}] is a typical deposition rate derived empirically.

Finally, the third parameterized eco-sedimentary process regards the enhanced settling of inorganic sediments. Indeed, in addition to the process of sediment trapping by plant stems, the concomitant influence of plants on velocity and turbulence during tidal flooding also participates in the settling of inorganic sediments. A number of researchers have found that these two hydrodynamic quantities tend to reduce with increasing stem density (Leonard and Luther, 1995; Leonard and Croft, 2006). As customary in numerical models dealing with physical-biological interactions, the flow resistance due to the presence of vegetation is parameterized by means of the bed roughness to implicitly account for the effect of plant flow interaction on deposition. Let us consider the total shear stress τ, which can be decomposed as follows:

$$\tau = \tau_g + \tau_r + \phi\,\tau_v\,, \tag{4.3.25}$$

where τ_r is the shear stress produced by any irregular topography or macro-roughness triggering local hydrodynamic dissipation, and τ_v is the shear stress due to the drag exerted by the vegetation, weighted by the parameter ϕ. The shear stress is typically evaluated as referred to roughness coefficients. Expressing therefore the shear stress in terms of the Gauckler-Strickler coefficient K_s, equation (4.3.25) yields:

$$K_s^{-2} = K_{s_g}^{-2} + K_{s_r}^{-2} + \phi\,K_{s_v}^{-2}\,, \tag{4.3.26}$$

where K_{s_g}, K_{s_r} and K_{s_v} are the coefficients evaluated for the processes described in equation (4.3.25). When the vegetation starts colonizing the marsh platform, ϕ increases leading to an increase in the right hand side term of equation (4.3.26), and so to a decrease in the effective total roughness K_s. The decrease in K_s determines a decrease in the velocity $\mathbf{q}$, and as a consequence a reduced value of the bottom shear stress, eventually favouring the settling of suspended sediments Q_ds included in equation (4.3.17). Since τ_v is mediated by the presence of biomass B, as a first approximation we assume that the weight factor is linearly proportional to the dimensionless biomass density, i.e. $\phi = b$.

Therefore, vegetation primarily contributes to surface sedimentation in the model by means of these eco-sedimentary processes, whose rates highly depend on elevation related vegetation characteristics and notably on vegetation productivity (i.e., biomass distribution within the tidal frame).

However, other eco-geomorphic processes remain still poorly understood. For instance, most of the mathematical models simulating marsh platform evolutions assume that the erosion flux Q_e vanishes over vegetated marsh platforms due to the impeded flow through the vegetation canopy, the resulting flow being too weak to produce excess shear stress and therefore net erosion. Although such an assumption stems from field observations (e.g., Christiansen et al., 2000), it also poses the question of the dependence of the erosion rate on the spatial distribution and the density of the already established vegetation. Indeed, the conceptual model of Yapp et al. (1917) and the more recent contribution of Temmerman et al. (2007) indicate that vegetation, distributed sparsely over the marsh platform in the form of hummocks, promotes instead channel erosion, depicting therefore a negative feedback between vegetation productivity and marsh elevation. Furthermore, Bouma et al. (2009) demonstrated in a laboratory experiment

that the prevalence of one of the feedbacks over the other is a function of vegetation density. In view of these considerations, we assume that, as a first approximation, the erosion decreases linearly as plant biomass increases, namely:

$$Q_e = Q_{e_0} (1 - b) \ , \tag{4.3.27}$$

where Q_{e_0} represents the erosion flux in absence of vegetation, calculated in equation (4.3.14) as Q_e. This formulation, although simplified, retains the overall dynamics of the eco-geomorphic process.

4.3.2 Model setup

The sets of numerical experiments were performed on a computational domain of dimensions 600 m $\times$ 400 m. The domain, although conceptual, seeks to be representative, by dimension, configuration and bathymetry of a typical shallow mudflat located in the innermost areas of a lagoon; the reduced water depth, as well as the possible presence of vegetation, allow to neglect the effect of wind waves in the subsequent analyses.

The initial bathymetry consists of an intertidal mudflat deprived of existing tidal networks and characterized by random (normally distributed) elevation perturbations ε. Different amplitudes and degrees of smoothness of these perturbations are tested (see Figure 4.6), but the mean bottom elevation on the mudflat is kept at a value ζ = -0.10 m above MSL.

The initial conditions are set for the free surface elevation ($\eta = 0$, corresponding to MSL), the velocity (still water) and for the suspended sediment concentration ($C = 0$ mg.l^{-1}). As a note, the effect of these initial conditions rapidly vanishes given the short length of the domain.

Three boundaries of the rectangular domain are closed, with no-flux conditions applied, whereas the seaward channel bordering the lower edge of the domain constitutes the open boundary where a semi-diurnal sinusoidal tide with a reference amplitude $a =$ 0.5m (tidal range $R = 1$ m) is prescribed. This boundary condition is typical of tidal environments in micro-tidal regime (e.g., marshes in the Venice lagoon), for which the underlying morphodynamic modelling framework was designed. Along the open boundary condition, a uniform and stationary suspended sediment concentration C_0 is also applied, mimicking the supply of sediments to the tidal basin of which different scenarios of concentration values are considered.

The computational domain is discretized for the numerical solution using an unstruc-

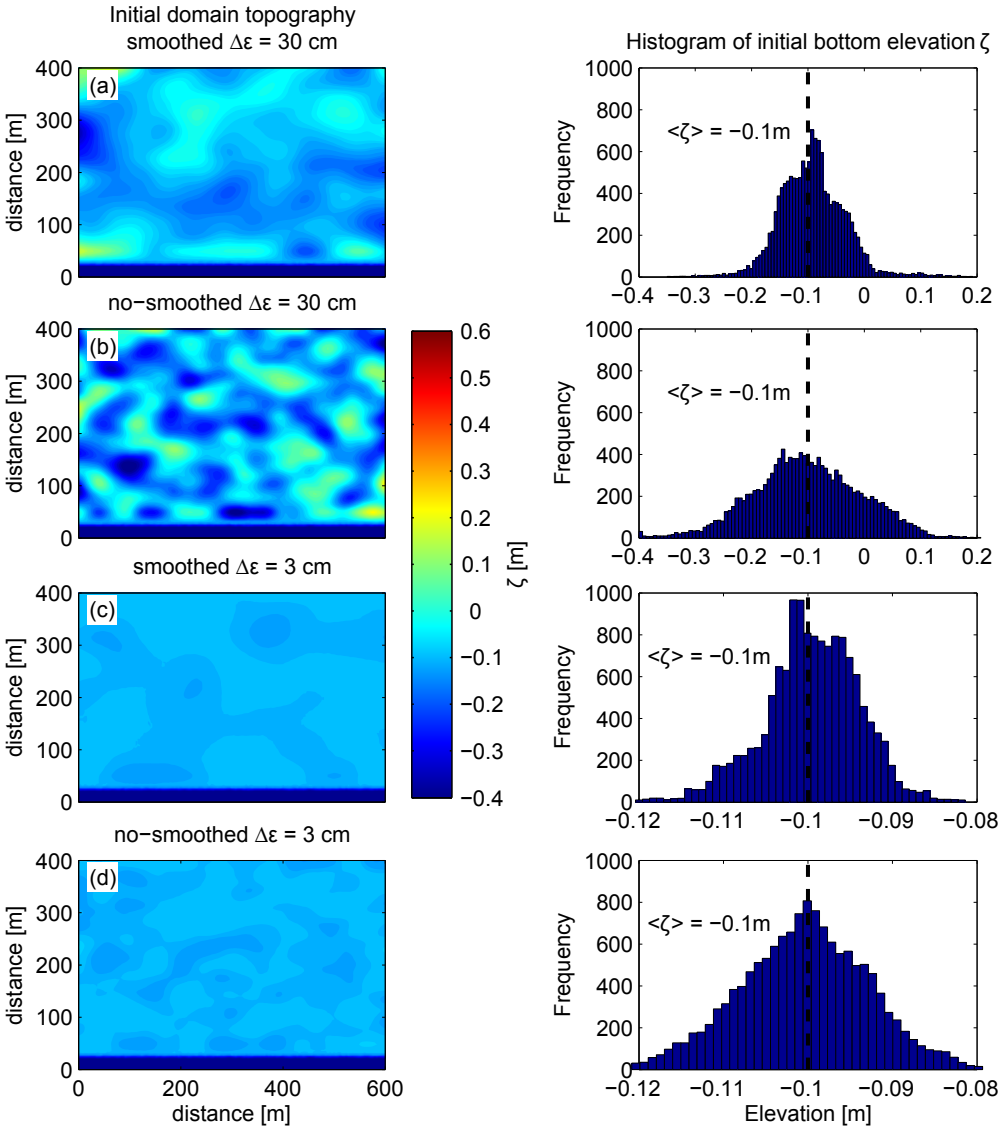

Figure 4.6: Four scenarios for the initial topographic configurations (left column) with their corresponding histograms of initial elevations ζ (right column), differing for the type of perturbations ε: (a) high and smoothed, (b) high and no-smoothed, (c) low and smoothed , (d) low and no-smoothed.

tured triangular mesh with a mean element size of 5 m. The computational sequence at each time step proceeds as follows: i) initial conditions provide information on the presence or absence of biomass and its related drag computed as in equation (4.3.25); ii) the hydrodynamic equations are solved by means of a semi-implicit staggered finite element numerical scheme, which is based on the classical Galerkin variational method; iii) the computed hydrodynamic field is fed into the sediment transport module in order to solve the advection-diffusion equation (4.3.12) and the different eco-geomorphic processes such as the eco-sedimentary contributions in equations (4.3.23) and (4.3.24), eventually summed up to compute the global deposition flux in equation (4.3.16), while vegetation mediation on the erosion flux is determined based on equations (4.3.14) and (4.3.27).

The bottom topography usually evolves on a longer time scale with respect to the hydrodynamics. This introduces the possibility to decouple the solution of the hydrodynamic field from the morphological evolution, an approach already implemented in several numerical modelling studies (e.g., Marciano et al., 2005; D'Alpaos et al., 2007b; Kirwan and Murray, 2007; van Maanen et al., 2013; Schwarz et al., 2014).

In addition, the computational effort required by the detailed hydrodynamic and sediment transport solvers makes impractical any long-term modelling application, unless the morphological changes, decoupled from the hydrodynamics, are artificially enhanced by using a "morphological factor".

In the present eco-geomorphic modelling framework, the increase in the rate of the morphological change is determined through a so-called "offline" method, as opposed to the "online" method (Roelvink, 2006). This method consists of multiplying the bed level changes integrated over a tidal cycle by a morphological factor M. This choice corresponds to adopt a morphodynamic time step for the evolution of bottom elevations given by M times the tidal period. Bed elevations are therefore updated, resulting in a new topographic configuration and consequently a new spatial biomass distribution. Then, a new morphodynamic iteration can be carried out. The computational sequence is summarised in Figure 4.7.

The morphological factor M is adjusted at every morphodynamic time step considering the actual bed change in relation to a reference value estimated as acceptable. Hence,

$$M = \frac{\Delta\zeta_{ref}}{\Delta\zeta_{max}}\,, \tag{4.3.28}$$

where $\Delta\zeta_{max}$ is the maximum bed level change over a tidal cycle calculated within the

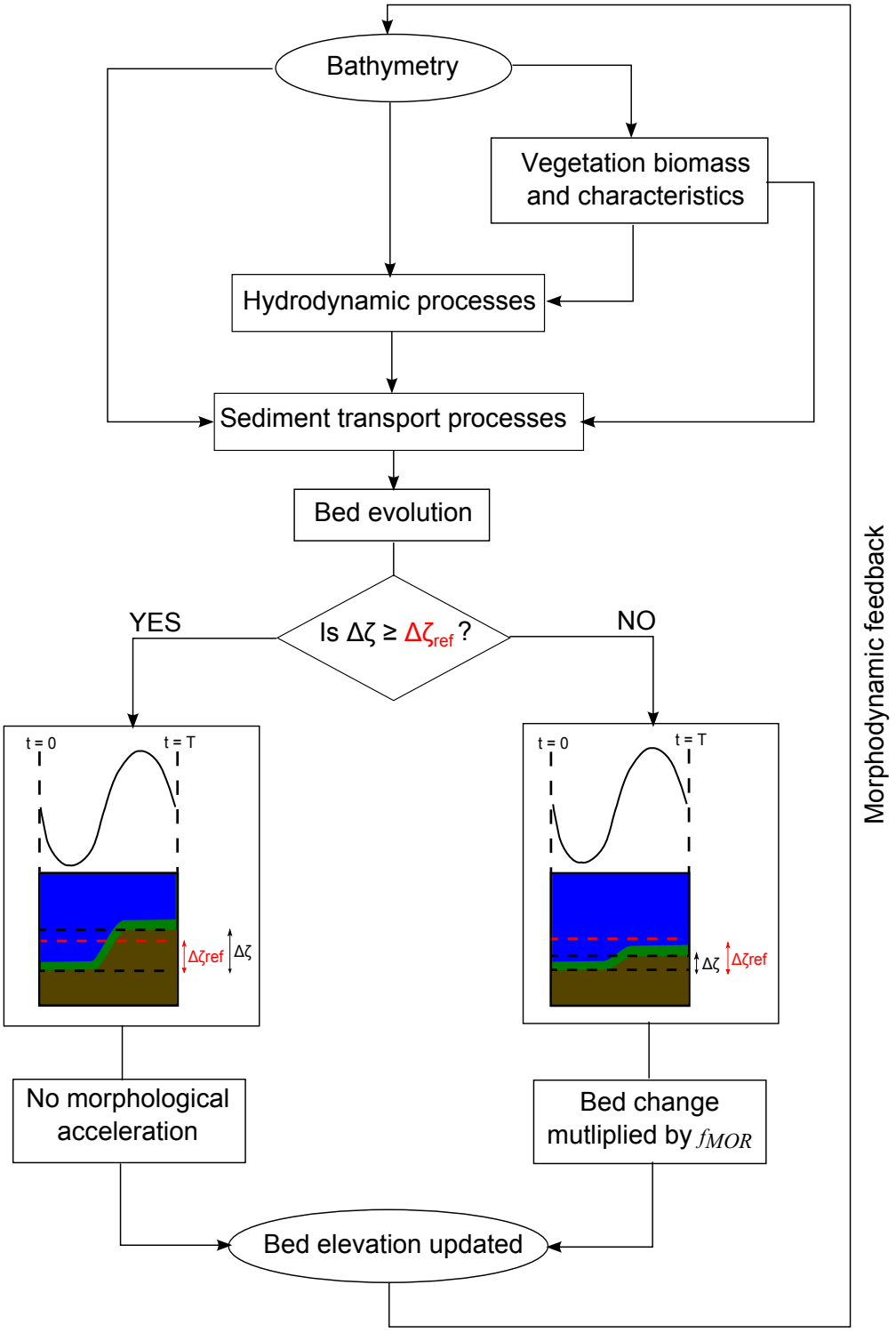

Figure 4.7: Flow diagram of a morphodynamic iteration.

domain, and $\Delta\zeta_{ref}$ is the maximum accepted change. Indeed, it is assumed that any morphological change lower than $\Delta\zeta_{ref}$ does not significantly affect the hydrodynamic computation during a tidal cycle, thus allowing for the theoretical repetition of the same hydrodynamic forcing determining the fluxes of sediments from and to the bottom (i.e., Q_e and Q_d). The morphological factor M, defined by equation (4.3.28), varies between 1 (which corresponds to a real-time morphodynamic computation) and a maximum value that is chosen arbitrarily to avoid excessively long morphological time steps.

The determination of the value of the reference bed level change $\Delta\zeta_{ref}$ followed a sensitivity analysis bearing in mind the idea that the applied artificial morphological acceleration must not alter the flow field. This consideration was transcribed by investigating the effect of applying different M values on hydrodynamic variables such as the bed shear stress and the magnitude of the flow velocities. Concretely, the sensitivity of M was explored by comparing two successive maps depicting the spatial distributions of the bed shear stress and/or the magnitude of the flow velocities: one map taken at the beginning of a tidal cycle and the other map taken at the end of the cycle once the morphology was updated by M. The comparison involves the computation of several statistics such as the absolute and percentage errors. Moreover, such an investigation was performed using different underlying topographic configurations (e.g., with semi developed, highly developed and without tidal networks) in order to assess the possible dependence of $\Delta\zeta_{ref}$ over different morphodynamic regimes.

This method allows one to adapt M to different morphodynamic rate of change in the various marsh evolutionary stages (we found a maximum value of $M \simeq 5$, 10 and 90 for topographic configurations with semi developed, with highly developed and without tidal networks, respectively), so that the morphodynamic time step varies throughout the simulation period.

Every simulation is run for a period of 30 years to grasp information on both channel initiation and further stages of elaboration. The values of the physical and empirical parameters adopted throughout the different simulation sets are displayed in Table **??**.

4.4 Results

In the following, results of a series of numerical experiments aiming to bring further insights into the mechanisms governing tidal network ontogeny are presented. At first, the influence of the sediment supply on tidal channel formation and further evolution is analysed by applying different sediment supply scenarios. In a second stage, the inves-

Table 4.1: Values of parameters used in the simulations

Parameter	Value	Ref.	Parameter	Value	Ref.
$\tau_{cr,e}$	0.4 Pa	[1]	γ_ϵ	2.08	[5]
$\tau_{cr,d}$	0.1 Pa	[2]	α_a	0.25	[6]
d_{50}	20 μm	[2]	β_a	0.5	[6]
p	0.4	[3]	α_d	0.0006	[7]
K_{s_v}	15 $\mathrm{m}^{1/3}\mathrm{s}^{-1}$	[4]	β_d	0.3	[8]
$Q_{db,0}$	0.002 m yr^{-1}	[1]	α_n	250	[6]
B_{max}	2000 g m^{-2}	[3]	β_n	0.3032	[6]
α_ϵ	0.224	[5]	α_h	0.0609	[7]
β_ϵ	0.718	[5]	β_h	0.1876	[8]
$\Delta\zeta_{ref}$	0.005 m		w_s	0.00034 m s^{-1}	
ζ_0 (veg. type-1)	-0.0183		ζ_0 (veg. type-2)	0.34785	
λ_1(veg. type-1)	15		λ_1 (veg. type-2)	1	
λ_2 (veg. type-1)	45		λ_2 (veg. type-2)	18	

References: [1]D'Alpaos et al. (2006); [2]Amos et al. (2004); [3]D'Alpaos et al. (2007b); [4]Chow (1959); [5]Palmer et al. (2004); [6]Mudd et al. (2004); [7]Gibbs (1985); [8]Fagherazzi and Furbish (2001).

tigation is devoted to the effect of applying different initial topographic configurations (from Figure 4.6) on the successive tidal channel development. Hence, this choice of controlling factors comes down to investigating the influence of a respective boundary and initial conditions, both being thought to control tidal channel morphodynamics. In parallel, through these different simulation sets, the morphological response of tidal channels to different ecological scenarios and their mathematical parameterisations is addressed.

4.4.1 Varying sediment supply

Figure 4.8, displays the final planview morphologies starting from an initial mudflat characterized by high and smoothed perturbations ε (i.e., Figure 4.6a). The different subplots show the final (after 30 years) morphological evolution of an initially unchannelised domain that was forced under different scenarios of sediment supply (rows are distinguished by the different values of the input sediment concentration C_0, ranging from 0 to 100 mg/l) and marsh ecology (the different columns refer to the case without vegetation, with vegetation type-1 and type-2, respectively). In this set of simulations, biomass distribution is estimated by means of the continuous formulation (see equation 4.3.19 and Figure 4.5 second row).

A variety of erosional and depositional mechanisms emerges from Figure 4.8, which highlights how the properties of the resulting tidal network change depending on sediment supply and vegetation type. Looking at the overall planview morphology, the sedimentation patterns, which increase with the sediment supply, are largely influenced by the course of the forming tidal channels and progressively slope away from them (e.g., Figure 4.8l). In fact, the inner areas of the simulated marshes are clearly lower than the edges, in accordance with previous observations in micro-tidal marshes such as in the Venice lagoon (e.g., Pignatti, 1966; Caniglia et al., 1997; Silvestri et al., 2005). Such a spatial distribution suggests that tidal waters and incoming suspended sediments are chiefly transported through the forming tidal channels rather than as sheet flow (Temmerman et al., 2005a), this hydrodynamics being consistent with flow regimes typically occurring in shallow basins under micro-tidal conditions.

It can be also noted, although with different planimetric and bathymetric characteristics, the formation of tidal channels is observed in all of the considered scenarios. The channel planview morphologies evoke an increase in channel maturity with increasing sediment supply. Indeed, while hydraulic path geometry in Figure 4.8a, b and c materialises the presence of ill-defined tidal channels characterized by shelving

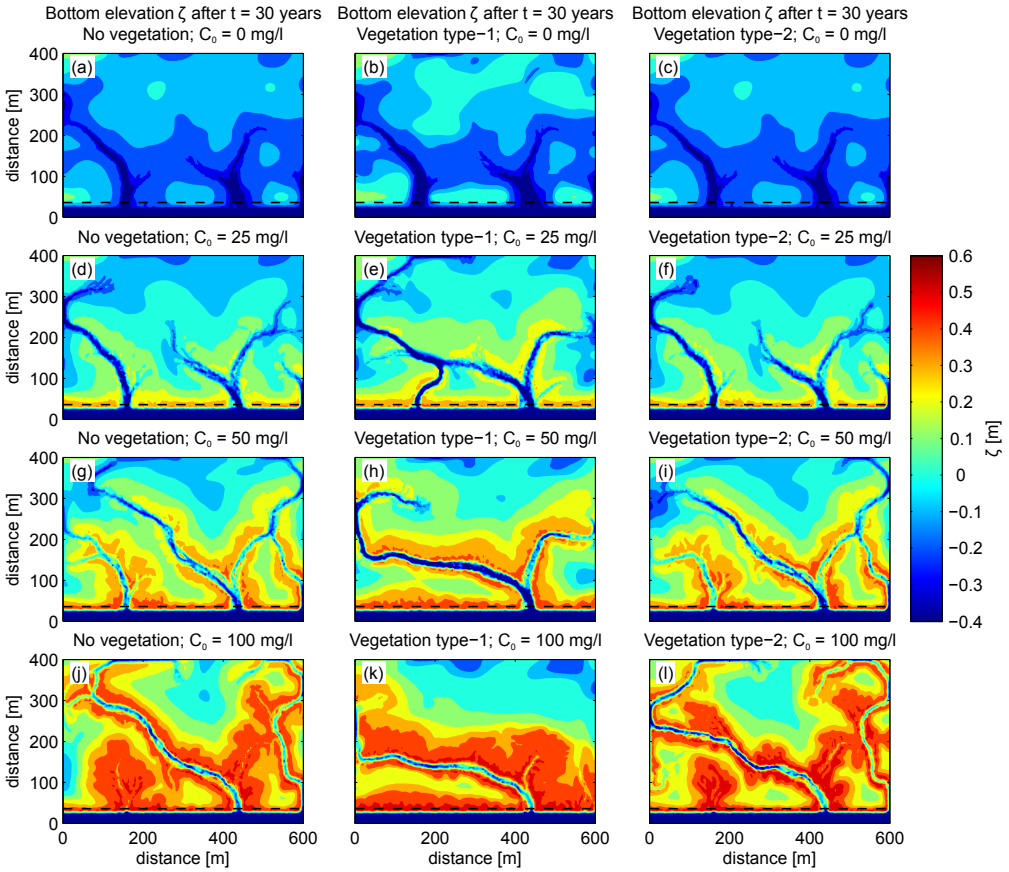

Figure 4.8: Simulated marsh morphologies after 30 years according to different sediment supply and marsh ecology, computed with the continuous formulation (equation 4.3.19). Columnwise: with different ecological scenarios. Rowise: with increasing sediment supply.

banks, more clearly defined features with marked banks describe, on the contrary, tidal channels developing under scenarios characterised by increasing sediment supply. The corresponding tidal networks also portray a higher degree of channel lengthening and sinuosity suggesting an increase in channel complexity together with sediment supply. Signs of channel senescence depict tidal networks developed under high incoming suspended sediment concentrations such as channel narrowing and even channel closure by sediment infilling (e.g., Figure 4.8j, k and l). These observations suggest that the various simulated tidal networks may be considered in different evolutionary stages.

As for the comparison between scenarios characterised by different ecological features, results point out to the importance of vegetation type in driving the overall morphodynamic evolution of the intertidal platform together with its biogeomorphic

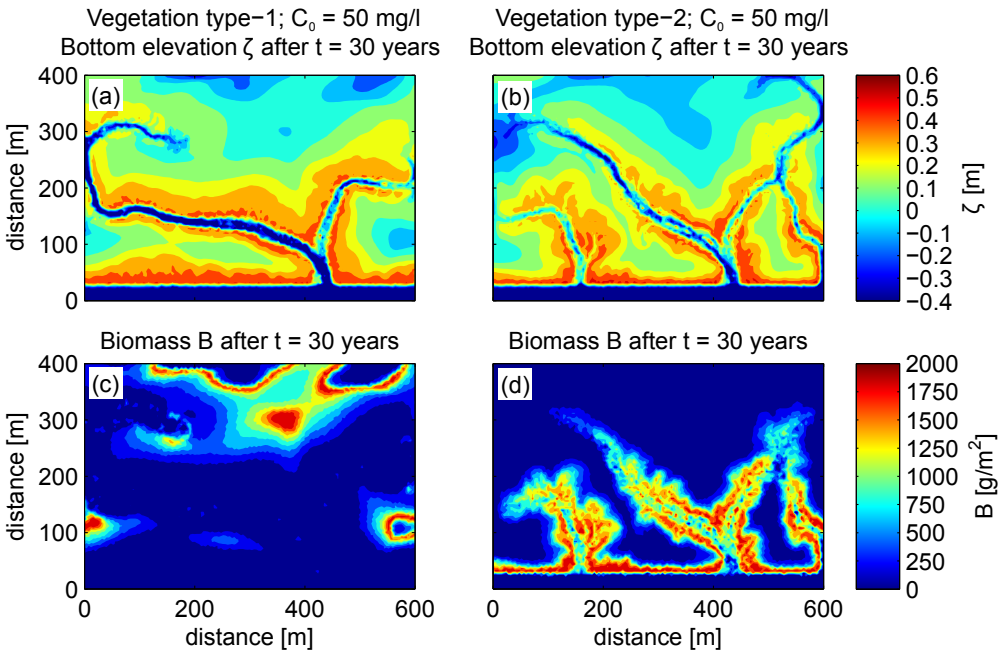

Figure 4.9: Biomass distribution for the simulated marsh morphologies (h) and (i) in Figure 4.8.

features. Notable discrepancies in marsh and channel planview morphologies arise when comparing simulations without vegetation (i.e., Figure 4.8d, g and j) and those characteristic of the type-1 (monospecific) vegetation scenario (i.e., 4.8e, h and k). On the other hand, although local discrepancies take place, the overall channel morphology remain fairly similar between simulations without vegetation and those characterized by type-2 (multiple species) vegetation scenario (i.e., 4.8f, i and l), the differences mainly regarding the presence of lateral shifts in channel location and elongation. Figure 4.9 compares the spatial distribution of bottom elevation and biomass for the cases (h) and (i) in Figure 4.8 ($C_0 = 50$ mg/l). The different ecological scenarios induce, in particular, distinct patterns of spatial biomass distribution.

In marshes colonized by monospecific vegetation species such as *Spartina alterniflora*, vegetated areas are pushed back to the landward side of the tidal basin (Figure 4.9c). This landward migration is explained by the inverse relationship between plant productivity and marsh elevation characterizing the vegetation type-1 scenario, as graphically illustrated in the left column of Figure 4.5. Indeed, surface sedimentation decreases with distance from the seaward channel and the forming tidal channels as a result of the decrease in sediment deposition due to the reduction of the advective

transport and hydroperiod. As a consequence, regions near the seaward channel, where the incoming flux of sediments originates, experience the highest sedimentation rates during the first simulation years. The resulting elevation gain leads to the progressive die-back of the already established pioneer species. Moreover, the forming channels promote the transport and subsequent deposition of suspended sediments further landward, constraining eventually vegetation to regions not yet intertwined by tidal channels, as it emerges form Figure 4.9c.

Conversely, due to the positive relationship between biomass and marsh elevation in the type-2 (multiple species) vegetation scenario, maximum biomass productivity is found in proximity of the tidal channels. As a matter of fact, once channels have developed, the deposition process becomes a function of the hydraulic distance from this geomorphological component. Accordingly, it is maximal near the channels owing to the high magnitude of the advective fluxes and progressively decreases as moving away from the channel banks. The local accretion alongside the tidal channels produces favourable conditions for plant growth, which in turn enhances further sedimentation. Biomass patterns following the forming tidal channels (see Figure 4.9) are a clear manifestation of these bio-physical dynamics, in agreement with field observations (e.g., Pignatti, 1966; Silvestri et al., 2005). Thus, the model correctly reproduces the well-documented positive feedback mechanism between marsh elevation and plant productivity for marshes colonized by multiple species.

Figure 4.10 depicts the temporal evolution of the simulated tidal basin whose final morphology was displayed in Figure 4.8i. In accordance with field observations (Steers, 1939; Collins et al., 1987; D'Alpaos et al., 2007a), Figure 4.10 indicates that tidal channel formation is rather rapid with the initiation process already materialised after 3 years of simulation. By 9 years of simulation period, most of the basic imprinting of the tidal network has taken place. Then, channel elaboration development stage comes into play which is notably manifested by channel elongation. Subsequently, progressive signs of channel narrowing, infilling of first order channels, and even the beginning of channel segmentation allude to manifestations of channel senescence which is typical of tidal channels being in a integration development stage in accordance with (Steel and Pye, 1997; Allen, 2000)

Figure 4.11 displays the hypsometries of the final morphologies and suggests that different platform and channel morphological characteristics occur. The growing upward shift of the hypsometric curves with increasing sediment supply alludes to the progressive accretion of the marsh platform. The curves also tend to loose the typical

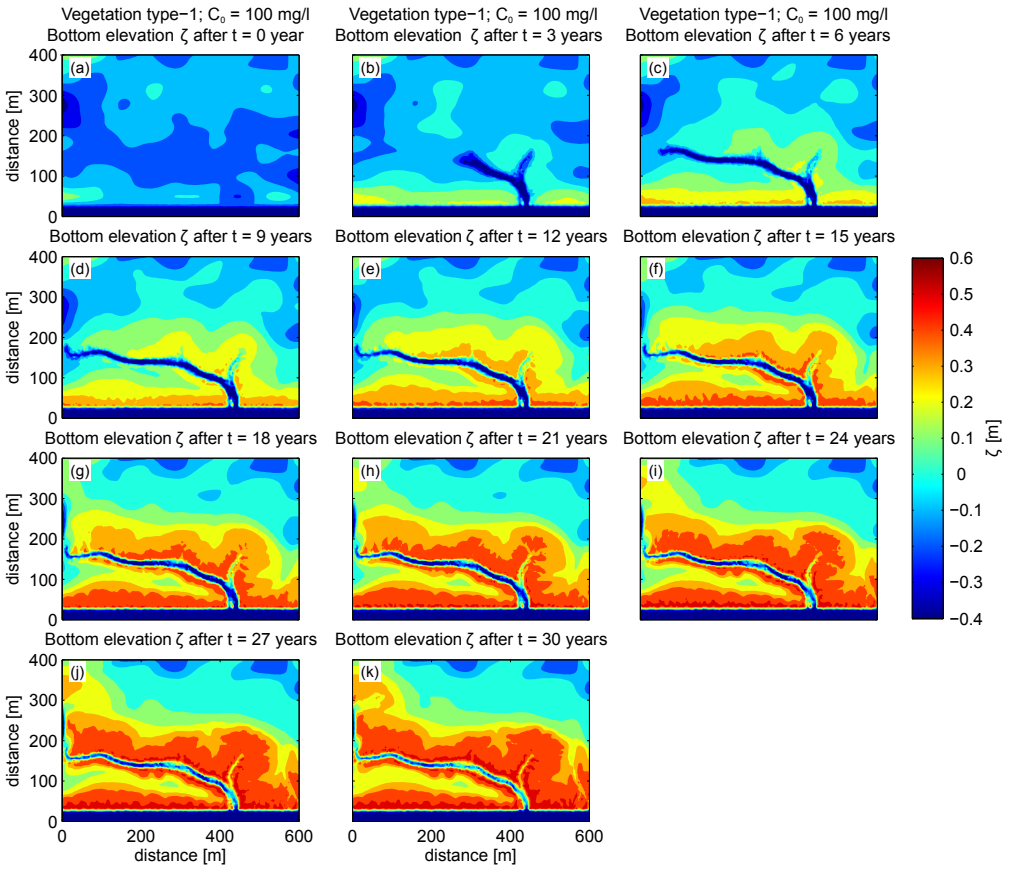

Figure 4.10: Time evolution of the simulation case depicted in Figure 4.8i characterised by an incoming suspended sediment concentration C = 100 mg/l and with a monospecific vegetation scenario computed by means of the continuous biomass-elevation relationship.

sigmoid shape towards the development of a linear profile followed by a sharp discontinuity. This is due to the transition from an initially perturbed topography characterized by depressions and rising ground features to a relatively flat topography being undercut by marked discontinuities represented by the presence of mature channels with distinct natural levees, and therefore corroborating with the observations from Figure 4.8.

Moreover, one can clearly distinguish the marked effect of vegetation enhancing sediment deposition. For instance, the sudden bump in curve (b) around MSL is clearly a manifestation of the production of organic sediments, which is the only depositional mechanism in this simulation due to the absence of inflowing suspended sediment concentration ($C_0 = 0$). Such eco-sedimentary processes are highlighted by this step-like pattern in some of the hypsometric curves (e.g., curves (h) and (k)). For a same sediment supply scenario, the hypsometry featuring tidal basins grown by single species (vegetation type-1) depicts the highest elevation with increasing domain area except for tidal basins under high accretional activity (e.g., compare curve (k) with respect to curves (j) and (l)). This peculiarity can be illustrated looking at the corresponding planview morphology of the specific case (k), (see Figure 4.8k), where the presence of a barrier-like depositional feature in the mid of the domain, and a relatively large area with low elevation landward (subject to little accretion over the simulation period), explain why the integrated elevation for the same percentage area is lower for this scenario compared to the two other ecological scenarios.

Figure 4.12 shows the temporal evolution of the relative difference of averaged bottom elevations between subsequent years. Morphological changes within the tidal basin appear to occur not only earlier but also higher in magnitude with increasing accretional activity. Except for the case of the simulations without sediment supply, this period of intense morphodynamic activity is then followed by a slower evolution indicated by the gradual decrease in relative changes, whose duration is also a function of the sediment supply.

Additionally, a stagnation in the landscape morphological evolution seems to portray the last years of the simulation period. This suggests that the different simulated morphologies are approaching a dynamic equilibrium configuration, in a sense that changes still occur in time but at a similar pace. This quasi-equilibrium state is typical of intertidal landscapes where static equilibrium is difficult to grasp owing to the variety of external drivers coming into play (De Vriend et al., 1993). This comparison further supports the observation that the synthetic tidal networks across the different simulation cases are in different development stages.

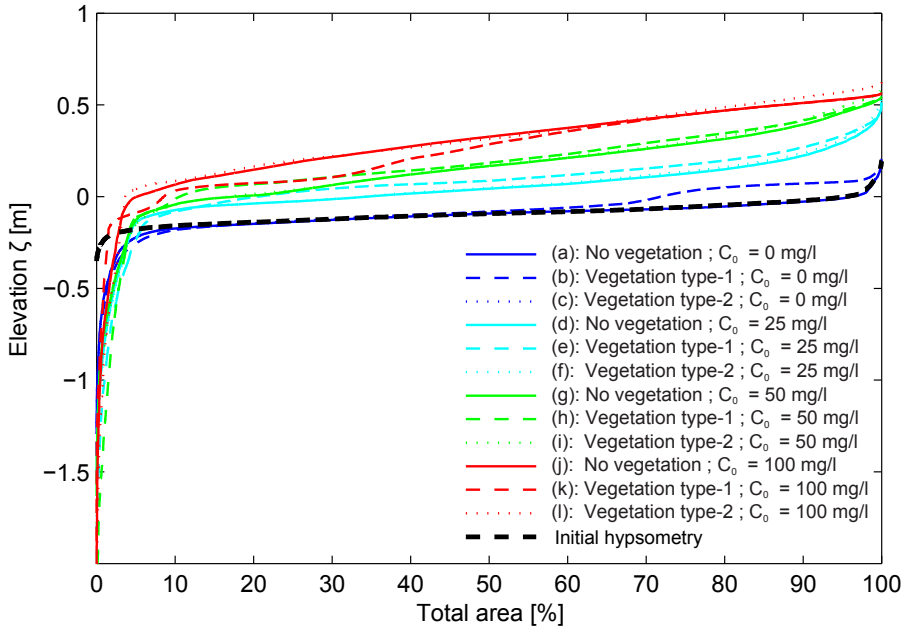

Figure 4.11: Hypsometric curves of the whole tidal basin for the simulated marsh morphologies after 30 years.

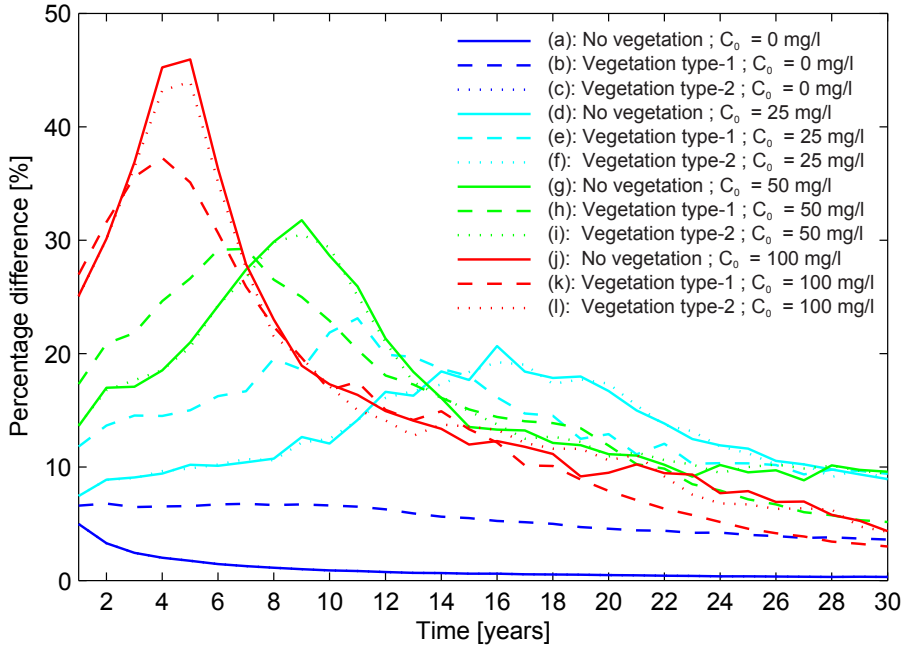

Figure 4.12: Relative change of averaged bottom elevations between consecutive years for the simulated morphologies.

A further analysis was performed to assess whether the synthetic tidal networks meet observed network statistical metrics in order to quantitatively validate the modeling framework. Figure 4.13 reports on the channel mouth cross-sectional area Ω (computed at MSL) of the tidal network common to all the simulated morphologies against the tidal prism P flowing through the corresponding outlet and evaluated at $t = 30$ years. The tidal prism P is computed as follows:

$$P = \frac{1}{2} \int_0^T q_y w \mathrm{d}w \tag{4.4.1}$$

where T is the tidal period [s], and w is the width of the network mouth [m], obtained by applying the network extraction procedure of Fagherazzi et al. (1999), described in Chapter 3.

Data in figure 4.13 are arranged in two clusters: a first cluster gathering the simulation cases with no external sediment supply and a second one comprising the remaining simulation cases. This clustering likely results from the different evolutionary stages of the underlying tidal networks. Indeed, the previous observations suggest that tidal networks developed under marsh regression context (i.e., absence of sediment supply, first cluster) are far from any morphological equilibrium.

A regression analysis between P and Ω performed on the second cluster shows that the data can be approximated by means of a power law regression model, in agreement with the well-established O'Brien-Jarrett-Marchi law (e.g., D'Alpaos et al., 2010):

$$\Omega = k\, P^{\alpha}\,, \tag{4.4.2}$$

where k and α are empirical coefficients. The value of the exponent α (see Figure 4.13) lies in the range $0.85 - 1.10$ in accordance with the empirical law (O'Brien, 1969; Jarrett, 1976) and is very close to the value $6/7$ theoretically derived by Marchi (1990).

As mentioned in Chapter 2, this scaling relationship provides a synthesis of the complex and site-specific feedbacks occurring between tidal channel geometry and tidal hydrodynamic regime.

The temporal evolution of the geomorphic relationship between Ω and P is also explored in Figure 4.14. A clear distinction emerges again between the simulations under marsh retrogression and those in marsh progradation contexts. Regardless of the ecology scenario, the channel cross-sectional area Ω for the three runs with no sediment supply (i.e., Figure 4.14a, b and c) increases throughout the simulation period. On the contrary, a global decrease with time in Ω and P characterises the simulation cases

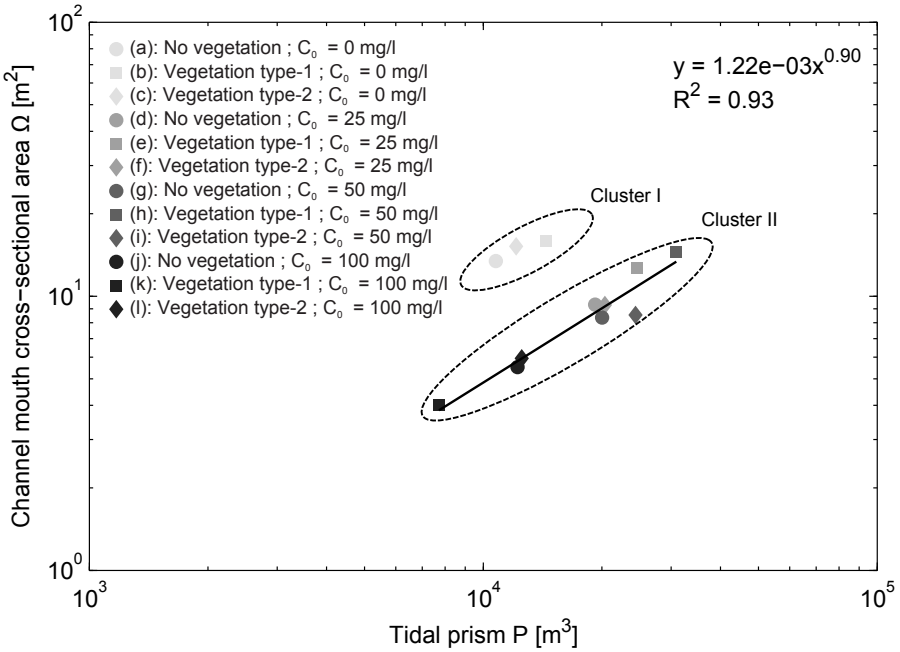

Figure 4.13: Log-log plot of the channel mouth cross-sectional area Ω versus spring tidal prism P for the mouth of the tidal sub-basin common to the simulated marsh morphologies (see Figure 4.8).

with high sediment supply.

An overall gradient from channel scouring towards progressive channel infilling is covered by the set of different simulations. These two contrasting processes acting on the morphological evolution of tidal channels imply that the synthetic tidal networks are in different morphological ages. More precisely, the time evolution of the relationship between Ω and P for simulations under high accretional activity exhibits an increase for the first years followed by a decrease until the end of the simulation period. In this latter period, the data may be approximated by a power law (e.g., Figure 4.14j, k and l). Such a pattern is qualitatively consistent with a similar investigation reported in D'Alpaos et al. (2010).

Another geomorphic measure addresses the drainage density of the synthetic tidal networks. According to Marani et al. (2003) and as previously pointed out in Chapter 3, the conventional Hortonian metrics appear to be unable to distinguish peculiarities in tidal network structures. Instead, site-specific features and important differences in network morphologies may only be captured by evaluating the unchanneled flow lengths l within the domain, namely the distance from any marsh point to the nearest channel. In tidal networks, determining such a measure requires the definition of flow

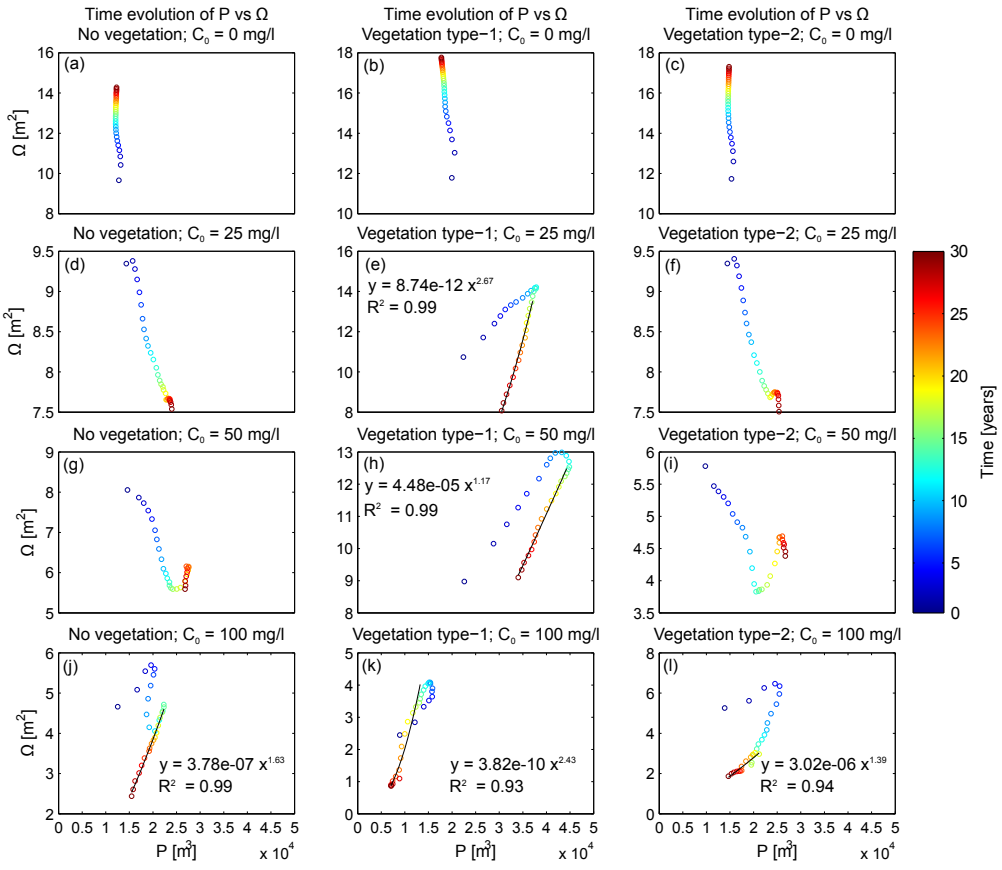

Figure 4.14: Log-log plot of the time evolution of the channel mouth cross-sectional area Ω versus spring tidal prism P for the mouth of the tidal sub-basin common to the simulated marsh morphologies (see Figure 4.8).

directions on the basis of hydrodynamic rather than topographic gradients. In the present contribution, we use the method proposed by Rinaldo et al. (1999a), introduced in Section 4.1.2, which consists of suitably simplifying the classical shallow water equations to a Poisson boundary value problem to solve the free surface elevations and thereby deduce drainage directions through the associated gradients. Figure 4.15 displays the semilog plot of the exceedance probability of the unchanneled flow lengths $(P \geq l)$ for the various simulated marsh morphologies. The statistical properties allow to perceive the tidal network capability to drain its basin, and therefore provide an appropriate definition of drainage density. The approximate linear trend of the curves alludes to exponential probability distributions, and therefore a pointed absence of scale-free properties in network structures. Such a property implies that the synthetic tidal networks manifest a scale dependency as opposed to scale invariance which is a chracteristic of fractals so prevalent in their fluvial counterparts, in agreement with previous studies (e.g., Marani et al., 2003; Feola et al., 2005).

Furthermore, apart from the simulation case characterized by $C_0 = 100$ mg/l with monospecific vegetation scenario (i.e., distribution (k)), the overall results point out to a decrease in the mean unchanneled flow length l, hence an increase in the drainage density, as the sediment supply increases. Such an observation reflects that the various synthetic tidal networks present different degrees of complexity, and so different evolutionary stages, corroborating the previous results.

The departure of the distribution (k) from this general relationship may be explained by the fact that the respective tidal network presents a course location that is restricted to the lower left region of the domain (see Figure 4.8k) because of a barrier-like structure produced by the intense deposition interacting with vegetation. Such a structure leaves a large portion of the tidal basin unchanneled, and consequently high unchanneled flow lengths.

4.4.2 Varying initial bathymetry

A further step of the analysis is devoted to investigate the influence of the initial conditions on the tidal network development. Figure 4.16 shows final planview morphologies obtained starting from the four initial topographic configurations displayed in Figure 4.6, keeping the three ecological scenarios but with a constant value of suspended sediment concentration $C_0 = 50$ mg/l.

The diversity in final morphologies is indicative of the crucial role of the initial topography in driving tidal channel morphodynamics. Indeed, network lengthening, sin-

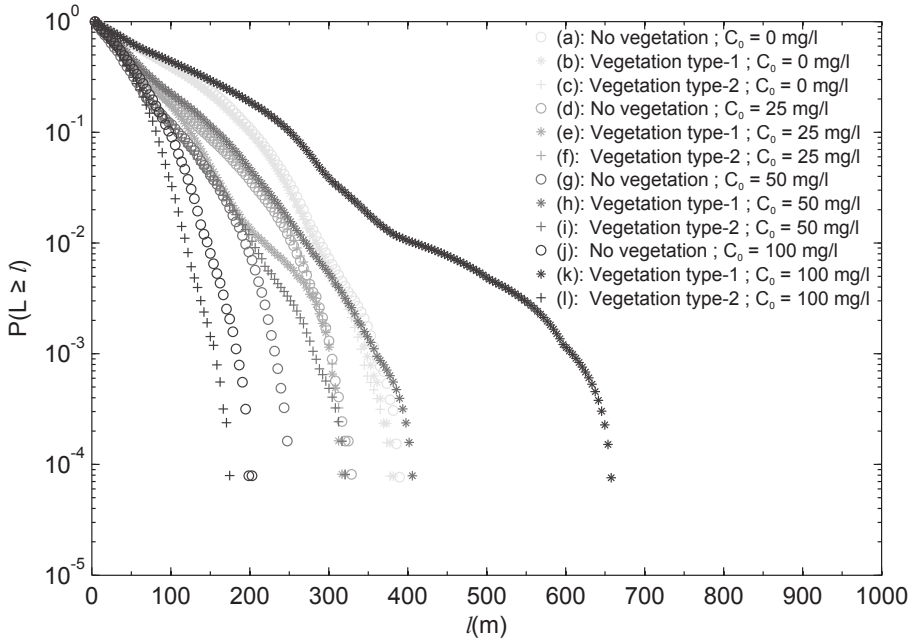

Figure 4.15: Semilog plot of the exceedance probability of unchanneled flow lengths $(P \geq l)$ for the synthetic tidal networks of the simulated marsh morphologies. The approximate linear trends suggest an exponential distribution whose slope represents the mean unchanneled flow length, while the drainage density is estimated by its inverse value.

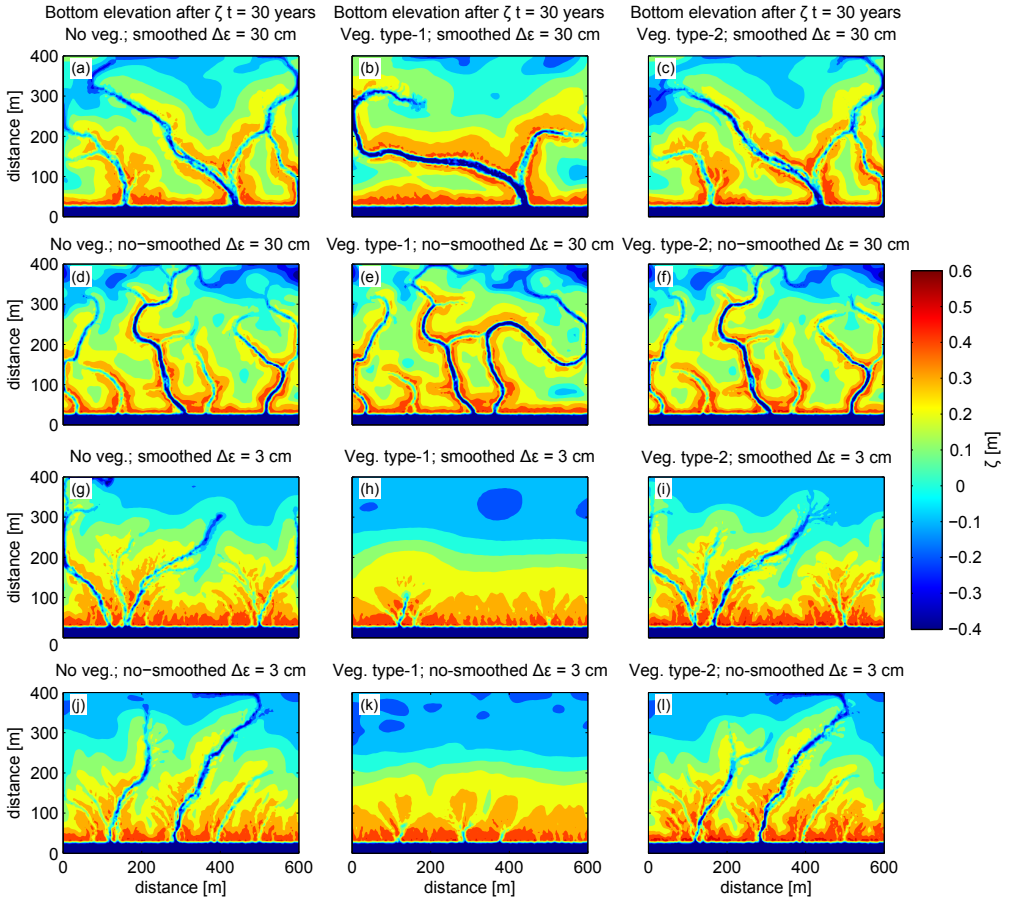

Figure 4.16: Simulated marsh morphologies after 30 years under a sediment supply $C_0 = 50$ mg/l for different initial topographic configurations and marsh ecology scenarios, computed with the continuous formulation (4.3.19). Columnwise: different ecological scenarios; rowise: different amplitudes and degree of smoothness of initial perturbation reported in Figure 4.6.

uosity and complexity highly differ within this simulation set. Precisely, the amplitude of the initial topographic perturbations ε seems to influence tidal network characteristics with a notable increase in channel density and complexity as the height of the topographic noises increases.

The degree of smoothness of these perturbations may affect the planar patterns with the presence of more sinuous tidal channels as the topography becomes rougher (e.g., Figure 4.16d, e and f with $\Delta\varepsilon = 30$ cm). Yet, this seems to be still a function of the size of the initial perturbations as the degree of smoothness no longer influences channel morphology when the perturbation amplitude is low (e.g., Figure 4.16g to l with $\Delta\varepsilon = 3$ cm).

On the whole, results emphasise that network morphological evolution and complexity occur more rapidly and in greater extent when tidal channels develop onto an initial perturbed bathymetry.

4.5 Discussion

4.5.1 Tidal network development in different marsh sedimentary contexts

The various numerical experiments bring interesting results that are worth to be further discussed. Firstly, Figure 4.8 exhibits the formation and evolution of tidal networks throughout the range of sedimentary and ecological scenarios investigated, which yet result from different morphological processes. Figure 4.17 brings further insights into this concern. The different subplots display the time evolution of a cross-sectional profile for the simulated morphologies (the location is highlighted by the dashed line in Figure 4.8). Results point out that channel deepening results from the progressive bottom scouring for the simulations in the absence of sediment supply (Figure 4.17a, b and c), whereas it chiefly results from the continuous aggradation and progradation of the flanking marsh platform for the simulations with high sediment supply (e.g., Figure 4.17j, k and l).

Such observations constitute good testimonies of the occurrence of two channel-forming processes: differential erosional formation in marsh retrogradation context and differential depositional formation in marsh progradation context (Stefanon et al., 2010, 2012). Nevertheless, a detailed examination of Figure 4.17 evokes a more complex picture of the problem. As a matter of fact, throughout the different simulations, the mouth of the main tidal network, which represents the outlet of the common sub-basin

examined in previous figures, occurs at the same location where an initial topographic depression exists. This analogy suggests a similar underlying mechanism participating in channel initiation regardless of the sedimentary and ecological contexts. Indeed, here, channel initiation is ascribed to the incision process as a result of flux concentration into the local initial depression producing excess bed shear stress.

Recalling the global picture of tidal network ontogeny, the different interpretations indicate that, for tidal networks developing under high accretional activity, the two channel-forming processes in reality co-exist but act at different time scales. Channel formation is attributed to the erosional process of channel incision that gives a basic imprinting to the network, in line with previous observations (e.g. Beeftink, 1966; French and Stoddart, 1992) and modeling studies (e.g. Fagherazzi and Sun, 2004; D'Alpaos et al., 2005). Then, channel incision and headward erosion occur during channel elaboration together with the prevalent depositional process of differential deposition, contributing to channel deepening. Eventually, channel narrowing, segmentation and even closure, due to the further aggradation and progradation of the marsh platform, represent other depositional processes acting over the longer timescales where depositional processes cancel out erosion.

Another point that arises from the analysis suggests that the morphological evolution of the tidal network is accelerated in marsh progradation context. Various results justify this interpretation. For instance, the qualitative observations from Figure 4.8 depict higher degree of channel lengthening as the sediment supply increases, which alludes to more elaborated channels as opposed to the presence of young ill-defined channels when sediment supply is limited. Furthermore, the channel senescence features such as channel narrowing and channel infilling portrayed in the highest accretional scenarios in Figure 4.8 denote that tidal networks have gone beyond maturity, and are experiencing a reduction (or integration) evolutionary stage, in agreement with Steel and Pye (1997). In addition, the progressive adjustment of the simulated basin hypsometries as sediment supply increases in Figure 4.11, the change in the temporal evolution patterns of the scaling relationship between Ω and P translating a gradient from channel scouring to channel infilling under higher accretional activity put forward in Figure 4.14, and the increase in drainage density, hence network complexity, with increasing suspended sediment concentrations highlighted in Figure 4.15, constitute quantitative observations arguing that the synthetic tidal networks age faster under marsh accretional context. This appears to be a critical feature of tidal network dynamics that previous studies missed to address.

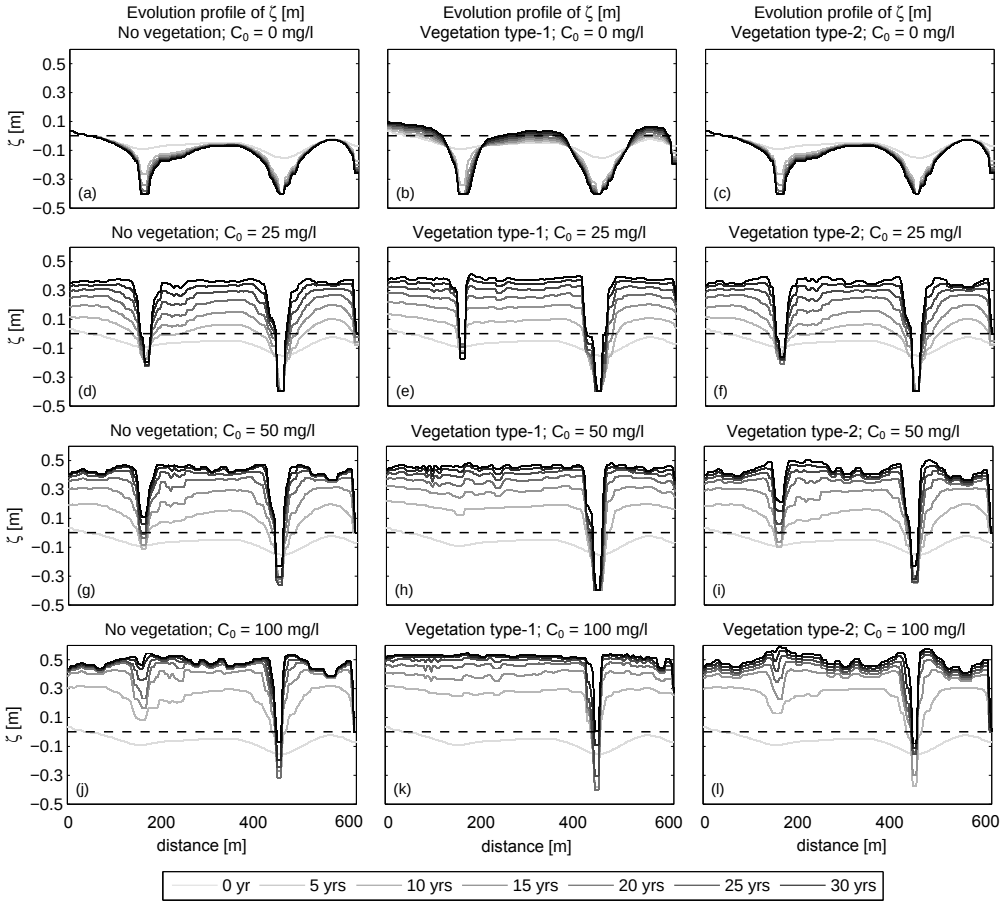

Figure 4.17: Time evolution of a cross-sectional profile (see dashed line in Figure 4.8) for the simulated morphologies.

This accelerated morphological evolution of tidal networks with higher sediment supply is ascribed to the more pronounced aggradation and progradation of the marsh platform which constrict faster and to a greater extent tidal channels. In response, channels rapidly extend and elaborate notably through elongation or first orders tributary initiation in order to accommodate the tidal prism that passes through it, leading eventually to high degree of channel complexity. Similarly, the critical point whereby channels start depicting signs of senescence due to the progressively reduced tidal prism and tidal velocities in the channel as the marsh platform reaches high elevations within the tidal frame occurs faster.

Evidences for accelerated tidal network development under high accretional activity can be also deduced from Figure 4.12. Indeed, the described morphological evolution of the simulated tidal landscape can be juxtaposed to the morphodynamics of the tidal channels. Therefore, the first period of high morphological change which appears earlier and in greater extent as sediment supply increases is manifested by the channel initiation process, triggering the whole morphodynamic system being far from its equilibrium configuration. Then, the slow and gradual decrease in the system morphological evolution is associated with the progressive elaboration of the channels, being particularly marked in simulations characterized by high suspended sediment concentration, while the system approaches dynamic equilibrium.

4.5.2 Tidal network development from different initial tidal flat bathymetries

The initial basin topography reveals also to play a crucial role in determining tidal network evolution. The characteristics of the planview morphologies from Figure 4.16 have notably indicated that network complexity seems to be linked to the heterogeneity of topographic surface.

To quantify this relationship, Figure 4.18 displays the values of the mean unchanneled flow lengths l for the simulated morphologies from Figure 4.16. Results show that the lowest values of the mean unchanneled flow lengths l occur for tidal networks formed over initial highly perturbed tidal basins. Accordingly, their corresponding high drainage densities evoke tidal networks characterized by an intricate morphology consisting of elongated and sinuous tidal channels, and with the appearance of lower order creeks (Figure 4.16 - subplots (d), (e) and (f)). This observation may be explained by the fact that the local topographic bumps and troughs composing the initial mudflat tend to guide the course of the forming tidal channels resulting therefore in a complex

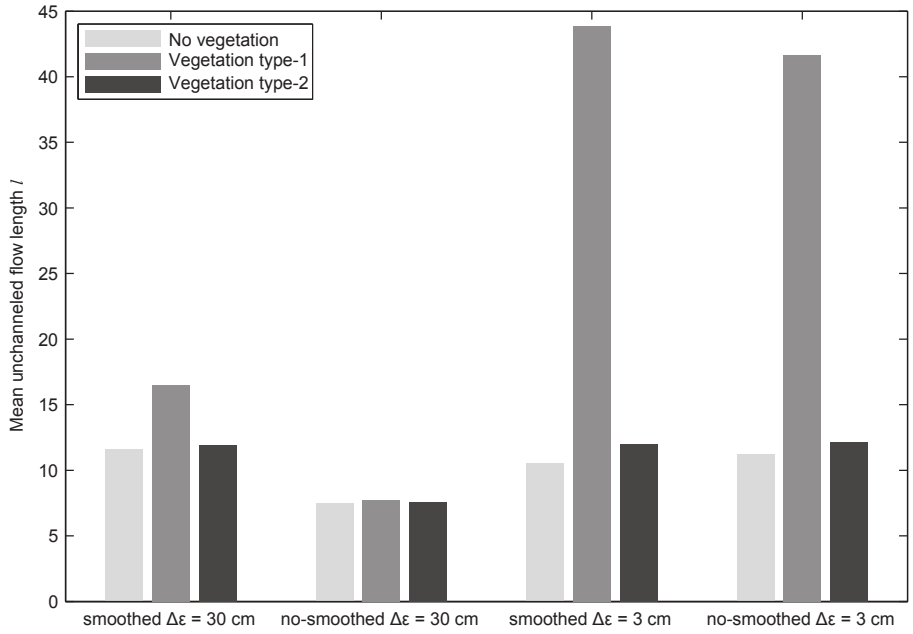

Figure 4.18: Mean unchanneled flow lengths l for the simulated morphologies from Figure 4.16. The drainage density is defined as the corresponding inverse value.

and elaborated tidal network as the topographic surface becomes rougher.

In truth, these results support the concept of inheritance of the major tidal channel features from the morphological characteristics of the underlying mudflat (Allen, 2000; Marani et al., 2003; Friedrichs and Perry, 2001). This confirms the legacy left by the initial conditions, in this case the topography, on landscape evolution, as put forward also in previous studies (e.g., French and Stoddart, 1992; Fagherazzi and Sun, 2004; Perron and Fagherazzi, 2012; Stefanon et al., 2012).

4.5.3 Role of vegetation in tidal network morphodynamics

The role of vegetation on tidal channel morphodynamics, particularly its impact on network development, highly depends on its vertical biomass distribution within the tidal frame. Figure 4.8 and Figure 4.16 show that the vegetation type-1 (monospecific) scenario characterized by a high biomass productivity at the lower positions in the tidal frame, alluding therefore to its presence in the initial mudflat, may influence channel initiation processes. This is particularly illustrated looking at the high discrepancies in channel morphologies between the simulations with vegetation type-1 scenario and those without vegetation colonization.

On the other hand, the vegetation type-2 (multiple species) scenario characterized

by a high biomass productivity at the upper positions in the tidal frame, alluding therefore to its absence in the initial mudflat, may only contribute to channel elaboration processes, such as channel lengthening and channel lateral migration as the network imprinting already arose prior to vegetation colonization. As a matter of fact, only local differences exist which concern shifts in channel course locations and degree of extension, while channel mouth location remains identical between the simulations with vegetation type-2 scenario and those without vegetation colonization.

Therefore, depending on its presence or absence during the short time span in which channel initiation occurs, vegetation may be seen either as an erosive or a stabilizing agent for tidal channel development, as documented also by Temmerman et al. (2007) and Schwarz et al. (2014).

Up to this point, the different simulation sets have addressed vegetation biomass growth using the continuous formulation (4.3.19). Owing to the current challenge in transcribing mathematically the vegetation dynamics, one may question the sensitivity of the present mathematical expression in reproducing accurately such a dynamical process.

Figure 4.19 displays final planview morphologies for the two different marsh ecological scenarios, keeping a constant suspended sediment concentration value $C_0 =$ 50 mg/l, and focusing on the comparison between the two mathematical biomass formulations (continuous and discontinuous). Results show a diversity of morphologies even for a same ecological scenario. Particularly, substantial discrepancies in channel density and location occur between the two mathematical functions simulating marsh colonized by vegetation type-1 (Figure 4.19a and c) because, as discussed above, vegetation in this scenario immediately intervenes in the imprinting of the tidal network.

Such discrepancies indicate that the landscape morphological evolution appears to be highly sensitive to the way the biomass growth is formulated. Consequently, there is a need to further comprehend the vertical distribution of halophyte biomass in salt marshes together with accurate mathematical representations which will be discussed in Chapter 5.

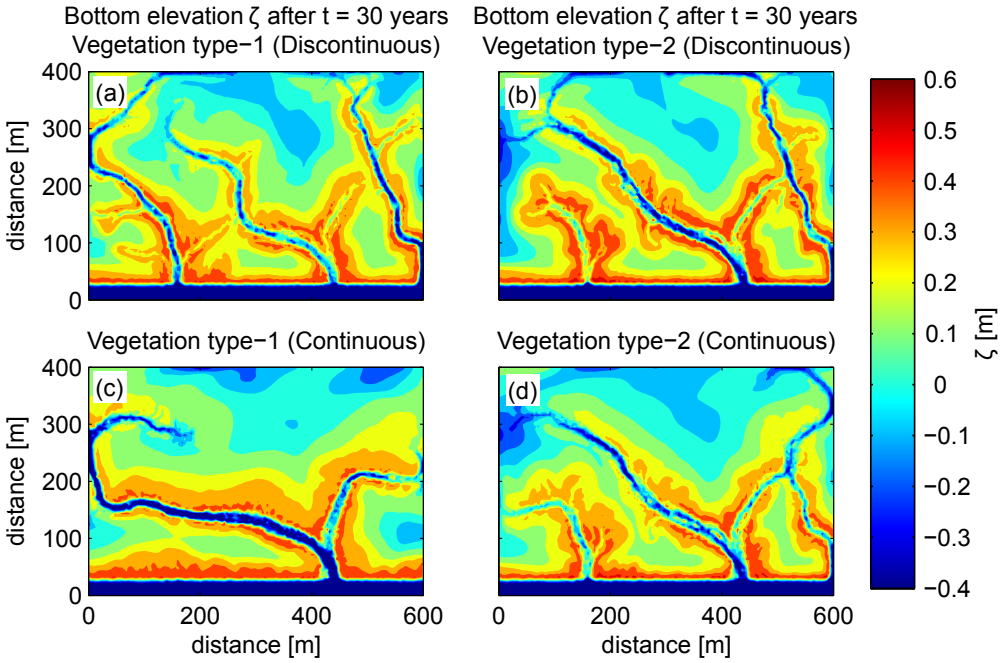

Figure 4.19: Simulated marsh morphologies after 30 years under a sediment supply $C_0 = 50$ mg/l and according to the two vegetation type scenarios, each being computed using the continuous formulation (4.3.19) and the discontinuous formulations (4.3.20) - (4.3.21).

Chapter 5

Assessing vegetation spatial distribution and productivity in a temperate salt marsh

This chapter discusses on vegetation distribution and productivity with respect to the elevation gradient in a temperate salt marsh. Firstly, broad knowledge of vegetation dynamics in salt marshes will be reviewed so as to introduce the scope of this study. Secondly, the field work approach adopted to tackle the problem will be presented and its main outcomes will eventually conclude this chapter.

5.1 Vegetation dynamics in salt marshes

Vegetation in salt marshes is mostly dominated by halophytic species, which consists of macrophytes adapted to salty conditions to complete their cycles of growth and decay (Silvestri et al., 2005), but various algae can be present (Allen, 2000). Terms such as "foundation species" (Bertness et al., 2001) or "ecosystem engineers" (Jones et al., 1994) are used to refer to these plants due to their ability to modify the physical environment, to influence species interactions, resource availability and community structure (Bruno and Bertness, 2001). Consequently, halophytes play a big part in sustaining the biological richness and diversity of the wetland and their presence is essential to salt marsh and tidal network evolution (Marani et al., 2006a,b; Garofalo, 1980; Gabet, 1998).

In fact, it has been long observed and recognised that marsh vegetation highly

contributes to the building-up of the marsh platform (e.g., Yapp et al., 1917), through a range of physical-biological interactions. Correspondingly, salt marsh halophytes influence sediment deposition by reducing tidal flow velocities and turbulence within vegetation canopies (Leonard and Luther, 1995; Nepf, 1999; Leonard and Croft, 2006), by capturing mineral and organic sediments (Leonard and Luther, 1995; Palmer et al., 2004), and by producing organic matter (Neubauer, 2008; Langley et al., 2009), thus raising marsh elevation. Due to these ecogeomorphic processes, the rate of sediment deposition is proportional to vegetation properties such as stem diameter, length, density as well as projected plant area, which themselves depend on plant productivity (i.e., biomass) (Mudd et al., 2004; D'Alpaos et al., 2006). However, vegetation productivity partly relies upon the elevation of the marsh relative to sea-level (Morris et al., 2002). This two-way bio-physical coupling highlights thus the presence of a strong feedback between salt marsh ecology and morphology which stands out perhaps more clearly than in any other environment (Murray et al., 2008).

Together with the fundamental feedback between marsh surface sedimentation and tidal inundation that it complements, this eco-geomorphic feedback allows the wetland to maintain its position in the intertidal zone under moderate accelerations in the rate of sea level rise (Kirwan et al., 2010). Nevertheless, the current observed trend of marsh degradation and submergence occurring in various worldwide regions points out to a limit of these eco-geomorphic processes in allowing the marsh to keep pace with today's high rates of sea level rise (Fagherazzi et al., 2012), although locally other extrinsic factors may come into play (Kirwan and Temmerman, 2009). In fact, models of marsh morphological evolution have revealed that an increase in sea level rise would cause a decrease in marsh platform elevation relative to mean sea level, leading eventually to vegetation disturbance (e.g., D'Alpaos et al., 2007a). Thereby, all the aforementioned eco-geomorphic interactions would be progressively hindered, and the concurrent action of erosional processes such as peat collapse as well as channel and wave erosion would eventually induce the marsh to submerge beyond depths that preclude vegetation regrowth (Marani et al., 2007; Kirwan and Murray, 2007; Kirwan et al., 2008). A number of field studies have notably confirmed these manifestations following the onset of modern accelerations in the rate of sea level rise (e.g., Morris et al., 2005; Hughes et al., 2009). A full comprehension of the vegetation productivity - marsh elevation feedback is therefore fundamental in order to better grasp and predict the overall resilience of wetlands facing climatic change.

As the previously listed eco-geomorphic interactions are a function of vegetation

productivity, important is to investigate factors determining spatio-temporal variations in vegetation productivity. In general, a variety of environmental factors influence the distributions of halophyte species and their productivity on the salt marsh. Salinity (Phleger, 1971; Morris, 2000), tidal range (Kirwan and Guntenspergen, 2010), latitude (Pratolongo et al., 2009; Kirwan et al., 2009), temperature, sediment supply, CO_2 concentration (Langley et al., 2009), nutrient availability (Gallagher, 1975), substrate stability and oxygenation (Mendelssohn and Morris, 2000) are among factors controlling plant establishment on the marsh platform. As previously mentioned, the marsh elevation relative to mean sea level is however the most dominant factor in controlling plant biomass, because marsh relative elevation is correlated with many of the above-mentioned variables and hence lumps the combined effects of these variables (Fagherazzi et al., 2012). Indeed, marsh elevation determines the duration and frequency of tidal inundation over the marsh habitat that is extremely important for the local biota, including the marsh vegetation community (Morris et al., 2002). Correspondingly, salt marsh macrophytes occupy a narrow elevation window being delimited by the mean sea level and the mean high tide in which productivity varies strongly. For instance, Morris et al. (2002) reported that the productivity of *Spartina alterniflora* increases with increasing depth to a maximum productivity at an inundation depth between 40 cm and 60 cm below mean high tide, where the tidal amplitude is 60 cm locally, following an 18-year field measurement record of biomass and morphometric characteristics of this pioneer halophytic species collected at North-Inlet, South Carolina. This indicates the existence of an optimum elevation relative to sea-level for plant productivity, which has been previously documented by other authors (e.g., Redfield, 1972; Orson et al., 1985). They also noticed that the vertical distribution of *Spartina alterniflora* does not extend below this optimum elevation. Indeed, at depths greater than this optimum, periodic fluctuations in sea-level would cause the plants to succumb to hypoxic conditions, and the corresponding decrease in surface sedimentation would eventually induce the marsh to submerge. Such a behaviour reveals the presence of a negative feedback between plant growth, sea-level rise and marsh sedimentation for elevations below the optimum, which is responsible for the formation of a bimodal elevation distribution of salt marshes and tidal flats (Fagherazzi et al., 2006; Marani et al., 2007). To the contrary, if the marsh relative elevation is above this optimum, salinity in pore waters would increase as salinity typically rises in mid marsh elevation where prolonged periods between tidal inundations combined with evaporation favours the accumulation of salt (Adam, 1990), which can limit the growth or be fatal to *Spartina alterniflora* (e.g.,

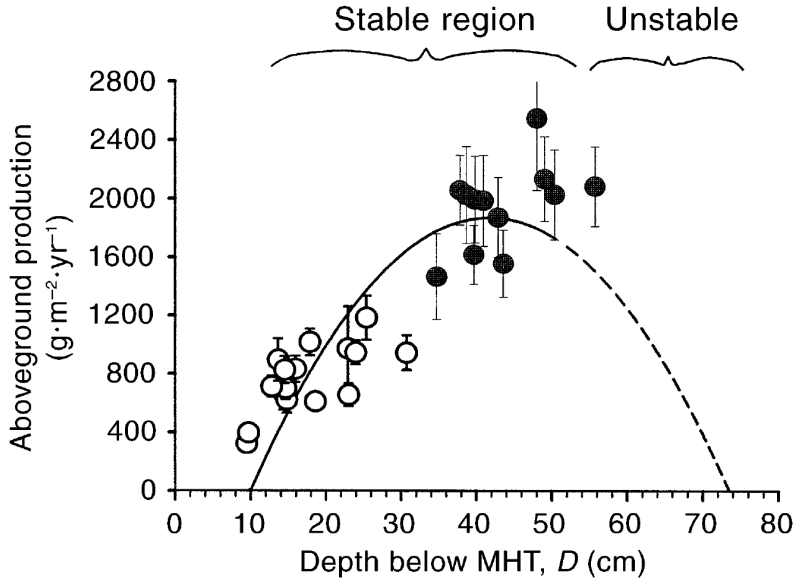

Figure 5.1: Relationship between *Spartina alterniflora* aboveground productivity and depth below Mean High Tide (MHT) of sites located in the high (open circles) and in the low (solid circles) marsh (from Morris et al., 2002).

Morris, 2000; Phleger, 1971; Webb, 1983). In light of these considerations, Morris et al. (2002) formulated a non-linear mathematical relationship of plant productivity, whereby aboveground biomass first increases with inundation until an optimum depth (or marsh relative elevation) where biomass production is maximum and then decreases with further inundation, depicting thus a hump-shaped curve as displayed in Figure 5.1. Mudd et al. (2004) further assumed plant biomass to be a linear decreasing function of inundation depth (or marsh relative elevation) with the presence of a threshold depth (or elevation) beyond which the halophyte community drowns, and which have been adopted by other authors (e.g., D'Alpaos et al., 2006, 2007a). The eco-geomorphic model introduced in Chapter 4 makes also use of this two types of mathematical relationship.

While these observed vegetation dynamics are peculiar to marshes dominated by monospecific plant populations such as in the Eastern and Gulf Coast of USA, (Figure 5.2), in other salt marshes worldwide, such as Mediterranean and Northern European marshes, different ecological dynamics may prevail (Fagherazzi et al., 2012).

Typically, a variety of halophytic species colonise these environments (see Figure 5.3), and exhibit spatial distributions in the form of organised, rather uniform and sharply bounded vegetation patches (Da Lio et al., 2013), alluding to the phenomenon

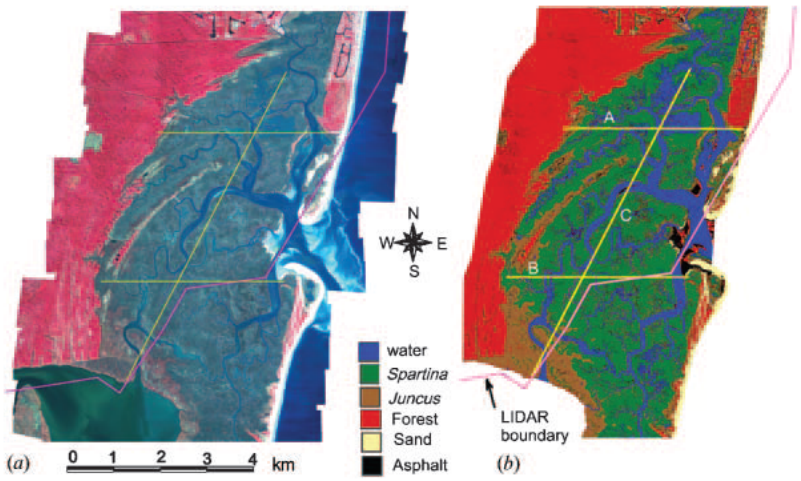

Figure 5.2: (a) A False colour composite image of North Inlet, South Carolina; (b) derived land cover classification map (from Morris et al., 2005).

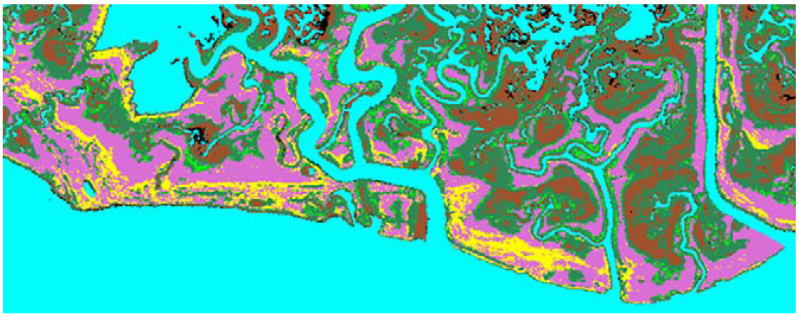

Figure 5.3: Land cover classification map of the San Felice salt marsh in the Venice lagoon using San Felice CASI 2002 data. Vegetation classes include *Spartina maritime* (dark green), *Limonium narbonense* (purple), *Sarcocornia fruticosa* (yellow), *Juncus spp.* (light green), soil (brown) and water (blue) (from Marani et al., 2006a).

of zonation.

Zonation patterns have been first hypothesised to be the result of interspecific competition among species (Glenn-Lewin et al., 1992), and of the adaptation of marsh vegetation to edaphic conditions (Bertness and Ellison, 1987; Bockelmann et al., 2002; Silvestri et al., 2005; Moffett et al., 2010). However, Marani et al. (2013) have shown that zonation patterns are the product of marsh areas being actively engineered by competing vegetation species through the plant biomass - marsh elevation feedback. This contrasts with the common vision of vegetation regarded as a passive agent with respect to environmental controls. Studies on vegetation spatial distribution and abundance in the Venetian salt marshes have demonstrated that vegetation zonation is

characterised by an increase in species richness and density with soil elevation (e.g., Marani et al., 2004; Silvestri et al., 2005). As increased plant diversity is generally associated with increased plant biomass (Tilman, 2000), one can hypothesise that in marshes colonised by multiple halophytes, plant biomass can be expressed as an increasing function of marsh elevation.

5.2 Objectives

The previously mentioned contributions have provided definite insights into vegetation dynamics in salt marshes. Consequently, a number of models dealing with the eco-geomorphology of salt marshes and tidal networks have progressively arisen in the literature, whereby vegetation growth, described by its biomass, is expressed as a function of marsh elevation through the use of process-based equations (e.g., Mudd et al., 2004; van de Koppel et al., 2005; D'Alpaos et al., 2006, 2007a; Kirwan and Murray, 2007; Marani et al., 2007, 2010, 2013; Kirwan et al., 2010; Larsen and Harvey, 2010; Lorenzo-Trueba et al., 2010; Mariotti and Fagherazzi, 2010). Except for a few exceptions (e.g., van de Koppel et al., 2005; Marani et al., 2013), the parameterization of the vegetation growth in these models emanates from the quadratic relationship derived by Morris et al. (2002), based on field measurements carried out at North Inlet, South Carolina. In reality, this field site is atypical in several aspects. As a matter of fact, in addition to the monospecific plant ecology specific to this salt marsh system, the sub-tropical climate that characterises this location enhances the building up of high concentrations of salt in pore waters for marshes mid to high in the intertidal zone (Pratolongo et al., 2009). This hot climate acts therefore as an important stress factor on plant growth, leading to the strong decline in primary production observed in high marsh elevations at North Inlet, causing the hump-shaped productivity curve. Accordingly, one should be careful with the sue of site-specific biomass-elevation relationships in global model studies. For instance, Kirwan et al. (2012) found biomass production persisting at marsh elevations well above mean high tide, following a decade long measurement of *Spartina alterniflora* productivity in seven marshes located in Virginia, further north from North Inlet, which therefore did not give support for a hump-shaped relationship between plant productivity and marsh elevation. Although a significant body of work exists on the relationship between halophytes and marsh elevation, surprisingly, only a very few field surveys have addressed this relationship through direct biomass measurements, particularly in European salt marshes despite their

different plant ecology. As put forward by Mudd et al. (2004), in view of the observed regional dependence of such a relationship, further field research should be conducted to see whether it holds for marshes in different locations and depicting different climatic or ecological settings. In the following will be presented a field analysis carried out in a European temperate salt marsh grown by a mixture of halophytes. This study aims to assess i) how halophytes are distributed in the tidal frame, ii) whether the total biomass responds to marsh elevation and, if so, what relationship exists and, recalling the previously derived relationships reported in the literature, iii) whether a relationship exists between total biomass and vegetation characteristics that determine sediment deposition, including stem diameter, height, density and plant projected area per unit volume.

5.3 Materials and methods

5.3.1 Study area

The field survey was conducted in a salt marsh system right adjacent to the Paulina marsh in the Scheldt Estuary, SW Netherlands (Figure 5.4a).

The study area is dominated by a semi diurnal macro-tidal regime with a mean tidal range of 3.9 m (Claessens and Meyvis, 1994). Different stages of geomorphological development and plant succession allow for the distinction of 3 marsh zones: a high, medium and low salt marsh zones. The high marsh zone is the oldest and is characterised by a relatively flat topography (Temmerman et al., 2005a). Together with the medium marsh zone, it can be intertwined by various creek tributaries of several orders. To the contrary, the younger low marsh zone also called pioneer zone, as it materialises the transition between the salt marsh and the bordered tidal flat, shows some slope degrees and is intersected by fewer tidal creeks (Temmerman et al., 2005a). The study site depicts a number of halophytic species common to Northwest European salt marshes. The high marsh zone is mostly colonised by *Elymus athericus* (see Figure 5.4b), while the medium marsh zone is dominated by *Aster tripolium* and *Atriplex portulacoides*. The pioneer marsh zone is typically characterised by a more patchy vegetation cover of the pioneer *Spartina anglica* (see Figure 5.4d).

5.3.2 Sampling methodology

The field campaign took place early September in order to measure end-of-season biomass as a proxy of annual, aboveground primary production. Measurements were

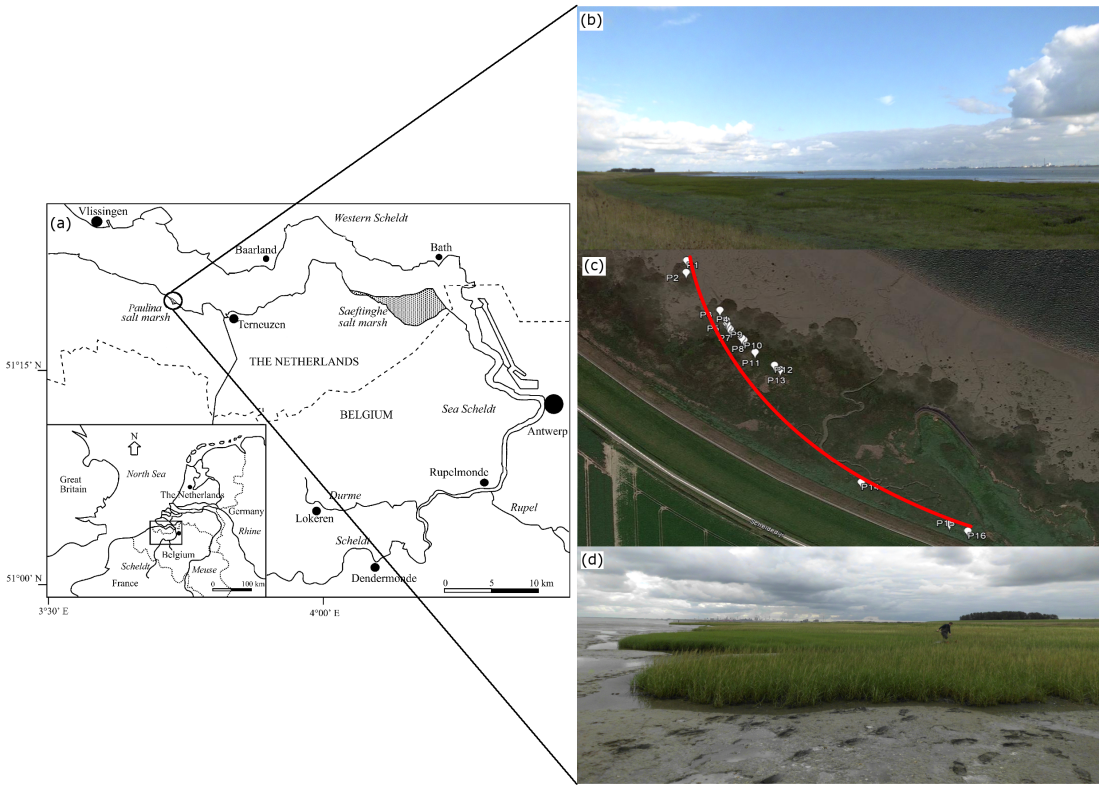

Figure 5.4: Location of study area and measurement transect.

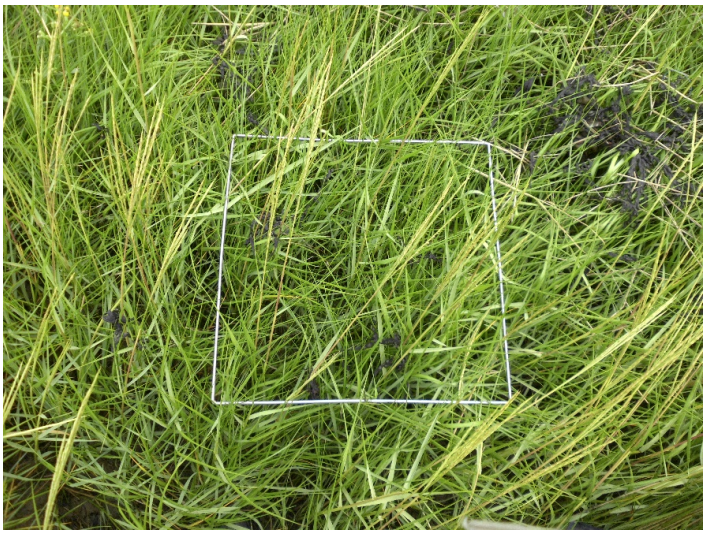

Figure 5.5: 25 $\times$ 25cm quadrat used to delineate plot for subsequent vegetation harvesting.

carried out along a single transect stretching from the marsh seaward edge to its furthest inland side. The location of the transect was determined according to a randomly stratified selection that attempted to cover the different marsh domains and vegetation zonation patterns while seeking the direction of the topographic slope. Tidal creeks were omitted along the transect as sub-surface creek drainage influences soil aeration and therefore plant productivity (Ursino et al., 2004; Silvestri et al., 2005). Similarly, artificial features such as embankments were avoided. In order to cope with the moderate elevation gradient typically characterising these environments, measurement points along the transect were taken about every 10 cm in elevation with the help of a RTK differential GPS whose elevation value was tied to the Dutch ordnance datum NAP with a vertical error +/- 1 cm. At every elevation point, 3 replicate plots were delimited using quadrats of dimensions 25 $\times$ 25 cm as seen in Figure 5.5.

Plant species composing the plots were first identified. Their respective percentage cover was then estimated and their relative abundance-dominance score was evaluated according to the Braun-Blanquet method (e.g., Bockelmann et al., 2002; Silvestri et al., 2005), based on 6 cover classes (<1, 1-5, 5-25, 25-50, 50-75, 75-100%). A species is thus considered as dominant if it covers > 50% of the plot. Then, all total standing biomass was harvested in the 3 replicate plots. Biomass samples were stored in a cool chamber and washed in the laboratory. A representative sub-sample of 30 plant individuals was selected from one replicate biomass sample per elevation point to perform direct morphometric measurements of stem diameter and height. Stem density

was derived by cross-multiplying the measured sub-sample biomass with known number of plant individuals to the total biomass of the respective sample. Projected plant area per unit volume was defined as the product of stem diameter and stem density (Nepf, 1999). Finally, biomass samples were dried in an oven at 70°C for 48 hours until they reach a constant weight, and dry biomass was determined afterwards by weighting.

5.3.3 Statistical analysis

In total, 16 elevation points were measured along the transect which allow for the extraction of 48 biomass samples. The resulting data set was first explored using descriptive statistics and exploratory graphs including boxplots, bar charts, etc. in order to summarise the main features of the considered variables. In a second stage, correlations between factor (e.g., elevation) and dependent variables (e.g., biomass) were assessed using Pearson product moment correlation coefficient r (Pearson, 1896), or Spearman's rank correlation coefficient ρ (Spearman, 1904),when the data were not normally distributed. Ordinary Least Square (OLS) regression analyses were subsequently carried out on variables showing high correlation. Models were validated by ensuring that the different assumptions underlying linear regression were satisfied. Normality of the residuals was thus assessed using different normality tests (e.g., Kolmogorov-Smirnov test (Kolmogorov, 1941; Smirnov, 1939), Anderson-Darling test (Anderson and Darling, 1952), etc.), heteroscedasticity was evaluated using White test (White, 1980), and the presence of autocorrelation structures was assessed graphically by plotting the residuals versus observation orders. To test the overall significance of the regression model and its parameters, lack-of-fit sum of square test (F-test) as well as T-tests were also conducted. Outliers were detected using the Grubbs test (Grubbs, 1950). All statistical tests were carried out with a 95% confidence interval. This statistical analysis was performed using MINITAB v17.

5.4 Results

5.4.1 Vegetation species spatial distribution

The topographic profile of the measurement transect, whose planar course is depicted in Figure 5.4c, is shown in Figure 5.6. The elevation gradient from the seaward to the landward edge of the marsh is 1.5 m, resulting in the measurement of 16 elevation points (i.e., about every 10 cm in height). Some contrasting morphologies can be

observed. Indeed, the marsh pioneer zone and, to a lesser extent, the lower elevations of the medium marsh zone clearly slope down towards the sea, although the marsh slope is not gradual and is the steepest some distance away from the marsh seaward edge, towards the end of the pioneer zone. To the contrary, the upper elevations of the medium marsh zone and the high marsh zone are rather flatter. Such observations relatively corroborate with the previously described topographic characteristics of the different marsh domains. In addition, Figure 5.6 displays the halophytic species identified per elevation point. A total number of 7 species were found along the course of the transect, namely *Spartina anglica (Sp)*, *Aster tripolium (As)*, *Suaeda maritima (Su)*, *Salicornia europea (Sa)*, *Spergularia marina (Spe)*, *Atriplex portulacoides (At)* and *Elymus athericus (El)*. Some elevation points are characterised by a monospecific plant cover whereas others, especially in the marsh medium zone, are featured with a multiple species cover. Correspondingly, a maximum of 4 plant species was found at location P11. Looking at the vertical distribution of the observed halophytes, *Spartina anglica* exclusively occupies the lower marsh domain but appears also to extend well above the pioneer zone. On the other hand, some species are present in narrow elevation ranges such as *Elymus athericus* which is solely found in the high marsh zone.

Figure 5.7 shows the proportion of plant cover as an average from the 3 replicate plots per elevation point for every identified species. Despite the fact that some elevation points in the medium marsh zone portray a vegetation cover composed of a mixture of several species (e.g., P10 to P14), in reality only *Spartina anglica* and *Aster tripolium* represent the abundant and dominant species with respect to the other recorded halophytes. The proportion of the species and the associated elevation values show a certain dependence of the presence of certain species on soil elevation such as *Elymus athericus*, *Salicornia europea* and *Spergularia marina*. To the contrary, the rather flat spatial distribution of *Spartina anglica* suggests that such a dependence may be weaker. In fact, its decrease in proportion in the intermediate zone seem to be connected to the interspecific competition with *Aster tripolium* and to a lesser extent *Atriplex portulacoides* and *Suaeda maritima*, until its proportion becomes null when a new zonation pattern characterised by the nearly exclusive abundance and dominance of *Elymus Athericus* establishes in the high marsh zone (e.g., P15 and P16). Particularly, one may discern that the proportion of *Spartina anglica* is strongly uncorrelated with the proportion of *Aster tripolium*. In other words, the abundance and dominance of *Spartina anglica*corresponds to an absence or weak presence of *Aster tripolium* and vice-versa.

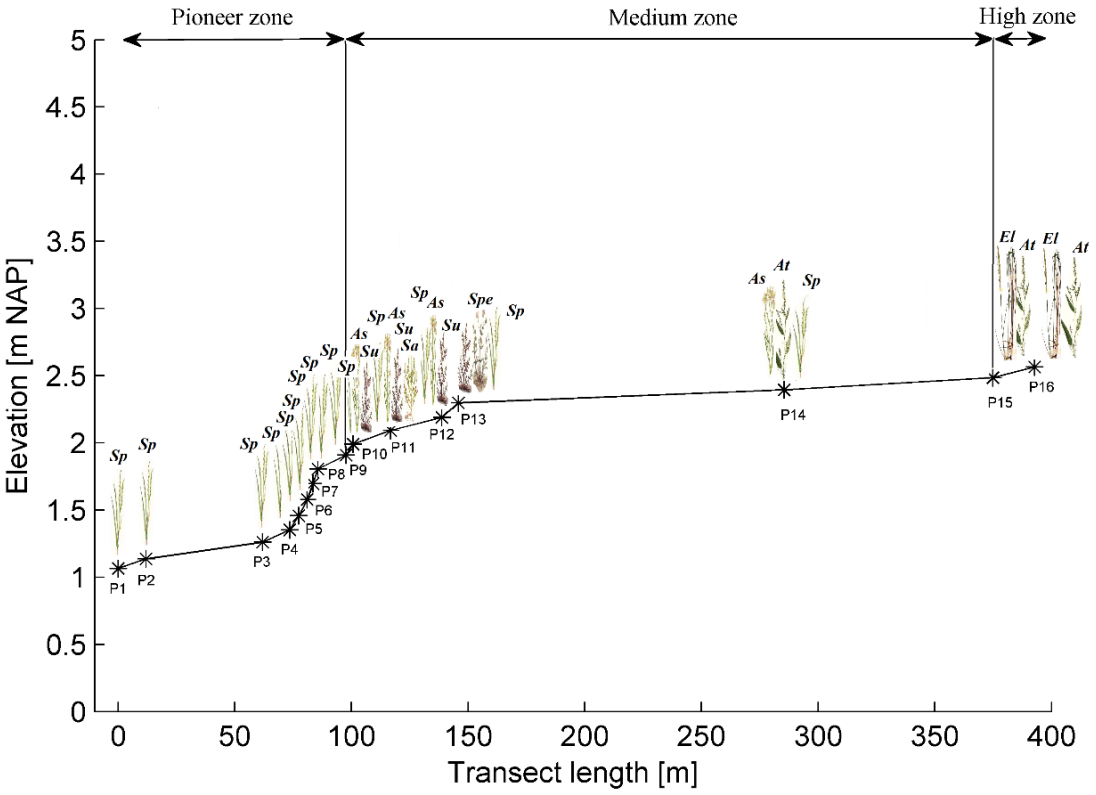

Figure 5.6: Topographic and plant distribution profile along the measurement transect

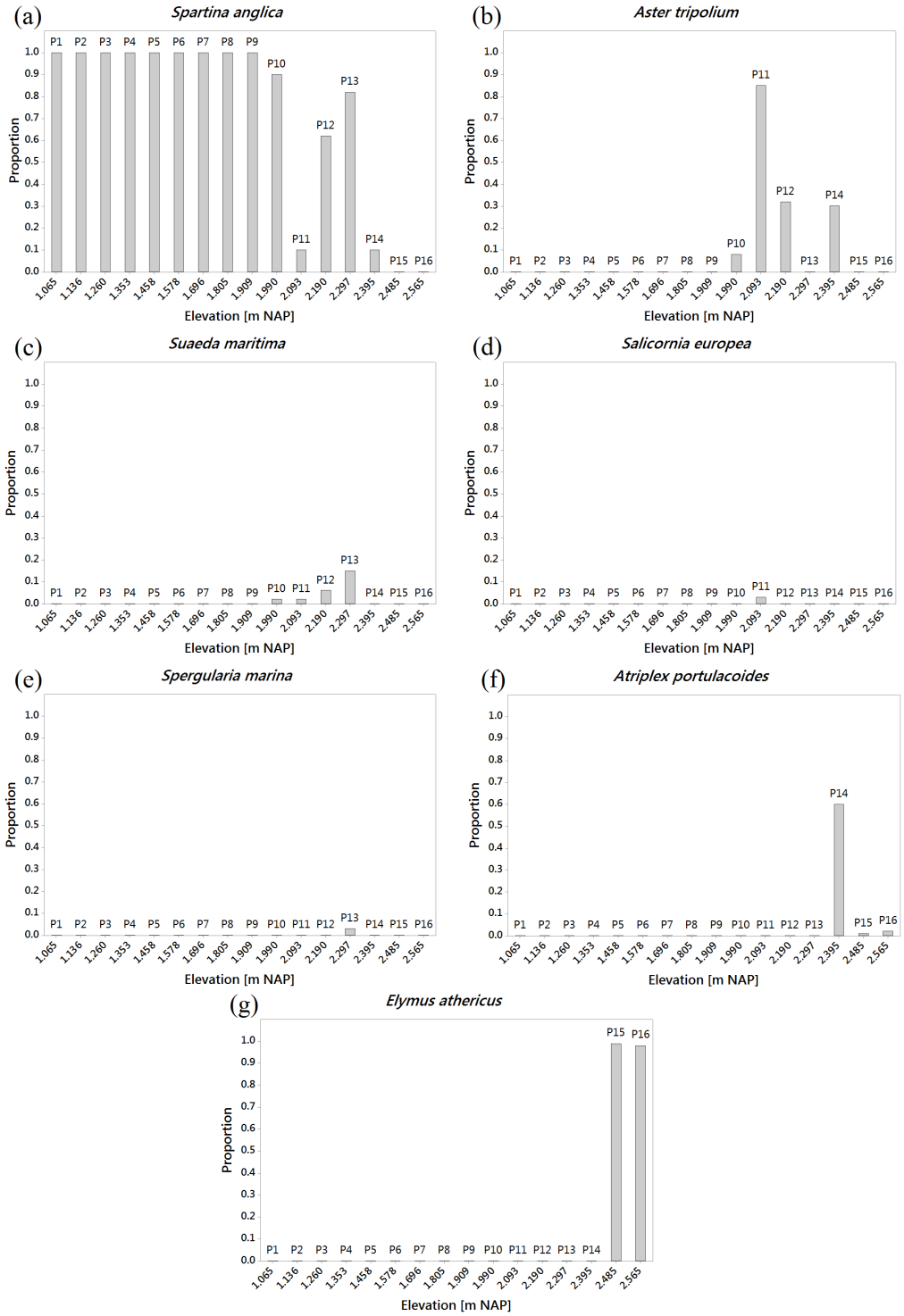

Figure 5.7: Proportion of plant cover with respect to soil elevation for the different identified halophytic species (a) *Spartina anglica*; (b) *Aster tripolium*; (c) *Suaeda maritime*; (d) *Salicornia europea*; (e) *Spergularia marina*; (f) *Atriplex portulacoides*; (g) *Elymus athericus*.

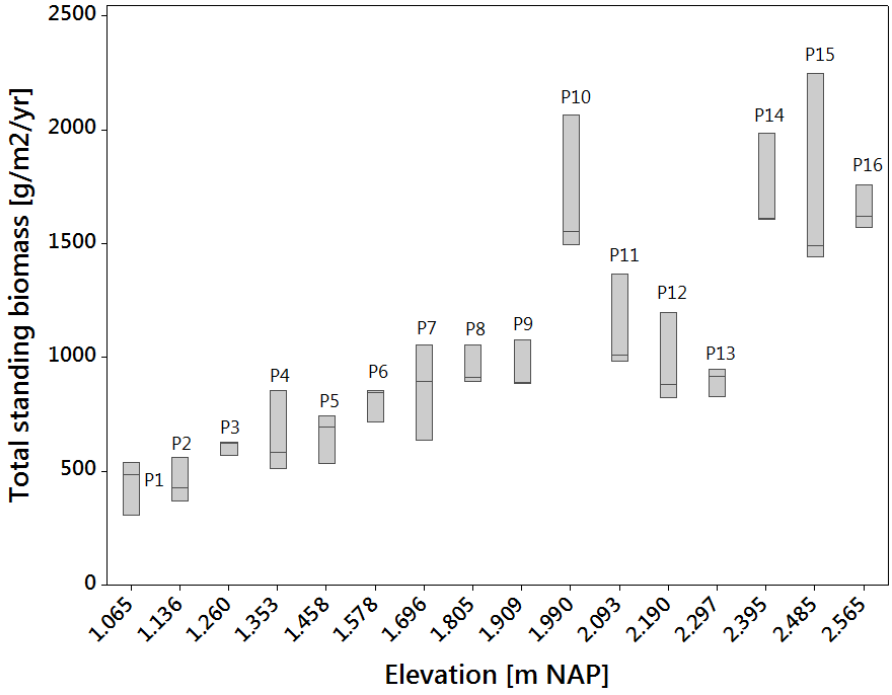

Figure 5.8: Box plot of total standing biomass against elevation.

5.4.2 Vegetation biomass vertical distribution

Table 5.1 summarises the main descriptive statistics based upon the biomass averaged per elevation point.

The total standing biomass seems to increase with elevation. The lowest biomass value is indeed measured at one of the lowest elevation points (P1 or P2) and the highest value at one of the highest elevation points (P14 or P16), depending on the measure of central tendency considered (i.e., mean or median). Moreover, biomass data depicts a higher degree of dispersion for elevation points characterised by a multiple plant species cover. The following statistics can be better appreciated by visualising the box plot of replicate biomass against marsh elevation, as displayed in Figure 5.8.

Figure 5.8 puts in evidence the presence of two regions in the plot of which the delineation coincides with the distribution of the halophytes along the measurement transect. A first region comprises the elevation points situated in the pioneer zone (P1 to P9) which shows a gradual increase in biomass with elevation. The second region includes the elevation points located in the medium and high marsh zones (P10 to P16) which displays more scatter in the distribution of biomass with respect to the marsh

Table 5.1: Summary of descriptive statistics of plant biomass per elevation.

Elevation point	Elevation (m NAP)	Plant species	AD scale[1]	Average biomass[2] ($g.m^{-2}.yr^{-1}$)	Std dev.	Min. biomass[2] ($g.m^{-2}.yr^{-1}$)	Median biomass[2] ($g.m^{-2}.yr^{-1}$)	Max. biomass[2] ($g.m^{-2}.yr^{-1}$)
P1	1.065	*Spartina anglica*	5	442.9	121.4	306	485.4	537.4
P2	1.136	*Spartina anglica*	5	452.9	99.1	369.8	426.4	562.6
P3	1.260	*Spartina anglica*	5	607.7	31.7	571.2	624	628
P4	1.353	*Spartina anglica*	5	649.7	181	512	583	854
P5	1.458	*Spartina anglica*	5	656.3	107.7	535.2	692	741.6
P6	1.578	*Spartina anglica*	5	804.1	76.9	715.4	844	852.8
P7	1.696	*Spartina anglica*	5	861.4	212	635	893	1056
P8	1.805	*Spartina anglica*	5	952.9	109.3	892.8	912.8	1053
P9	1.909	*Spartina anglica*	5	950.7	87.3	884.2	891	1076.8
P10	1.99	*Spartina anglica* *Aster tripolium* *Suaeda maritima*	5 2 1	1705.1	314	1495	1554	2006
P11	2.093	*Aster tripolium* *Spartina anglica* *Salicornia europea* *Suaeda maritima*	5 2 1 +	1119.6	214	984	1008	1366
P12	2.19	*Spartina anglica* *Aster tripolium* *Suaeda maritima*	4 3 2	967.0	202	822	881	1197
P13	2.297	*Spartina anglica* *Suaeda maritima* *Spergularia marina*	5 2 +	896.9	62.6	826.6	917.4	946.6
P14	2.395	*Atriplex portulacoides* *Aster tripolium* *Spartina anglica*	4 3 2	1734.5	218	1608	1609	1986
P15	2.485	*Elymus athericus* *Atriplex portulacoides*	5 +	1725.4	452	1440	1490	2246
P16	2.565	*Elymus athericus* *Atriplex portulacoides*	5 +	1648.1	97.4	1569.2	1618	1757

[1] Braun Blanquet Abundance-Dominance scale : + (< 1% cover and not abundant) ; 1 (< 1% cover); 2 (1 - 5% cover) ; 2 (5 - 25% cover.) ; 3 (25 - 50% cover) ; 4 (50 - 75% cover) ; 5 (75 - 100% cover)

[2] Total standing (live + dead plant material) end-of-season dry biomass ($g.m^{-2}.yr^{-1}$) averaged over the elevation point.

elevation. Furthermore, the relatively larger interquartile ranges characterising the latter elevation points indicate that the replicate biomass measurements vary strongly from each other, as opposed to what occurs for the low elevation points.

Correlation was subsequently tested between the replicate biomass measurements and their respective soil elevation values, which appeared to be highly positive ($\rho = 0.861$, significant at $p < 0.001$). This indicates that the two variables covariate strongly in a similar way (i.e., in the same direction). In fact, Figure 5.8 reflects this linear association between biomass and elevation since the plot depicts one main direction.

As a result, an OLS regression analysis was carried out to model total standing biomass as a function of marsh elevation. The exclusion of one outlying data, detected by means of the Grubbs test, allowed to correct for the non-normality of the residuals (significant at $p > 0.150$ after correction). No further corrections on the residuals were necessary to meet the other assumptions (homoscedastic residuals, significant just on the threshold α level of $p = 0.05$, uncorrelated residuals). Results of the regression analysis show that the marsh elevation is able to explain 70% of the plant biomass through a linear model. Figure 5.9 displays the response of plant biomass to marsh elevation.

5.4.3 Vegetation biomass - morphometrics relationships

On the basis of an 18-year record of *Spartina alterniflora* productivity at North Inlet, South Carolina (Morris and Haskin, 1990), Mudd et al. (2004) found that vegetation morphometric characteristics including stem diameter, projected plant area per unit volume and, by extension, stem height and stem density could be individually related to vegetation aboveground biomass via a power law relationship, as previously described in Chapter 4. Table 5.2 lists some descriptive statistics of stem diameter d_s, stem height h_s, stem density n_s and projected plant area per unit volume a_s.

Stem height seems to depict an increasing trend with the total standing biomass averaged over every elevation point (see Table 5.2 and Figure 5.10b. However, it appears difficult to discern any particular trend between mean biomass and each of the other vegetation morphometric characteristics. Box plots can be produced on the direct measurements of stem diameter and stem height against mean biomass as displayed in Figure 5.10, helping in visualising any trend between the variables.

Figure 5.10a reveals that stem diameter remains fairly constant with increasing biomass. Low variation in diameter values occurs for elevation points grown by a monospecific plant population (e.g., P1 to P9 with *Spartina anglica* and P15 to P16

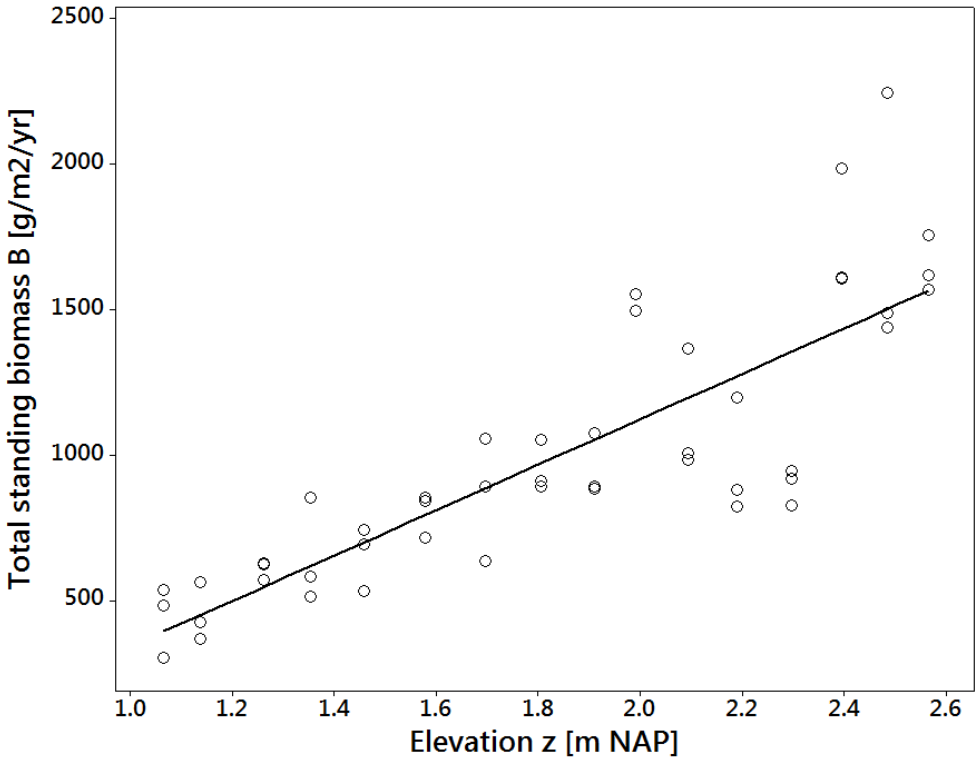

Figure 5.9: Scatter plot of total standing biomass against marsh elevation with the corresponding regression line of equation $B = -435.8 + 779.9z$. Model intercept is significant at p = 0.004 as well as slope at p<0.001. F-test on the regression model is significant at p<0.001. The coefficient of determination (R^2) is equal to 0.696.

Table 5.2: Average value of vegetation morphometric characteristics.

Elevation point	Elevation (m NAP)	Average biomass B (g.m^{-2}.yr^{-1})	Average stem diameter d_s (cm)	Average stem height h_s (cm)	Average stem density n_s (m^{-2})	Average proj. plant area per unit vol. a_s[3] (m^{-1})
P1	1.065	442.9	3.9	45.18	505.86	19.74
P2	1.136	452.9	3.35	42.61	466.13	15.6
P3	1.26	607.7	3.58	50.42	611.69	21.9
P4	1.353	649.7	4.26	52.33	608.69	25.93
P5	1.458	656.3	4.07	51.02	534.36	21.74
P6	1.578	804.1	4.27	55.71	502.26	21.43
P7	1.696	861.4	3.74	68.44	487.83	18.27
P8	1.909	952.9	4.31	69.03	472.83	20.4
P9	1.805	950.7	3.08	63.41	863.85	26.61
P10	1.99	1705.1	4.47	69.28	381.72	17.06
P11	2.093	1119.6	7.18	63.71	261.25	18.75
P12	2.19	967.0	4.93	61.02	387.21	19.09
P13	2.297	896.9	2.97	57.96	761.33	22.6
P14	2.395	1734.5	3.96	49.88	615.26	24.39
P15	2.485	1725.4	1.86	72.5	1259.24	23.45
P16	2.565	1648.1	2.00	76.74	1419.55	28.45

[3] Projected plant are per unit volume a_s, defined as $a_s = d_s \times n_s$. The projected plant area per unit volume represents the total area of plant material projected orthogonal to the flow direction within a 1 m^3 volume (Nepf, 1999; Mudd et al., 2010).

Table 5.3: Pearson product moment correlation coefficients r supplemented with hypothesis testing p-values between biomass or elevation and each of the vegetation characteristics.

Variable	Biomass	Elevation
Stem diameter d_s	-0.188 (p = 0.484)	-0.167 (p = 0.536)
Stem height h_s	**0.663** (p = **0.005**)	**0.708** (p = **0.002**)
Stem density n_s	0.460 (p = 0.073)	0.490 (p = 0.054)
Proj. plant area per unit vol. a_s	0.363 (p = 0.166)	0.297 (p = 0.264)

with *Elymus athericus*) as opposed to elevation points colonized by several species. Unlike stem diameter, stem height gradually increases with biomass Figure 5.10b, although a higher variation occurs all along the measurement transect.

Correlations between mean stem height and mean biomass yielded a certain degree of linear association ($r = 0.66$, significant at $p = 0.005$) which appeared to be even slightly stronger when replacing mean biomass by marsh elevation ($r = 0.71$, significant at $p = 0.002$). To the contrary, no correlation arose between mean stem diameter and mean biomass (r = -0.19, insignificant at $p = 0.484$) or marsh elevation (r = -0.17, insignificant at $p = 0.536$). Correlation test on the median diameter values did not improve the result. Similarly, despite a somewhat better Pearson score compared to stem diameter, all correlations between mean biomass and mean stem density or between mean biomass and mean projected plant area per unit volume were insignificant at 95% confidence interval. Analogous outcomes occur if substituting mean biomass with marsh elevation.

Consequently, stem height shows some degrees of linearity with mean biomass, which does not seem to hold however for the other vegetation characteristics, indicating either the existence of a non-linear function linking these plant morphometrics with mean biomass or simply an absence of relationship.

Based on the correlation results, an OLS regression analysis was therefore performed to model mean stem height as a function of mean biomass. Grubbs test revealed the presence of an outlier among the residuals (significant at p = 0.035). Despite the validity of the derived regression model as regards the assumptions on residuals (normality significant at p>0.150, homoscedasticity significant at p = 0.273, no autocorrelation structure) and the involved hypothesis tests, the outlier was discarded from the data series since regression attempts including and excluding the outlier have shown its influence in lowering the quality of the model (lower R^2 and higher S-score).

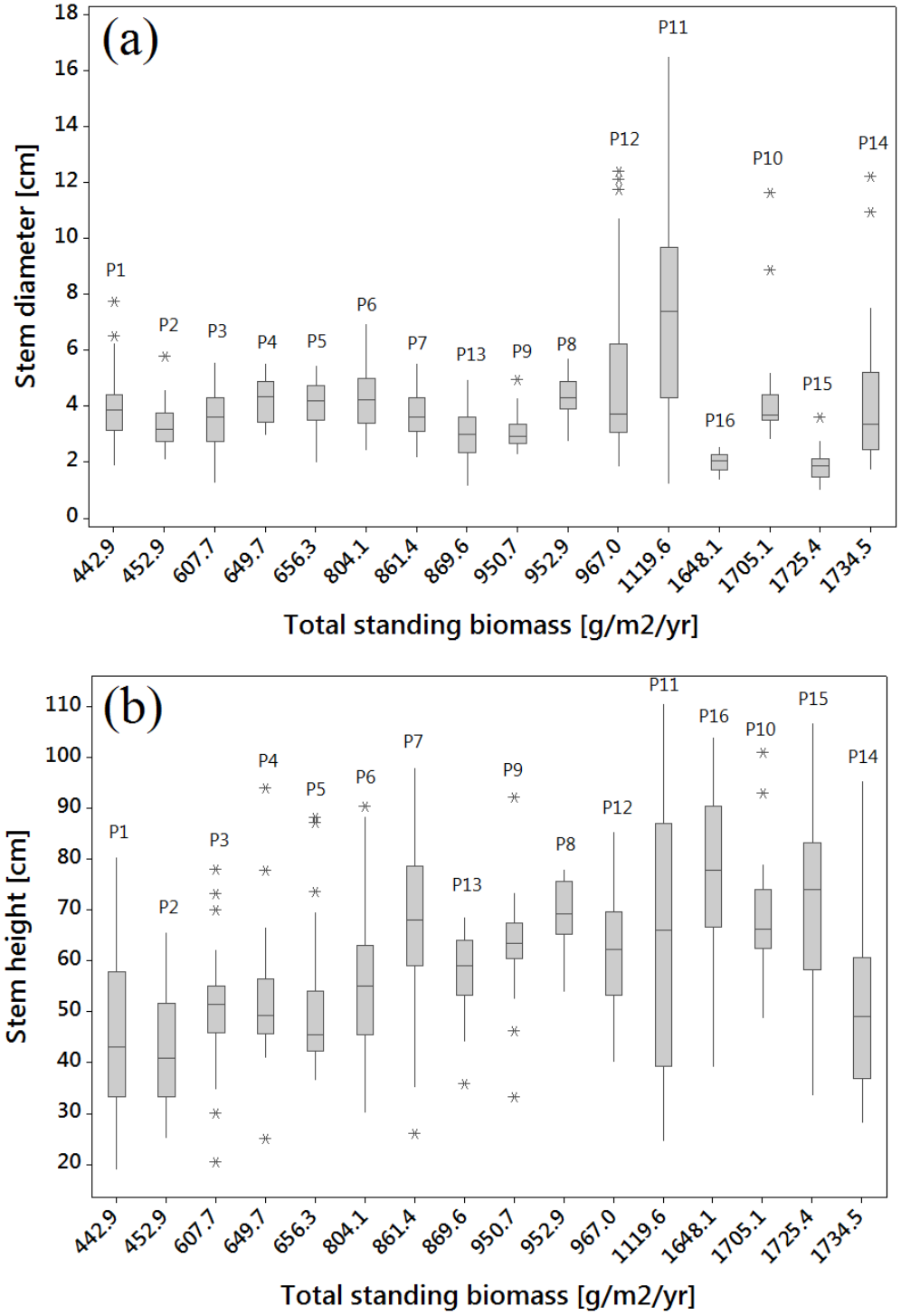

Figure 5.10: Box plots of (a) stem diameter and (b) stem height with respect to the total standing biomass averaged over every elevation point.

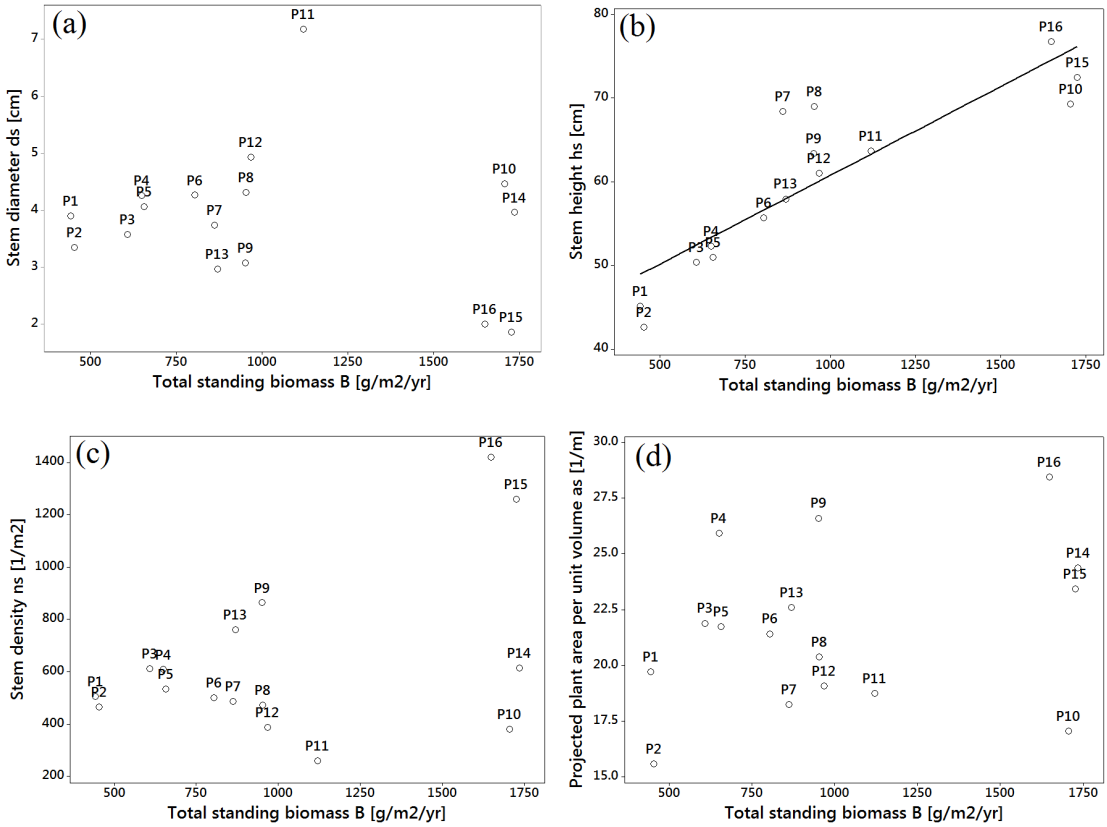

Figure 5.11: Scatter plot of (a) stem diameter d_s; (b) stem height h_s; (c) stem density n_s and (d) projected plant area per unit volume as against total standing biomass B. The fitted regression line in (b) has the equation $h_s = 39.56 + 0.02123B$. Model intercept and slope are significant at p<0.001. F-test on the regression model is significant at p<0.001. The coefficient of determination (R^2) is equal to 0.750.

Results of the regression analysis show that the total standing biomass describes 75% of the stem height via a linear function. Figure 5.11 displays the scatter plots of the different vegetation characteristics against mean total standing biomass and including the regression model derived for the stem height data. As clearly observed in Figure 5.11, except for the stem height, a broad scatter characterises the distribution of every vegetation characteristics with respect to the mean biomass which illustrates the absence of relationships between these respective variables.

5.5 Discussion

5.5.1 Halophyte vertical distribution and primary production

The topographic and species identification surveys discussed in the previous section suggest that some halophytic species exhibit preferential soil elevations for their establishment (e.g., *Suaeda maritimaa*, *Salicornia europea*, *Spergularia marina*, *Atriplex portulacoides* and *Elymus athericus*). To the contrary, the relatively uniform spatial distribution of the pioneer *Spartina anglica* (see Figure 5.7a) indicates that this species does not strictly depend on the position within the intertidal zone and can therefore adapt to varying edaphic conditions, such as flooding duration and frequency induced by the change in marsh elevation. In fact, the occurrence of *Spartina anglica* in the study area appears to be primarily conditioned to the presence and density of *Aster tripolium* and *Elymus athericus* (compare Figure 5.7a with b and with g). Therefore, species inter-specific competition reveals to be important in driving plant establishment as well. Although this key biotic process is common to salt marshes colonised by multiple plant species, this clearly contrasts with the distribution of *Spartina alterniflora* at North Inlet, South Carolina which can be explained by the local marsh elevation globally (Morris et al., 2005). This observation therefore confirms that zonation patterns do not only respond to the marsh elevation and the associated abiotic factors (i.e., inundation duration and frequency), but to a variety of interacting factors of different nature (Bockelmann et al., 2002).

Another interesting observation regards the diversity of plant species in the study site. Indeed, Figure 5.6 and Figure 5.7 point to an increase in species richness with distance from the seaward edge of the salt marsh up to an optimum elevation beyond which a progressive decline in species richness occurs towards eventually the return to a monospecific plant population at the highest elevations. This spatial diversity is surprising as usually less frequently flooded soils leads to a better aeration which should favour the colonisation of a number of species. In fact, this observation differs from other multiple species vegetated salt marshes, especially those in the Venice lagoon, where an increase in soil elevation is typically correlated with an increase in species diversity (e.g., Silvestri et al., 2005). In those marsh systems, the highest elevated areas are commonly found near the creek edges (e.g., Caniglia et al., 1997; Marani et al., 2004), and as shown by the herein ecogeomorphic model (see Chapter 4), whose drainage influences edaphic conditions and favour the growth of multiple plant species. In the present case however, this decrease in vegetation diversity in the high intertidal

zone may be the result of habitat adaptation to local edaphic conditions coupled with biotic processes such as competition between species. Indeed, *Elymus athericus* which almost exclusively dominates the highest elevation points is characterised by the highest stem height, density and projected plant area per unit volume (see Figure 5.11b, c and d), therefore leaving little space left for other salt marsh macrophytes to develop.

As expected, the observed distribution of vegetation productivity in the tidal frame does not give support to the quadratic relationship put forward by Morris et al. (2002), which is explained by the difference in ecological and climatic conditions between this present study site and North Inlet, the study side of Morris et al. (2002). Results have shown instead that vegetation aboveground production increases with marsh elevation (see Figure 5.9), corroborating thus with previous investigations on the vertical distribution of vegetation density in multiple species vegetated salt marshes (e.g., Silvestri et al., 2005). The present data set has notably shown that the total standing biomass can be expressed as an increasing linear function of marsh elevation. This direct finding therefore provides empirical proof for the use of such assumption in several modelling studies (e.g., D'Alpaos et al., 2006, 2007a). However, as previously raised, unlike the Venetian marshes, this linear increase in biomass is surprisingly not associated with an increase in plant diversity.

5.5.2 Relationships between vegetation biomass and morphometric vegetation characteristics

The field work analysis has revealed that only stem height depicts a relationship with vegetation productivity (see Figure 5.11b). Results have also shown a strong positive correlation between stem height and marsh elevation. This indicates thus that plant biomass is primarily materialised by stem height. On the opposite side, stem diameter does not yield any correlation with plant biomass which can be visualised by the lack of trend in Figure 5.11a. In truth, this broad scatter of data is associated with the segregation in diameter values between the different identified halophytes as displayed in Figure 5.12. By reason of their different plant composition and proportion, biomass samples being composed of different plant species therefore greatly differ from each other in their diameter statistics.

As the projected plant area per unit volume is a function of stem diameter, this vegetation characteristics does not correlate with plant biomass analogously (see Figure 5.11d). Similar outcome also characterises the paired stem density and plant biomass variables (see Figure 5.11c). Therefore, despite Mudd et al. (2004, 2010) documented

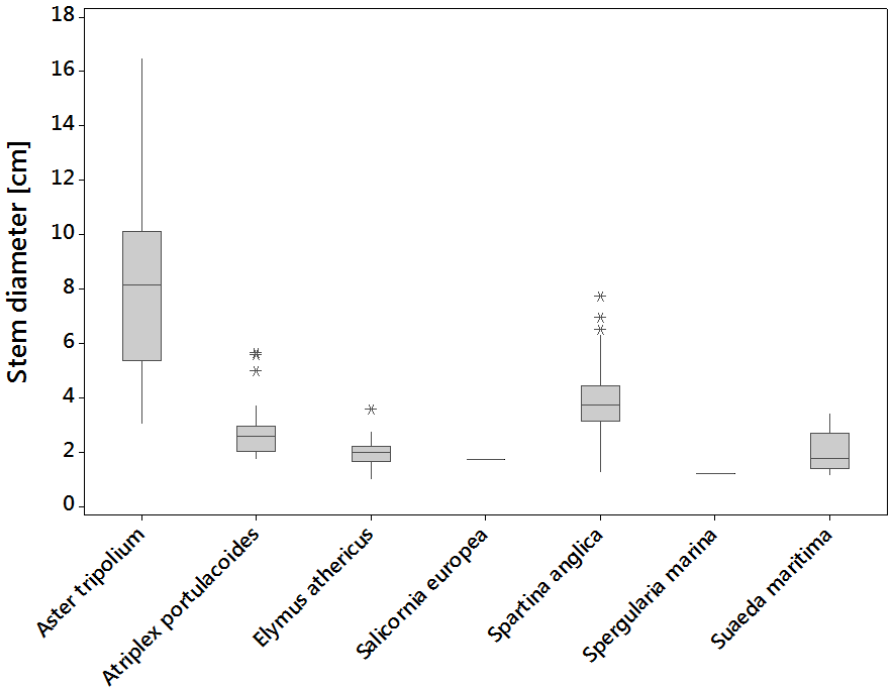

Figure 5.12: Box plot of stem diameter per observed salt marsh macrophytes.

a series of power law functions linking *Spartina alterniflora* characteristics to its aboveground biomass, the present data set does not provide evidence for these non-linear relationships, and the only derived relationship linking stem height with plant biomass is linear.

However, some patterns arise if considering only the response of *Spartina anglica* vegetation characteristics to its corresponding biomass. Regression attempts on the corresponding paired observations have led to the identification of quadratic relationships linking individually *Spartina anglica* stem density and projected area per unit volume with its biomass as highlighted in Figure 5.13. This allows for comparisons between the two *Spartina* pioneer species. Thus, despite *Spartina anglica* density and projected area per unit volume can be expressed as a function of its biomass, this relationship contrasts from the power law that its American counterpart exhibits. In truth, the existence of quadratic relationships in the present case, thence the decline in *Spartina anglica* density and projected area with higher biomass, clearly alludes to competition between species, a biotic process which is yet absent in the case of monospecific *Spartina alterniflora* marshes in North Inlet, hence the manifestation of a different relationship.

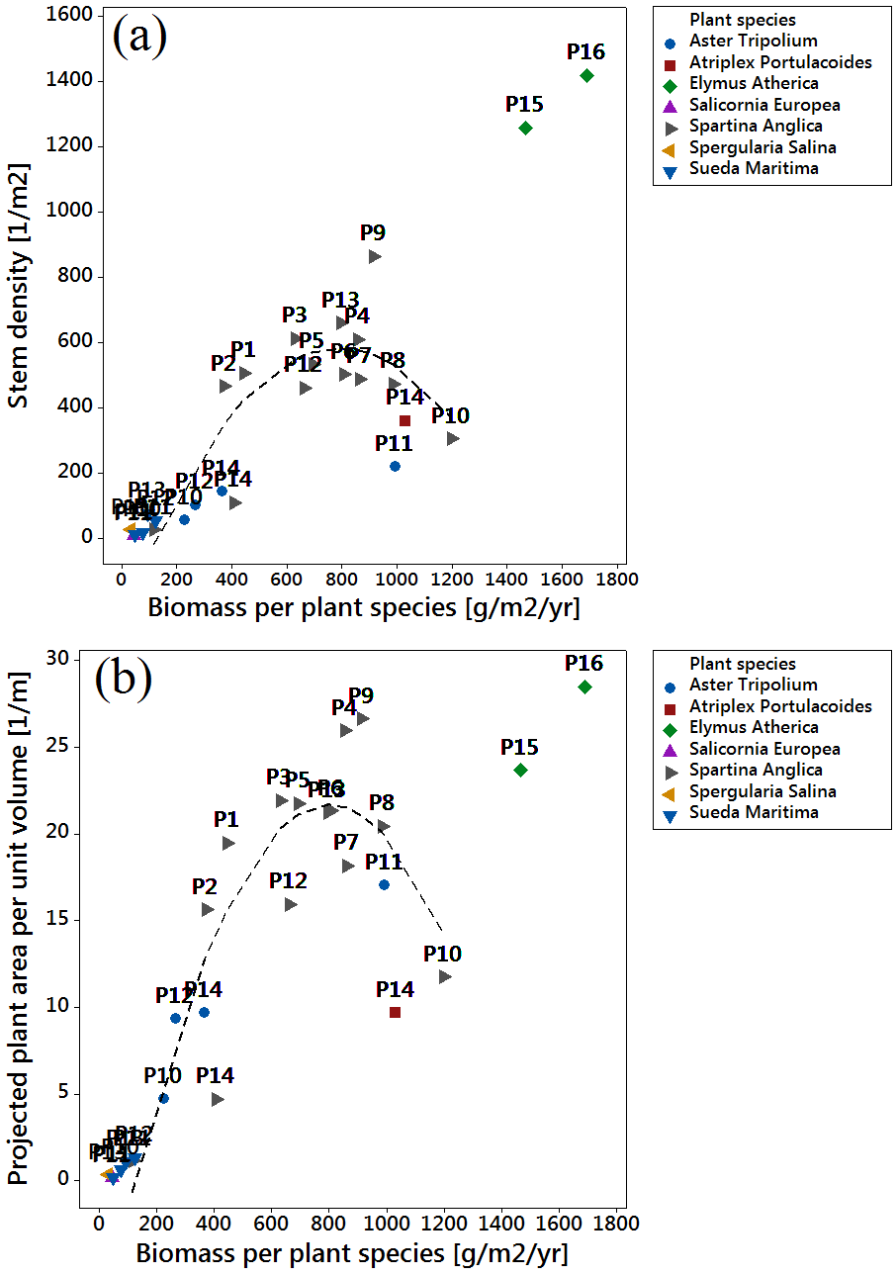

Figure 5.13: Scatter plot of (a) stem density per plant species and (b) projected plant area per unit volume and per plant species against its respective aboveground biomass. Regression line in (a) models *Spartina anglica* stem density as a function of its biomass ($n_s = -240.02 + 2.08B - 1.31B^2$). Assumptions on residuals are satisfied. R^2 = 0.60. Regression line in (b) models *Spartina anglica* projected plant area per unit volume as a function of its biomass ($a_s = -8.79 + 7.6.10^{-2}B - 4.74.10^{-5}B^2$). Assumptions on residuals are satisfied. R^2=0.70.

In sum, vegetation characteristics are typically parameterised in global models in the form of power laws as a function of the aboveground biomass (Morris and Haskin, 1990; Mudd et al., 2004, 2010). The present data set has however shown that a relationship between these characteristics and plant productivity disappears particularly for multiple species vegetated marshes exhibiting high biomass or elevations (see Figure 5.11). Owing to the important role of these vegetation morphometrics in enhancing sediment deposition either via enhanced settling of suspended sediments or their direct capture, results suggest that these models may overestimate sedimentation rates in marsh regions colonised by a variety of macrophytes and located high in the intertidal zone. This inability to capture the proper ecological dynamics in this portion of the tidal landscape should be highly considered in view of the implications this has in wetland resiliency notably facing sea level rise.

Chapter 6

Conclusions

Through this study of the nature, configuration and development of tidal networks and their relationships with associated landforms and biotic components (e.g., vegetation), this research has aimed to bring further insights into the geomorphology of this particular tidal landform. This concluding chapter exposes a summary picture based on the main outcomes per research element, while incorporating future research recommendations.

6.1 Variability of tidal network patterns

The study on the variability of tidal network patterns discussed in Chapter 3 has indicated that the investigated network types can be characterised based on measures of network size and complexity, with each pattern depicting proper morphometric characteristics. Particularly, the median depth of the network main channel and stream Strahler order provide the greatest discrimination between network patterns. Comparisons of network main channel aspect ratios have notably suggested that linear, linear-dendritic and dendritic networks followed a transitional gradient approximated by a power law and thus are seen to depict similar erosional processes. To the contrary, meandering networks clearly depart from this relationship, and show particular segregation in their aspect ratios with those of dendritic networks, thence on the type of incisions, which has shown to be controlled by the marsh sediment composition. In truth, differentiation on network pattern morphometrics has been linked to global environmental conditions characteristic of the marsh physiographic setting within which tidal networks occur. On one hand, in well-exposed tidal systems, tidal networks portray only single or few linear tidal channels as the corresponding high marine energy may directly contribute to the flooding and drainage of the salt marshes notably via sheet flows, leaving therefore

the tidal network with a simplistic structure. On the other hand, in more sheltered tidal systems, tidal networks must depict a higher degree of elaboration to compensate the corresponding low marine energy, and ensure an efficient drainage of the tidal basin. This higher level of complexity is manifested by an increasing drainage density, stream order and network size (through channel depth and/or width), which have shown to characterise dendritic and above all meandering networks. Accordingly, tidal networks seem to be able to adapt to global environmental conditions by adopting suitable morphologies to serve their tidal basin effectively.

The modelling results presented in Chapter 4 have also pointed out to a higher degree of channel elaboration with increasing sediment supply. This observation connected with the fact that corresponding numerical experiments were performed on a computational domain being representative of a lagoonal environment through its configuration, bathymetry and prescribed hydrodynamic as well as sedimentological boundary conditions recalls sheltered physiographic settings where deposition prevails, therefore corroborating the findings from the geo-spatial analysis. In truth, the present modelling framework was designed for micro-tidal basins such as in the Venice lagoon. However, the model is, in principle, flexible and can be applied to study different tidal environments, upon the implementation of suitable initial and boundary conditions. Therefore, one recommendation would be to model tidal network development within different physiographic settings in order to provide further evidence for the conceptual model derived from the geo-spatial analysis. Indeed, the role of landscape setting as a potential control on tidal network morphodynamics has not been explored in previous modelling studies, which adopted a computational domain representing a hypothetical closed tidal basin with the presence of an inlet where boundary conditions were typically prescribed. Additionally, one might consider the parameterization of explicit bank erosion processes together with secondary circulation in the model to simulate the development of meandering networks. However, implementing these physical processes remains fairly difficult and implies solving hydro-geomorphic feedbacks at fast and detailed scales, which would lead to severe computational efforts and eventually challenge the model applicability at the long term (Coco et al., 2013).

Moreover, although the derived data set of the geo-spatial analysis has allowed grasping inter- and intra-site variability of tidal network patterns, its dimensionality should be further increased in order to extend the overall population representativity and thus minimises the limitations inherent to the use of remotely-sensed data. As a matter of fact, the accuracy of the data highly depends on the resolution provided by the

corresponding medium. In the present case, the extraction of the different morphometric variables was based on high resolution data, and only a threshold was imposed for the determination of the total network length.

In addition, limitations can also regard data availability. A typical example in the present geo-spatial analysis refers to the determination of the vegetation area proportion consequent to the estimation of the vegetation cover for a particular tidal sub-basin. As mentioned previously, particular concerns were placed in using Google Earth images dated as close as possible to the date of the corresponding LiDAR survey. Yet, sometimes these dates were not coinciding and shifts from months to years could have occurred depending on the amount of historical images available at a particular site. Therefore, the selected aerial image may not have captured the exact plant spatial distribution at the particular date, leading instead to either an underestimation or overestimation of the plant cover since halophyte biomass depicts seasonal variations despite their biennial to perennial life cycle. This might explain why vegetation area proportion did not show overall significance in the statistical analysis, although the model has highlighted the potential control of salt marsh vegetation on tidal network morphodynamics. Perhaps the selection of other vegetation properties may be more relevant to detect its impact on tidal network morphology. For instance, halophyte density could be estimated based on formulations using Normalised Difference Vegetation Index (NDVI). However, this would require the use of multispectral images such as satellite images in order to obtain the vegetation spectral signature in the near infra-red region of the spectrum, to the detriment of a coarser pixel resolution.

6.2 Tidal network ontogeny

The modelling experiments have shown that the development of tidal networks and their intrinsic channels in marsh accretion and progradation contexts becomes the product of erosional and depositional processes, acting on different ontogenic stages: channel initiation stems from bottom incisions in regions where initial local depressions occur, while channel elaboration mostly results from differential deposition contributing to the deepening of the tidal channels relative to the adjacent marsh platform. The further evolutionary stages including channel reduction proceed from the horizontal progradation of the marsh platform leading to channel narrowing and eventually channel segmentation, and closure.

Both qualitative and quantitative modelling results have also indicated that tidal

network development is accelerated with increasing sediment supply. Although such effect seems trivial when looking at the marsh morphological evolution, because marshes typically age as they build up along the tidal frame (Pethick, 1981), transposing such a concept to the tidal network landform appears to be rather counter-intuitive as the majority of conceptual and mathematical models assume channel development as mainly resulting from erosional activity.

These previous observations emphasise thus the prevalence of the depositional processes in shaping the tidal network, and which has been disregarded in previous modelling studies. Evidently, such a geomorphic control on tidal channel development arises particularly in marshes experiencing high sedimentation rates, which may allude to a situation where relative sea level rise is null or even negative (i.e., soil uplift by sediment accretion), and which characterises a series of wetland locations worldwide (Redfield, 1965, 1972; Beeftink, 1966; Hood, 2006). However, it is well-known that mostly tidal environments are nowadays experiencing sea-level rise (Boesch et al., 1994; Marani et al., 2007; Kirwan et al., 2008, 2009, 2010). Therefore, one recommendation would be to complement the actual picture provided by the model with the implementation of the sea-level rise process, to study its impact not only on tidal network development but also on the spatial redistribution of the sediments in the system which may possibly lead to new topographic configuration, and the prominence of a new landscape setting.

Moreover, the modelling experiments have also emphasised that network morphological evolution and complexity occur more rapidly and in greater extent when tidal channels develop onto an initial perturbed bathymetry, this additional landscape characteristics complementing the environmental conditions related to the marsh physiographic setting derived from Chapter 3. In particular, these observations have exposed the legacy of the initial topography on tidal channel morphological features.

Lastly, modelling results have also confirmed the potential control of the salt marsh vegetation in driving tidal channel morphological evolution. Such an influence is linked to the vegetation biomass distribution within the tidal frame in relation to the characteristic time scale of channel initiation. In fact, depending on its presence or absence during the short time span where drainage patterns start initiating, vegetation may be seen either as an erosive or stabilizing control for tidal channel development. However, the comparison of network morphological development based upon the parameterization of two different mathematical representations of vegetation growth has pointed out to the sensitivity of the system morphodynamics to the way vegetation

productivity is formulated. This calls for the necessity to derive accurate mathematical representations of such a dynamic process.

6.3 Vegetation productivity in salt marshes

Direct measurements of vegetation properties including biomass and morphometric characteristics presented in Chapter 5 were carried out in a salt marsh to attempt to provide evidences for vegetation properties relationships reported in the literature (e.g., Morris and Haskin, 1990; Morris et al., 2002; Mudd et al., 2004, 2010; Marani et al., 2010, 2013), some of which have been set in the present modelling framework. In this respect, the field survey was conducted in a temperate salt marsh populated with different halophytic species in order to test the likely presence and validity of these previously derived relationships in different climatic and ecological conditions, and within the scope of deriving global eco-geomorphic models.

Field work analysis has revealed that vegetation biomass increases with marsh elevation, confirming therefore such a consideration which was previously assumed based on the spatial distribution of plant diversity and density in multiple species vegetated salt marshes. Surprisingly however, this increase in biomass is not accompanied with an increase in plant diversity in the present study site. Specifically, regression analysis yielded an increasing linear relationship between total standing biomass and marsh relative elevation, providing empirical validation for corresponding mathematical representations implemented in the modelling framework in Chapter 4 and in other modelling studies (D'Alpaos et al., 2006, 2007b).

Analysis of likely association between vegetation morphometrics and total standing biomass provided only a single linear relationship linking the latter to stem height. Lack of relationships for other vegetation characteristics was attributed to the multiple species marsh ecological character whereby different plant composition and proportion between samples induced clear distinctions in morphometric values. As these vegetation characteristics intervene in the formulation of some eco-sedimentary processes, the corresponding absence of relationship linking these morphometric variables with plant biomass should be taken cautiously in view of the implications this may have in wetland resiliency facing sea-level rise. The validity of such outcomes should be however further tested as the field survey was only conducted along a single transect, leading to the determination of biomass distribution exclusively in the vertical frame. However, horizontal variability in biomass distribution should be also considered, and

the observed variation in biomass values between replicate samples for some elevation points argues its importance.

6.4 Concluding remark

On overall, the research has outlined the tight coupling of the tidal network with the associated tidal flat and salt marsh landforms and their biological components (e.g., vegetation), thence the necessity to adopt a holistic research approach by considering the tidal wetland as a whole reference system and the need for integrated interdisciplinary studies over the involved characteristic scales when studying the geomorphology of tidal networks.

Bibliography

Adam, P. (1990). *Saltmarsh ecology*. Cambridge University Press.

Allen, J. R. (1989). Evolution of salt-marsh cliffs in muddy and sandy systems: a qualitative comparison of British west-coast estuaries. *Earth Surface Processes and Landforms*, 14(1):85–92.

Allen, J. R. (1990). Salt-marsh growth and stratification: a numerical model with special reference to the Severn Estuary, southwest Britain. *Marine Geology*, 95(2):77–96.

Allen, J. R. (2000). Morphodynamics of Holocene salt marshes: a review sketch from the Atlantic and Southern North Sea coasts of Europe. *Quaternary Science Reviews*, 19(12):1155–1231.

Allen, J. R. and Duffy, M. (1998). Medium-term sedimentation on high intertidal mudflats and salt marshes in the Severn Estuary, SW Britain: the role of wind and tide. *Marine Geology*, 150(1):1–27.

Allen, J. R. and Pye, K. (1992). Coastal saltmarshes: their nature and importance. In Allen, J. R. and Pye, K., editors, *Saltmarshes: morphodynamics, conservation, and engineering significance*, pages 1–18. Cambridge University Press.

Amos, C., Bergamasco, A., Umgiesser, G., Cappucci, S., Cloutier, D., DeNat, L., Flindt, M., Bonardi, M., and Cristante, S. (2004). The stability of tidal flats in Venice lagoon—the results of in-situ measurements using two benthic, annular flumes. *Journal of Marine Systems*, 51(1):211–241.

Anderson, T. W. and Darling, D. A. (1952). Asymptotic theory of certain "goodness of fit" criteria based on stochastic processes. *The annals of mathematical statistics*, pages 193–212.

Ashley, G. M. and Zeff, M. L. (1988). Tidal channel classification for a low-mesotidal salt marsh. *Marine Geology*, 82(1):17–32.

Ashworth, P. J. (1996). Mid channel bar growth and tis relationship to local flow strength and direction. *Earth Surface Processes and Landforms*, 21(2):103–123.

Barbier, E. B., Hacker, S. D., Kennedy, C., Koch, E. W., Stier, A. C., and Silliman, B. R. (2011). The value of estuarine and coastal ecosystem services. *Ecological Monographs*, 81(2):169–193.

Bayliss-Smith, T., Healey, R., Lailey, R., Spencer, T., and Stoddart, D. (1979). Tidal flows in salt marsh creeks. *Estuarine and Coastal Marine Science*, 9(3):235–255.

Beeftink, W. (1966). *Vegetation and habitat of the salt marshes and beach plains in the south-western part of the Netherlands*. Wentia.

Beeftink, W. and Rozema, J. (1988). The nature and functioning of salt marshes. In *Pollution of the North Sea*, pages 59–87. Springer.

Bendoni, M., Francalanci, S., Cappietti, L., and Solari, L. (2014). On salt marshes retreat: Experiments and modeling toppling failures induced by wind waves. *Journal of Geophysical Research: Earth Surface*, 119(3):603–620.

Bertness, M. D. and Ellison, A. M. (1987). Determinants of pattern in a New England salt marsh plant community. *Ecological Monographs*, pages 129–147.

Bertness, M. D., Gaines, S., and Hay, M. (2001). Salt marsh communities. In *Marine community ecology*, pages 289–316. Sinauer Associates, Sunderland, MA.

Best, J. L. (1988). Sediment transport and bed morphology at river channel confluences. *Sedimentology*, 35(3):481–498.

Bird, E. C. F. and Bird, E. (2000). *Coastal geomorphology: an introduction*. Wiley Online Library.

Bockelmann, A.-C., Bakker, J. P., Neuhaus, R., and Lage, J. (2002). The relation between vegetation zonation, elevation and inundation frequency in a Wadden Sea salt marsh. *Aquatic Botany*, 73(3):211–221.

Boesch, D. F., Josselyn, M. N., Mehta, A. J., Morris, J. T., Nuttle, W. K., Simenstad, C. A., and Swift, D. J. (1994). Scientific assessment of coastal wetland loss, restoration and management in Louisiana. *Journal of Coastal Research*, pages i–103.

Bouma, T., Friedrichs, M., Van Wesenbeeck, B., Temmerman, S., Graf, G., and Herman, P. (2009). Density-dependent linkage of scale-dependent feedbacks: A flume study on the intertidal macrophyte *Spartina anglica*. *Oikos*, 118(2):260–268.

Boyer, C., Roy, A. G., and Best, J. L. (2006). Dynamics of a river channel confluence with discordant beds: Flow turbulence, bed load sediment transport, and bed morphology. *Journal of Geophysical Research: Earth Surface)*, 111(F4).

Bridge, J. S. and Bennett, S. J. (1992). A model for the entrainment and transport of sediment grains of mixed sizes, shapes, and densities. *Water Resources Research*, 28(2):337–363.

Bruno, J. F. and Bertness, M. D. (2001). Habitat modification and facilitation in benthic marine communities. *Marine community ecology*, pages 201–218.

Burd, F. (1989). Saltmarsh survey of great britain: an inventory of British Saltmarshes. Technical report, Nature Conservancy Council, Peterborough.

Burgin, S. (2010). 'Mitigation banks' for wetland conservation: a major success or an unmitigated disaster? *Wetlands Ecology and Management*, 18(1):49–55.

Burns, R. P. and Burns, R. (2008). Chapter 25: Discriminant Analysis. In *Business research methods and statistics using SPSS*. Sage.

Byrne, R., Gammisch, R., and Thomas, G. (1980). Tidal prism-inlet area relations for small tidal inlets. In *Proceedings of the 17th Conference on Coastal Engineering*, volume 1, pages 2517–2533, New York. American Society of Civil Engineers.

Caniglia, G., Contin, G., Fusco, M., Anoé, N., and Zanaboni, A. (1997). Confronto su base vegetazionale tra due barene della laguna di venezia. *Fitosociologia*, 34:111–119.

Carniello, L., D'Alpaos, A., and Defina, A. (2011). Modeling wind waves and tidal flows in shallow micro-tidal basins. *Estuarine, Coastal and Shelf Science*, 92(2):263–276.

Carniello, L., Defina, A., and D'Alpaos, L. (2012). Modeling sand-mud transport induced by tidal currents and wind waves in shallow microtidal basins: Application to the Venice Lagoon (Italy). *Estuarine, Coastal and Shelf Science*, 102:105–115.

Carniello, L., Defina, A., Fagherazzi, S., and D'alpaos, L. (2005). A combined wind wave–tidal model for the Venice lagoon, Italy. *Journal of Geophysical Research: Earth Surface (2003–2012)*, 110(F4).

Cattell, R. B. (1966). The scree test for the number of factors. *Multivariate behavioral research*, 1(2):245–276.

Chapman, V. J. (1960). Salt marshes and salt deserts of the world. *London, New York*.

Chow, V. T. (1959). Open-channel hydraulics. In *Open-channel hydraulics*. McGraw-Hill Book Company.

Christiansen, T., Wiberg, P., and Milligan, T. (2000). Flow and sediment transport on a tidal salt marsh surface. *Estuarine, Coastal and Shelf Science*, 50(3):315–331.

Claessens, J. and Meyvis, L. (1994). *Overzicht van de tijwaarnemingen in het Zeescheldebekken gedurende het decennium 1981-1990*. Ministerie van de Vlaamse Gemeenschap AWZ Afdeling Maritieme Schelde, Antwerpen, Belgium.

Coco, G., Zhou, Z., van Maanen, B., Olabarrieta, M., Tinoco, R., and Townend, I. (2013). Morphodynamics of tidal networks: Advances and challenges. *Marine Geology*, 346:1–16.

Collins, L., Collins, J., and Leopold, L. (1987). Geomorphic processes of an estuarine marsh: preliminary results and hypotheses. *International geomorphology*, 1:1049–1072.

Costanza, R., d'Arge, R., De Groot, R., Farber, S., Grasso, M., Hannon, B., Limburg, K., Naeem, S., O'Neill, R. V., Paruelo, J., et al. (1997). The value of the world's ecosystem services and natural capital. *Nature*, 387.

Crooks, S., Schutten, J., Sheern, G. D., Pye, K., and Davy, A. J. (2002). Drainage and elevation as factors in the restoration of salt marsh in Britain. *Restoration Ecology*, 10(3):591–602.

Da Lio, C., D'Alpaos, A., and Marani, M. (2013). The secret gardener: Vegetation and the emergence of biogeomorphic patterns in tidal environments. *Philosophical Transactions of the Royal Society A: Mathematical, Physical and Engineering Sciences*, 371(2004).

D'Alpaos, A., Lanzoni, S., Marani, M., Bonometto, A., Cecconi, G., and Rinaldo, A. (2007a). Spontaneous tidal network formation within a constructed salt marsh: observations and morphodynamic modelling. *Geomorphology*, 91(3):186–197.

D'Alpaos, A., Lanzoni, S., Marani, M., Fagherazzi, S., and Rinaldo, A. (2005). Tidal network ontogeny: Channel initiation and early development. *Journal of Geophysical Research: Earth Surface (2003–2012)*, 110(F2).

D'Alpaos, A., Lanzoni, S., Marani, M., and Rinaldo, A. (2007b). Landscape evolution in tidal embayments: Modeling the interplay of erosion, sedimentation, and vegetation dynamics. *Journal of Geophysical Research: Earth Surface (2003–2012)*, 112(F1).

D'Alpaos, A., Lanzoni, S., Marani, M., and Rinaldo, A. (2009). On the O'Brien–Jarrett–Marchi law. *Rendiconti Lincei*, 20(3):225–236.

D'Alpaos, A., Lanzoni, S., Marani, M., and Rinaldo, A. (2010). On the tidal prism-channel area relations. *Journal of Geophysical Research F: Earth Surface*, 115(1).

D'Alpaos, A., Lanzoni, S., Mudd, S. M., and Fagherazzi, S. (2006). Modeling the influence of hydroperiod and vegetation on the cross-sectional formation of tidal channels. *Estuarine, Coastal and Shelf Science*, 69(3):311–324.

Dalrymple, R. W. and Choi, K. (2007). Morphologic and facies trends through the fluvial–marine transition in tide-dominated depositional systems: a schematic framework for environmental and sequence-stratigraphic interpretation. *Earth-Science Reviews*, 81(3):135–174.

Day Jr, J., Rybczyk, J., Scarton, F., Rismondo, A., Are, D., and Cecconi, G. (1999). Soil accretionary dynamics, sea-level rise and the survival of wetlands in Venice Lagoon: a field and modelling approach. *Estuarine, Coastal and Shelf Science*, 49(5):607–628.

De Swart, H. and Zimmerman, J. (2009). Morphodynamics of tidal inlet systems. *Annual Review of Fluid Mechanics*, 41:203–229.

De Vriend, H., Capobianco, M., Chesher, T., De Swart, H. d., Latteux, B., and Stive, M. (1993). Approaches to long-term modelling of coastal morphology: a review. *Coastal Engineering*, 21(1):225–269.

Defina, A. (2000). Two-dimensional shallow flow equations for partially dry areas. *Water Resources Research*, 36(11):3251–3264.

Di Silvio, G., Dall'Angelo, C., Bonaldo, D., and Fasolato, G. (2010). Long-term model of planimetric and bathymetric evolution of a tidal lagoon. *Continental Shelf Research*, 30(8):894–903.

Dijkema, K., Bossinade, J., Bouwsema, P., and De Glopper, R. (1990). *Salt marshes in the Netherlands Wadden Sea: rising high-tide levels and accretion enhancement*. Springer.

Dronkers, J. (2005). *Dynamics of coastal systems*. World Scientific, Singapore.

Eisma, D. (1998). *Intertidal deposits: river mouths, tidal flats, and coastal lagoons*, volume 16. CRC Press.

Elsey-Quirk, T., Middleton, B. A., and Proffitt, C. E. (2009). Seed dispersal and seedling emergence in a created and a natural salt marsh on the Gulf of Mexico coast in southwest Louisiana, USA. *Restoration Ecology*, 17(3):422–432.

Environment Agency (2014a). Environment agency - river and sea levels. `http://apps.environment-agency.gov.uk/river-and-sea-levels/default.aspx`.

Environment Agency (2014b). Geomatics - environment agency, national operations. `https://www.geomatics-group.co.uk/geocms/`.

EstSim Consortium (2007). Development and demonstration of systems-based estuary simulators. R&d technical report fd2117/tr, Joint Defra/EA Flood and Coastal Erosion Risk Management R&D Programme.

European Parliament and the Council of the European Union (2000). Directive 2000/60/EC of the European Parliament and of the Council establishing a framework for the Community action in the field of water policy. Technical report, Official Journal of the European Communities.

Fagherazzi, S., Bortoluzzi, A., Dietrich, W. E., Adami, A., Lanzoni, S., Marani, M., and Rinaldo, A. (1999). Tidal networks: 1. automatic network extraction and preliminary scaling features from digital terrain maps. *Water Resources Research*, 35(12):3891–3904.

Fagherazzi, S., Carniello, L., D'Alpaos, L., and Defina, A. (2006). Critical bifurcation of shallow microtidal landforms in tidal flats and salt marshes. *Proceedings of the National Academy of Sciences*, 103(22):8337–8341.

Fagherazzi, S. and Furbish, D. J. (2001). On the shape and widening of salt marsh creeks. *Journal of Geophysical Research: Oceans (1978–2012)*, 106(C1):991–1003.

Fagherazzi, S., Gabet, E. J., and Furbish, D. J. (2004). The effect of bidirectional flow on tidal channel planforms. *Earth Surface Processes and Landforms*, 29(3):295–309.

Fagherazzi, S., Hannion, M., and D'Odorico, P. (2008). Geomorphic structure of tidal hydrodynamics in salt marsh creeks. *Water resources research*, 44(2).

Fagherazzi, S., Kirwan, M. L., Mudd, S. M., Guntenspergen, G. R., Temmerman, S., D'Alpaos, A., Koppel, J., Rybczyk, J. M., Reyes, E., Craft, C., et al. (2012). Numerical models of salt marsh evolution: Ecological, geomorphic, and climatic factors. *Reviews of Geophysics*, 50(1).

Fagherazzi, S. and Overeem, I. (2007). Models of deltaic and inner continental shelf landform evolution. *Annu. Rev. Earth Planet. Sci.*, 35:685–715.

Fagherazzi, S. and Sun, T. (2004). A stochastic model for the formation of channel networks in tidal marshes. *Geophysical Research Letters*, 31(21).

Feola, A., Belluco, E., D'Alpaos, A., Lanzoni, S., Marani, M., and Rinaldo, A. (2005). A geomorphic study of lagoonal landforms. *Water resources research*, 41(6).

French, J. R. (1993). Numerical simulation of vertical marsh growth and adjustment to accelerated sea-level rise, north Norfolk, UK. *Earth Surface Processes and Landforms*, 18(1):63–81.

French, J. R. and Stoddart, D. (1992). Hydrodynamics of salt marsh creek systems: Implications for marsh morphological development and material exchange. *Earth surface processes and landforms*, 17(3):235–252.

French, P. W. (2006). Managed realignment–the developing story of a comparatively new approach to soft engineering. *Estuarine, Coastal and Shelf Science*, 67(3):409–423.

Frey, R. W. and Basan, P. B. (1978). Coastal salt marshes. In *Coastal sedimentary environments*, pages 101–169. Springer.

Friedrichs, C. T. (1995). Stability shear stress and equilibrium cross-sectional geometry of sheltered tidal channels. *Journal of Coastal Research*, pages 1062–1074.

Friedrichs, C. T. and Perry, J. E. (2001). A review of tidal salt marsh morphodynamics. In *AGU Spring Meeting Abstracts*, volume 1.

Gabet, E. J. (1998). Lateral migration and bank erosion in a saltmarsh tidal channel in San Francisco Bay, California. *Estuaries*, 21(4):745–753.

Gallagher, J. (1975). Effects of an ammonium nitrate pulse on the growth and elemental composition of natural strands of *Spartina alterniflora* and *Juncus roemeriamus*. *American Journal of Botany*, 62.

Gao, S. (2009). Geomorphology and sedimentology of tidal flats. In Perillo, G. M., Wolanski, E., Cahoon, D. R., and Brinson, M. M., editors, *Coastal Wetlands: An Integrated Ecosystem Approach*. Elsevier, Amsterdam.

Garbutt, R., Reading, C., Wolters, M., Gray, A., and Rothery, P. (2006). Monitoring the development of intertidal habitats on former agricultural land after the managed realignment of coastal defences at Tollesbury, Essex, UK. *Marine Pollution Bulletin*, 53(1):155–164.

Garofalo, D. (1980). The influence of wetland vegetation on tidal stream channel migration and morphology. *Estuaries*, 3(4):258–270.

Gehrels, W. R. (2010). Late Holocene land-and sea-level changes in the british isles: implications for future sea-level predictions. *Quaternary Science Reviews*, 29(13):1648–1660.

Gibbs, R. J. (1985). Estuarine flocs: their size, settling velocity and density. *Journal of Geophysical Research: Oceans (1978–2012)*, 90(C2):3249–3251.

Ginsberg, S. S. and Perillo, G. M. (2004). Characteristics of tidal channels in a mesotidal estuary of Argentina. *Journal of coastal research*, pages 489–497.

Glenn-Lewin, D. C., Peet, R. K., and Veblen, T. T. (1992). *Plant succession: theory and prediction*, volume 11. Springer.

Glock, W. S. (1931). The development of drainage systems: A synoptic view. *Geographical Review*, pages 475–482.

Goudie, A. (2013). Characterising the distribution and morphology of creeks and pans on salt marshes in England and Wales using Google Earth. *Estuarine, Coastal and Shelf Science*, 129:112–123.

Grass, A. J. (1970). Initial instability of fine bed sand. *Journal of the hydraulics division*, 96(3):619–632.

Gray, A. (1972). The ecology of Morecambe Bay. v. The salt marshes of Morecambe Bay. *Journal of Applied Ecology*, pages 207–220.

Grubbs, F. E. (1950). Sample criteria for testing outlying observations. *The Annals of Mathematical Statistics*, pages 27–58.

Hack, J. T. (1973). Stream-profile analysis and stream-gradient index. *Journal of Research of the US Geological Survey*, 1(4):421–429.

Hibma, A., Stive, M., and Wang, Z. (2004). Estuarine morphodynamics. *Coastal Engineering*, 51(8):765–778.

Hood, W. G. (2006). A conceptual model of depositional, rather than erosional, tidal channel development in the rapidly prograding Skagit River Delta (Washington, USA). *Earth Surface Processes and Landforms*, 31(14):1824–1838.

Hood, W. G. (2010). Tidal channel meander formation by depositional rather than erosional processes: examples from the prograding Skagit River Delta (Washington, USA). *Earth Surface Processes and Landforms*, 35(3):319–330.

Horton, R. E. (1945). Erosional development of streams and their drainage basins; hydrophysical approach to quantitative morphology. *Geological society of America bulletin*, 56(3):275–370.

Hughes, S. A. (2002). Equilibrium cross sectional area at tidal inlets. *Journal of Coastal Research*, pages 160–174.

Hughes, Z. J. (2012). Tidal channels on tidal flats and marshes. In Davis, R. and Dalrymple, R., editors, *Principles of Tidal Sedimentology*, pages 269–300. Springer.

Hughes, Z. J., FitzGerald, D. M., Wilson, C. A., Pennings, S. C., Więski, K., and Mahadevan, A. (2009). Rapid headward erosion of marsh creeks in response to relative sea level rise. *Geophysical Research Letters*, 36(3).

Hume, T. M. (1991). Empirical stability relationships for estuarine waterways and equations for stable channel design. *Journal of coastal research*, pages 1097–1111.

Jarrett, J. T. (1976). Tidal prism-inlet area relationships. Technical report, U.S. Army Coastal Engineering Research Center, Fort Belviour, VA.

Jones, C. G., Lawton, J. H., and Shachak, M. (1994). Organisms as ecosystem engineers. In *Ecosystem Management*, pages 130–147. Springer.

Jones, L., Angus, S., Cooper, A., Doody, P., Everard, M., Garbutt, A., Gilchrist, P., Hansom, J., Nicholls, R., Pye, K., Ravenscroft, N., Rees, S., Rhind, P., and Whitehouse, A. (2011). Coastal margins. In *The UK National Ecosystem Assessment Technical Report*. UK National Ecosystem Assessment UNEP-WCMC, Cambridge.

King, C. A. (1972). *Beaches and coasts*. Edward Arnold, London, 2nd edition.

Kirby, R. (2013). The long-term sedimentary regime of the Outer Medway Estuary. *Ocean & Coastal Management*, 79:20–33.

Kirchner, J. W. (1993). Statistical inevitability of horton's laws and the apparent randomness of stream channel networks. *Geology*, 21(7):591–594.

Kirwan, M., Christian, R., Blum, L., and Brinson, M. (2012). On the Relationship Between Sea Level and *Spartina alterniflora* Production. *Ecosystems*, 15(1):140–147.

Kirwan, M. and Temmerman, S. (2009). Coastal marsh response to historical and future sea-level acceleration. *Quaternary Science Reviews*, 28(17-18):1801–1808.

Kirwan, M. L. and Guntenspergen, G. R. (2010). Influence of tidal range on the stability of coastal marshland. *Journal of Geophysical Research: Earth Surface (2003–2012)*, 115(F2).

Kirwan, M. L., Guntenspergen, G. R., D'Alpaos, A., Morris, J. T., Mudd, S. M., and Temmerman, S. (2010). Limits on the adaptability of coastal marshes to rising sea level. *Geophysical Research Letters*, 37(23).

Kirwan, M. L., Guntenspergen, G. R., and Morris, J. T. (2009). Latitudinal trends in *Spartina alterniflora* productivity and the response of coastal marshes to global change. *Global Change Biology*, 15(8):1982–1989.

Kirwan, M. L. and Murray, A. B. (2007). A coupled geomorphic and ecological model of tidal marsh evolution. *Proceedings of the National Academy of Sciences*, 104(15):6118–6122.

Kirwan, M. L., Murray, A. B., and Boyd, W. S. (2008). Temporary vegetation disturbance as an explanation for permanent loss of tidal wetlands. *Geophysical Research Letters*, 35(5).

Kjerfve, B. (1978). Bathymetry as an Indicator of Net Circulation in Well Mixec. *Limnology and Oceanography*, 23(4):816–821.

Klein, G. d. V. (1985). Intertidal Flats and Intertidal Sand Bodies, second ed. In Davis, R., editor, *Coastal Sedimentary Envrionments*, pages 187–224. Springer-Verlag, New York.

Knighton, A. D., Woodroffe, C. D., and Mills, K. (1992). The evolution of tidal creek networks, Mary River, Northern Australia. *Earth Surface Processes and Landforms*, 17(2):167–190.

Kolmogorov, A. (1941). Confidence limits for an unknown distribution function. *The Annals of Mathematical Statistics*, 12(4):461–463.

Krone, R. (1987). A method for simulating historic marsh elevations. In *Coastal Sediments (1987)*, pages 316–323. ASCE.

Krone, R. B. (1962). Flume studies of the transport of sediment in estuarial shoaling processes. Technical report, Hydr, Eng. Laboratory, Univ of Berkely, USA.

Lachenbruch, P. A. (1975). *Discriminant analysis*. Wiley Online Library.

Langley, J. A., McKee, K. L., Cahoon, D. R., Cherry, J. A., and Megonigal, J. P. (2009). Elevated co_2 stimulates marsh elevation gain, counterbalancing sea-level rise. *Proceedings of the National Academy of Sciences*, 106(15):6182–6186.

Lanzoni, S. and Seminara, G. (2002). Long-term evolution and morphodynamic equilibrium of tidal channels. *Journal of Geophysical Research: Oceans (1978–2012)*, 107(C1):1–1.

Larsen, L. G. and Harvey, J. W. (2010). How vegetation and sediment transport feedbacks drive landscape change in the Everglades and wetlands worldwide. *The American Naturalist*, 176(3):E66–E79.

Lee, S. and Cundy, A. (2001). Heavy metal contamination and mixing processes in sediments from the Humber Estuary, Eastern England. *Estuarine, Coastal and Shelf Science*, 53(5):619–636.

Lehmann, E. (1975). *Nonparametrics: Statistical methods based on ranks*. Holden-Day, San Francisco, CA.

Leonard, L. A. and Croft, A. L. (2006). The effect of standing biomass on flow velocity and turbulence in *Spartina alterniflora* canopies. *Estuarine, Coastal and Shelf Science*, 69(3):325–336.

Leonard, L. A. and Luther, M. E. (1995). Flow hydrodynamics in tidal marsh canopies. *Limnology and Oceanography*, 40(8):1474–1484.

Lorenzo-Trueba, J., Voller, V., and Paola, C. (2010). Toward a model framework for sedimentary delta growth that accounts for biological processes. In *AGU Fall Meeting Abstracts*, volume 1, page 0427.

Marani, M., Belluco, E., D'Alpaos, A., Defina, A., Lanzoni, S., and Rinaldo, A. (2003). On the drainage density of tidal networks. *Water Resources Research*, 39(2).

Marani, M., Belluco, E., Ferrari, S., Silvestri, S., D'Alpaos, A., Lanzoni, S., Feola, A., and Rinaldo, A. (2006a). Analysis, synthesis and modelling of high-resolution observations of salt-marsh eco-geomorphological patterns in the Venice lagoon. *Estuarine, Coastal and Shelf Science*, 69(3):414–426.

Marani, M., Da Lio, C., and D'Alpaos, A. (2013). Vegetation engineers marsh morphology through multiple competing stable states. *Proceedings of the National Academy of Sciences*, 110(9):3259–3263.

Marani, M., D'Alpaos, A., Lanzoni, S., Carniello, L., and Rinaldo, A. (2007). Biologically-controlled multiple equilibria of tidal landforms and the fate of the Venice lagoon. *Geophysical Research Letters*, 34(11).

Marani, M., D'Alpaos, A., Lanzoni, S., Carniello, L., and Rinaldo, A. (2010). The importance of being coupled: Stable states and catastrophic shifts in tidal biomorphodynamics. *Journal of Geophysical Research: Earth Surface (2003–2012)*, 115(F4).

Marani, M., Lanzoni, S., Silvestri, S., and Rinaldo, A. (2004). Tidal landforms, patterns of halophytic vegetation and the fate of the lagoon of Venice. *Journal of Marine Systems*, 51(1):191–210.

Marani, M., Lanzoni, S., Zandolin, D., Seminara, G., and Rinaldo, A. (2002). Tidal meanders. *Water Resources Research*, 38(11):7–1.

Marani, M., Silvestri, S., Belluco, E., Ursino, N., Comerlati, A., Tosatto, O., and Putti, M. (2006b). Spatial organization and ecohydrological interactions in oxygen-limited vegetation ecosystems. *Water resources research*, 42(6).

Marchi, E. (1990). Sulla stabilitá delle bocche lagunari a marea. *Rendiconti Lincei*, 1(2):137–150.

Marciano, R., Wang, Z. B., Hibma, A., de Vriend, H. J., and Defina, A. (2005). Modeling of channel patterns in short tidal basins. *Journal of Geophysical Research: Earth Surface (2003–2012)*, 110(F1).

Mariotti, G. and Fagherazzi, S. (2010). A numerical model for the coupled long-term evolution of salt marshes and tidal flats. *Journal of Geophysical Research: Earth Surface (2003–2012)*, 115(F1).

Martínez, A. M. and Kak, A. C. (2001). Pca versus lda. *Pattern Analysis and Machine Intelligence, IEEE Transactions on*, 23(2):228–233.

Mendelssohn, I. A. and Morris, J. T. (2000). Eco-physiological controls on the productivity of *Spartina alterniflora Loisel*. In Weinstein, M. and Kreeger, D., editors, *Concepts and controversies in tidal marsh ecology*, pages 59–80. Dordrecht: Kluwer Press.

Miller, M., McCave, I., and Komar, P. (1977). Threshold of sediment motion under unidirectional currents. *Sedimentology*, 24(4):507–527.

Minkoff, D. R. (2007). *Geomorfología y dinámica de canales de mareas en ambientes internareales*. PhD thesis, Departamento de Ingeniería, Universidad Nacional del Sur, Bahía Blanca.

Minkoff, D. R., Escapa, M., Ferramola, F. E., Maraschín, S. D., Pierini, J. O., Perillo, G. M., and Delrieux, C. (2006). Effects of crab–halophytic plant interactions on creek growth in a SW atlantic salt marsh: a cellular automata model. *Estuarine, Coastal and Shelf Science*, 69(3):403–413.

Mitsch, W. J. and Gosselink, J. G. (2000). *Wetlands*. John Wiley, New York.

Moffett, K. B., Robinson, D. A., and Gorelick, S. M. (2010). Relationship of salt marsh vegetation zonation to spatial patterns in soil moisture, salinity, and topography. *Ecosystems*, 13(8):1287–1302.

Morris, J. T. (2000). Effects of Sea-level Anomalies on Estuatine Processes. In Hobbie, J., editor, *Estuarine science: A synthetic approach to research and practice*, page 107. Island Press, Washington DC.

Morris, J. T. and Haskin, B. (1990). A 5-yr record of aerial primary production and stand characteristics of *Spartina alterniflora*. *Ecology*, pages 2209–2217.

Morris, J. T., Porter, D., Neet, M., Noble, P. A., Schmidt, L., Lapine, L. A., and Jensen, J. R. (2005). Integrating LIDAR elevation data, multi-spectral imagery and neural network modelling for marsh characterization. *International Journal of Remote Sensing*, 26(23):5221–5234.

Morris, J. T., Sundareshwar, P., Nietch, C. T., Kjerfve, B., and Cahoon, D. (2002). Responses of coastal wetlands to rising sea level. *Ecology*, 83(10):2869–2877.

Mudd, S. M., D'Alpaos, A., and Morris, J. T. (2010). How does vegetation affect sedimentation on tidal marshes? Investigating particle capture and hydrodynamic controls on biologically mediated sedimentation. *Journal of Geophysical Research: Earth Surface (2003–2012)*, 115(F3).

Mudd, S. M., Fagherazzi, S., Morris, J. T., and Furbish, D. J. (2004). Flow, sedimentation, and biomass production on a vegetated salt marsh in South Carolina: Toward a predictive model of marsh morphologic and ecologic evolution. *Coastal and Estuarine Studies*, 59:165–188.

Murray, A., Knaapen, M., Tal, M., and Kirwan, M. (2008). Biomorphodynamics: Physical-biological feedbacks that shape landscapes. *Water Resources Research*, 44(11).

Murray, A. B. (2003). Contrasting the goals, strategies, and predictions associated with simplified numerical models and detailed simulations. *Geophysical Monograph Series*, 135:151–165.

Myrick, R. M. and Leopold, L. B. (1963). *Hydraulic geometry of a small tidal estuary*. US Government Printing Office Washington, DC.

National Oceanographic Centre (2014). National Tidal and Sea Level Facilities – Real-time data – UK National Tide Gauge Network. `http://www.ntslf.org/data/uk-network-real-time`.

Nepf, H. (1999). Drag, turbulence, and diffusion in flow through emergent vegetation. *Water resources research*, 35(2):479–489.

Neubauer, S. C. (2008). Contributions of mineral and organic components to tidal freshwater marsh accretion. *Estuarine, Coastal and Shelf Science*, 78(1):78–88.

O'Brien, M. P. (1969). Equilibrium flow areas of tidal inlets on sandy coasts. *Coastal Engineering Proceedings*, 1(10).

Orson, R., Panageotou, W., and Leatherman, S. P. (1985). Response of tidal salt marshes of the US Atlantic and Gulf coasts to rising sea levels. *Journal of Coastal Research*, pages 29–37.

Palmer, M. R., Nepf, H. M., Pettersson, T. J., and Ackerman, J. D. (2004). Observations of particle capture on a cylindrical collector: Implications for particle accumulation and removal in aquatic systems. *Limnology and Oceanography*, 49(1):76–85.

Partheniades, E. (1965). Erosion and deposition of cohesive soils. *Journal of the Hydraulics Division, ASCE*, 91(1):105–139.

Pearson, K. (1896). Mathematical contributions to the theory of evolution. iii. Regression, Heredity, and Panmixia. In *Philosophical Transactions of the Royal Society Ser.* The Royal Society.

Pendle, M. (2013). Estuarine and coastal managed realignment sites in England: A comparison of predictions and monitoring results for selected case studies. Technical report, HR Wallingford.

Perillo, G. M. (2009). Tidal courses: Classification, origin and functionality. In Perillo, G. M., Wolanski, E., Cahoon, D. R., and Brinson, M. M., editors, *Coastal Wetlands: An Integrated Ecosystem Approach*. Elsevier, Amsterdam.

Perillo, G. M. and Iribarne, O. O. (2003a). New mechanisms studied for creek formation in tidal flats: from crabs to tidal channels. *Eos, Transactions American Geophysical Union*, 84(1):1–5.

Perillo, G. M. and Iribarne, O. O. (2003b). Processes of tidal channel development in salt and freshwater marshes. *Earth Surface Processes and Landforms*, 28(13):1473–1482.

Perillo, G. M., Minkoff, D. R., and Piccolo, M. C. (2005). Novel mechanism of stream formation in coastal wetlands by crab–fish–groundwater interaction. *Geo-Marine Letters*, 25(4):214–220.

Perillo, G. M., Ripley, M. D., Piccolo, M. C., and Dyer, K. R. (1996). The formation of tidal creeks in a salt marsh: new evidence from the Loyola Bay Salt Marsh, Rio Gallegos Estuary, Argentina. *Mangroves and Salt Marshes*, 1(1):37–46.

Perron, J. and Fagherazzi, S. (2012). The legacy of initial conditions in landscape evolution. *Earth Surface Processes and Landforms*, 37(1):52–63.

Pestrong, R. (1965). The development of drainage patterns on tidal marshes. *Stanford University publications*, 10(2).

Pestrong, R. (1972). Tidal-flat sedimentation at Cooley Landing, southwest San Francisco Bay. *Sedimentary Geology*, 8(4):251–288.

Pethick, J. (1969). Drainage in tidal marshes. In Steers, J., editor, *The Coastline of England and Wales*, pages 725–730. Cambridge University Press, Cambridge.

Pethick, J. (1980). Velocity surges and asymmetry in tidal channels. *Estuarine and Coastal Marine Science*, 11(3):331–345.

Pethick, J. (1981). Long-term accretion rates on tidal salt marshes. *Journal of Sedimentary Research*, 51(2).

Pethick, J. (1992). Saltmarsh geomorphology. In Allen, J. and Pye, K., editors, *Saltmarshes: morphodynamics, conservation and engineering significance*, pages 41–62. The University Press, Cambridge, Cambridge.

Phleger, C. F. (1971). Effect of salinity on growth of a salt marsh grass. *Ecology*, pages 908–911.

Pignatti, S. (1966). *La vegetazione alofila della laguna veneta*, volume 33. Istituto Veneto di Scienze, Lettere ed Arti, Venezia.

Pratolongo, P., Kirby, J., Plater, A., and Brinson, M. (2009). Temperate coastal wetlands: morphology, sediment processes, and plant communities. In Perillo, G. M., Wolanski, E., Cahoon, D. R., and Brinson, M. M., editors, *Coastal Wetlands: An Integrated Ecosystem Approach*. Elsevier, Amsterdam.

Priestas, A. and Fagherazzi, S. (2011). Morphology and hydrodynamics of wave-cut gullies. *Geomorphology*, 131(1):1–13.

Pringle, A. (1995). Erosion of a cyclic saltmarsh in Morecambe Bay, north-west England. *Earth Surface Processes and Landforms*, 20(5):387–405.

Pritchard, D. and Hogg, A. (2003). Cross-shore sediment transport and the equilibrium morphology of mudflats under tidal currents. *Journal of Geophysical Research: Oceans (1978–2012)*, 108(C10).

Pye, K. (1995). Controls on long-term saltmarsh accretion and erosion in the Wash, eastern England. *Journal of Coastal Research*, pages 337–356.

Pye, K. (2000). Saltmarsh erosion in southeast England: mechanisms, causes and implications. In Sherwood, B., Gardiner, B., and Harris, T., editors, *British Saltmarshes*, pages 359–396. Westbury Publishing, Yorkshire.

Pye, K. (2005). Alde and Ore Estuary Flood Management Strategy-Assessment of Background Evidence and Recommendations for Further Action. Technical report, External Investigation Report EX509, Holloway,London.

Pye, K. and French, P. (1993). Volume One: Introduction: Saltmarsh process & morphology. In *Erosion & Accretion Processes on British Salt Marshes*, volume 1. Cambridge Environmental Research Consultants.

Ragotzkie, R. A. (1959). Drainage patterns in salt marshes. In *Proceedings of the Salt Marsh Conference*, pages 22–25.

Randerson, P. (1979). A simulation model of salt-marsh development and plant ecology. *Estuarine and coastal land reclamation and water storage*, pages 48–67.

Redfield, A. C. (1965). Ontogeny of a salt marsh estuary. *Science*, 147(3653):50–55.

Redfield, A. C. (1972). Development of a New England salt marsh. *Ecological Monographs*, pages 201–237.

Rinaldo, A., Fagherazzi, S., Lanzoni, S., Marani, M., and Dietrich, W. E. (1999a). Tidal networks: 2. watershed delineation and comparative network morphology. *Water Resources Research*, 35(12):3905–3917.

Rinaldo, A., Fagherazzi, S., Lanzoni, S., Marani, M., and Dietrich, W. E. (1999b). Tidal networks: 3. landscape-forming discharges and studies in empirical geomorphic relationships. *Water Resources Research*, 35(12):3919–3929.

Rinaldo, A., Rodriguez-Iturbe, I., and Rigon, R. (1998). Channel networks. *Annual Review of Earth and Planetary Sciences*, 26:289–327.

Rodríguez-Iturbe, I. and Rinaldo, A. (1997). *Fractal river basins: chance and self-organization*. Cambridge University Press.

Roelvink, J. (2006). Coastal morphodynamic evolution techniques. *Coastal Engineering*, 53(2):277–287.

Rotman, R., Naylor, L., McDonnell, R., and MacNiocaill, C. (2008). Sediment transport on the Freiston Shore managed realignment site: an investigation using environmental magnetism. *Geomorphology*, 100(3):241–255.

Schoeneberger, P. and Wysocki, D. (2012). Geomorphic description system. Technical Report Version 4.2, Natural Resources Conservation Service, National Soil Survey Center, Lincoln, NE.

Schuttelaars, H. and de Swart, H. (2000). Multiple morphodynamic equilibria in tidal embayments. *Journal of Geophysical Research: Oceans (1978–2012)*, 105(C10):24105–24118.

Schwarz, C., Ye, Q., Wal, D., Zhang, L., Bouma, T., Ysebaert, T., and Herman, P. (2014). Impacts of salt marsh plants on tidal channel initiation and inheritance. *Journal of Geophysical Research: Earth Surface*.

Scott, C., Armstrong, S., Townend, I., Dixon, M., and Everard, M. (2011). Lessons Learned from 20 Years of Managed Realignment and Regulated Tidal Exchange in the UK. In *nstitution of Civil Engineers Conference on Innovative Coastal Management*. ICE.

Shepard, F. P. (1954). Nomenclature based on sand-silt-clay ratios. *Journal of Sedimentary Research*, 24(3).

Silvestri, S., Defina, A., and Marani, M. (2005). Tidal regime, salinity and salt marsh plant zonation. *Estuarine, Coastal and Shelf Science*, 62(1):119–130.

Smirnov, N. V. (1939). On the estimation of the discrepancy between empirical curves of distribution for two independent samples. *Bull. Math. Univ. Moscou*, 2(2).

Solari, L., Seminara, G., Lanzoni, S., Marani, M., and Rinaldo, A. (2002). Sand bars in tidal channels part 2. tidal meanders. *Journal of Fluid Mechanics*, 451:203–238.

Spearman, C. (1904). The proof and measurement of association between two things. *The American journal of psychology*, 15(1):72–101.

Spencer, K. and Harvey, G. (2012). Understanding system disturbance and ecosystem services in restored saltmarshes: Integrating physical and biogeochemical processes. *Estuarine, Coastal and Shelf Science*, 106:23–32.

Spencer, K. L., Cundy, A. B., and Croudace, I. W. (2003). Heavy metal distribution and early-diagenesis in salt marsh sediments from the Medway Estuary, Kent, UK. *Estuarine, Coastal and Shelf Science*, 57(1):43–54.

Steel, T. and Pye, K. (1997). The development of salt marsh tidal creek networks: Evidence from the UK. In *Proceedings of the Canadian Coastal Conference*, volume 1, pages 267–280.

Steers, J. (1939). Scolt Head report. Technical report, Transactions of the Norfolk and Norwich Naturalists Society.

Steers, J. A. (1964). *The coastline of England and Wales*. Cambridge University Press Cambridge.

Stefanon, L., Carniello, L., D'Alpaos, A., and Lanzoni, S. (2010). Experimental analysis of tidal network growth and development. *Continental Shelf Research*, 30(8):950–962.

Stefanon, L., Carniello, L., D'Alpaos, A., and Rinaldo, A. (2012). Signatures of sea level changes on tidal geomorphology: Experiments on network incision and retreat. *Geophysical Research Letters*, 39(12).

Stoddart, D. R., Reed, D. J., and French, J. R. (1989). Understanding salt-marsh accretion, Scolt Head Island, Norfolk, England. *Estuaries*, 12(4):228–236.

Symonds, A. M. and Collins, M. B. (2007). The establishment and degeneration of a temporary creek system in response to managed coastal realignment: The Wash, UK. *Earth Surface Processes and Landforms*, 32(12):1783–1796.

Temmerman, S., Bouma, T., Govers, G., and Lauwaet, D. (2005a). Flow paths of water and sediment in a tidal marsh: Relations with marsh developmental stage and tidal inundation height. *Estuaries*, 28:338–352.

Temmerman, S., Bouma, T., Govers, G., Wang, Z., De Vries, M., and Herman, P. (2005b). Impact of vegetation on flow routing and sedimentation patterns: Three-dimensional modeling for a tidal marsh. *Journal of Geophysical Research: Earth Surface (2003–2012)*, 110(F4).

Temmerman, S., Bouma, T., Van de Koppel, J., Van der Wal, D., De Vries, M., and Herman, P. (2007). Vegetation causes channel erosion in a tidal landscape. *Geology*, 35(7):631–634.

Tilman, D. (2000). Causes, consequences and ethics of biodiversity. *Nature*, 405(6783):208–211.

Toffolon, M. and Crosato, A. (2007). Developing macroscale indicators for estuarine morphology: The case of the Scheldt estuary. *Journal of Coastal Research*, pages 195–212.

Toffolon, M. and Lanzoni, S. (2010). Morphological equilibrium of short channels dissecting the tidal flats of coastal lagoons. *Journal of Geophysical Research: Earth Surface (2003–2012)*, 115(F4).

Ursino, N., Silvestri, S., and Marani, M. (2004). Subsurface flow and vegetation patterns in tidal environments. *Water Resources Research*, 40(5).

van de Koppel, J., van der Wal, D., Bakker, J. P., and Herman, P. M. (2005). Self-organization and vegetation collapse in salt marsh ecosystems. *The American Naturalist*, 165(1):E1–E12.

van der Wal, D. and Pye, K. (2004). Patterns, rates and possible causes of saltmarsh erosion in the Greater Thames area (UK). *Geomorphology*, 61(3-4):373–391.

Van Maanen, B., Coco, G., Bryan, K., and Friedrichs, C. (2013). Modeling the morphodynamic response of tidal embayments to sea-level rise. *Ocean Dynamics*, 63(11-12):1249–1262.

van Maanen, B., Coco, G., and Bryan, K. R. (2013). Modelling the effects of tidal range and initial bathymetry on the morphological evolution of tidal embayments. *Geomorphology*, 191:23–34.

Vandenbruwaene, W., Meire, P., and Temmerman, S. (2012). Formation and evolution of a tidal channel network within a constructed tidal marsh. *Geomorphology*, 151:114–125.

Watts, C., Tolhurst, T., Black, K., and Whitmore, A. (2003). In situ measurements of erosion shear stress and geotechnical shear strength of the intertidal sediments of the experimental managed realignment scheme at Tollesbury, Essex, UK. *Estuarine, Coastal and Shelf Science*, 58(3):611–620.

Webb, J. (1983). Soil water salinity variations and their effects on *Spartina alterniflora*. *Contributions in Marine Science*.

White, H. (1980). A heteroskedasticity-consistant covariance matrix estimator and a direct test for heteroskedasticity. *Econometrica*, 48.

Wolanski, E. (2009). Coastal wetlands: A synthesis. In Perillo, G. M., Wolanski, E., Cahoon, D. R., and Brinson, M. M., editors, *Coastal Wetlands: An Integrated Ecosystem Approach*. Elsevier, Amsterdam.

Yapp, R., Johns, D., and Jones, O. (1917). The salt marshes of the Dovey Estuary. *The Journal of Ecology*, pages 65–103.